



TECHNISCHE
UNIVERSITÄT
WIEN

Vienna University of Technology

Master thesis

Mechanistic Investigations of C–H Activation Reactions

Conducted at the

Institute of Applied Synthetic Chemistry

Vienna University of Technology

under the supervision of

Assistant Prof. DI Dr. techn. Michael Schnürch

performed by

Robert Pollice

1026337

Au 190, 2880 Kirchberg am Wechsel

Acknowledgements

This thesis would not have been possible if it was not for the many people who helped and supported me during the time of my studies and my works. Therefore, before going into the matters of my thesis I would like to thank those people who were crucial for its successful completion.

First of all, I want to express my deepest gratitudes to my supervisor Assistant Prof. Michael Schnürch. He gave me the possibility to work very independently on my research project and always had an open door for discussing ideas and problems with me. He was a crucial person in order for me to become the chemist I am now.

Moreover, I would like to acknowledge Prof. Marko D. Mihovilovic who gave me the possibility to work in his research group and who always supported me to thrive as a scientist.

Furthermore, I would like to thank all the present and former members of our research group for all the support they could offer me. I would especially like to express my gratitude for measuring lots of NMR samples, for fixing problems with MPLC, GC and GC/MS equipment and for creating a pleasant working atmosphere. I really enjoyed being part of this research group.

In addition, I would like to thank Professor Gerd Mauschitz for his help with particle size distribution measurements, Dr. Sven Barth and Dr. Jingxia Yang for their help with nitrogen adsorption and desorption measurements and Fabian Glatz for proof-reading of mathematical derivations.

Finally, I owe my parents Elisabeth and Giancarlo everything in my life. They supported me throughout my whole life in every matter I had and therefore they made it possible for me to become a scientist.

Key

All compounds used or prepared in this thesis are labelled with bold Arabic numbers. Some compounds that are intended to be grouped together under the same Arabic number are labelled with bold Arabic numbers followed by Latin alphabetic characters. Proposed reaction intermediates are numbered in bold Roman numerals.

Literature citations are indicated by superscript Arabic numbers. Footnotes are indicated by superscript Latin alphabetic characters. Footnotes in the text are found at the bottom of the respective page, footnotes in Tables are found directly below the respective Table and are numbered independently from footnotes in the text.

List of Abbreviations

ax	axial
BET	Brunauer-Emmett-Teller
bipy	2,2'-bipyridine
but	butyl
cod	1,5-cyclooctadiene
coe	cyclooctene
Cy	cyclohexyl
d	doublet
EIE	equilibrium isotope effect
eq	equatorial
eq.	equivalent(s)
Et	ethyl
hex	hexyl
KIE	kinetic isotope effect
LP	light petroleum
Lut	lutidine
m	multiplet
mp	melting point
n.i.	not isolated
prop	propyl
q	quartet

List of Abbreviations

s	singlet
Sel.	selectivity
SF	stirring factor
t	triplet
terpy	2,2':6',2''-terpyridine

Abstract

The starting point of this master thesis was a Rh(I)-catalysed direct alkylation reaction of benzylic amines at the benzylic carbon atom directed by 3-substituted pyridin-2-yls employing either alkylbromides or alkenes. Preliminary mechanistic investigations have previously shown that during the reaction using alkylbromides β -H elimination is fast and the corresponding alkenes are formed intermediately. Since the reaction conditions are also almost identical, both reactions are likely to proceed via similar reaction mechanisms. The goal of this project was to investigate further into the reaction mechanisms of these reactions, especially focussing on the transformation using alkenes.

First of all, the reaction using alkenes, formally a $C(sp^3)$ -H activation, was revealed to proceed via imine intermediates and hence via a $C(sp^2)$ -H activation pathway. The reaction shows a primary KIE of 4.3 at the benzylic C–H position together with a reversible H-D exchange at the same position which indicates that there are at least 2 distinct steps in which the corresponding C–H bonds are broken. The imine intermediates, which are detected throughout the whole reaction period, are shown to be converted to the final product under the reaction conditions and a time course analysis of the alkylated imine intermediate shows that it is formed before the final amine product in the course of the reaction.

Second of all, K_2CO_3 , which is effectively insoluble in the reaction mixture under the reaction conditions, was shown to be needed only in the beginning of the reaction using alkenes. During this induction period K_2CO_3 dissolves to a very small extent and the Rh-catalyst irreversibly reacts with it to form the catalytically active species. The duration of this induction period is dependent on the concentration, the specific surface and the water content of K_2CO_3 and on the agitation of the reaction mixture and all these dependences can be rationalised on the basis of a detailed kinetic model.

Third of all, the reaction using alkylbromides was revealed to yield several unexpected sideproducts. The alkylated product is accommodated by an alkylated sideproduct with a one carbon atom shorter alkyl chain. In addition, one of the sideproducts is an amide of the benzylic amine bearing a carbon chain elongated by one carbon atom with respect to the employed alkylbromide. Intensive screenings were carried out to increase selectivity in the reaction employing alkylbromides and it could be shown that the addition of secondary alcohols proves to be effective in that matter in the beginning while slowing the reaction down significantly as well. However, this selectivity is lost when the reaction approaches full conversion.

Deutsche Kurzfassung

Der Ausgangspunkt dieser Masterarbeit war eine Rh(I)-katalysierte direkte Alkylierungsreaktion von benzyllischen Aminen am benzyllischen Kohlenstoffatom mit Unterstützung einer 3-substituierten Pyridin-2-yl dirigierenden Gruppe unter Verwendung von Alkylbromiden oder Alkenen. Erste mechanistische Studien konnten zeigen, dass β -H Eliminierung während der Reaktion mit Alkylbromiden schnell ist und daher zwischenzeitlich die entsprechenden Alkene gebildet werden. Ziel dieses Projekts war es die Mechanismen dieser Reaktionen weiter zu untersuchen, wobei der Fokus auf der Reaktion mit Alkenen lag.

Als Erstes konnte gezeigt werden, dass die Reaktion mit Alkenen über Imin-Intermediate abläuft und daher über einen $C(sp^2)$ -H Aktivierungsmechanismus. Die Reaktion zeigt einen primären kinetischen Isotopeneffekt von 4.3 an der benzyllischen C–H Position zusammen mit einem reversiblen H-D Austausch an derselben Position. Diese Beobachtungen zeigen, dass es zumindest 2 unterschiedliche Reaktionsschritte geben muss, in denen die benzyllischen C–H Bindungen gespalten werden. Die Iminintermediate werden unter den Reaktionsbedingungen zu den Endprodukten der Reaktion umgesetzt. Eine Analyse des Zeitprofils des alkylierten Iminintermediates offenbart, dass es zeitlich vor dem finalen alkylierten Amin gebildet wird.

Weiters wurde herausgefunden, dass K_2CO_3 , das unter den Reaktionsbedingungen quasi unlöslich ist, nur am Beginn der Reaktion mit Alkenen benötigt wird. Während dieser Induktionsperiode löst sich K_2CO_3 zu einem sehr geringen Anteil im Reaktionsgemisch auf und der Rh-Katalysator reagiert irreversibel mit gelöstem K_2CO_3 zur katalytisch aktiven Spezies. Die Dauer dieser Induktionsperiode ist abhängig von der Konzentration, von der spezifischen Oberfläche und vom Wassergehalt von K_2CO_3 und von der Agitation des Reaktionsgemisches.

Zuletzt wurde aufgedeckt, dass die Reaktion mit Alkylbromiden einige unerwartete Nebenprodukte bildet. Das alkylierte Hauptprodukt der Reaktion ist von einem Nebenprodukt begleitet, das eine Kohlenstoffkette mit einem Kohlenstoffatom weniger aufweist. Zusätzlich wird auch ein Amid des benzyllischen Amins beobachtet, das eine um ein Kohlenstoffatom längere Kette als das eingesetzte Alkylbromid aufweist. Intensive Screenings wurden durchgeführt um die Selektivität in der Reaktion mit Alkylbromiden zu erhöhen und es konnte gezeigt werden, dass der Zusatz von sekundären Alkoholen darin effektiv ist, jedoch nur in einer anfänglichen Reaktionsperiode. Die anfänglich deutlich erhöhte Selektivität bleibt nicht aufrecht, wenn die Reaktion sich vollständigem Umsatz annähert.

Contents

Acknowledgements	I
Key	II
List of Abbreviations	III
Abstract	V
Deutsche Kurzfassung	VI
1. General Synthetic Schemes	1
2. Introduction	3
2.1. C–H Activation	3
2.2. Cyclometalation	5
2.3. Direct C–H Alkylation	6
2.4. C–H Activation Reactions of Benzylic Amines	8
2.5. Starting Point in Direct Alkylation Reactions of Benzylic Amines	10
2.5.1. Direct Alkylation of Benzylic Amines with Alkylbromides	10
2.5.2. Direct Alkylation of Benzylic Amines with Alkenes	12
2.5.3. Motivation for Additional Investigations	13
3. Results and Discussion	14
3.1. Direct Alkylations using Alkenes	14
3.1.1. Investigations into the Mechanistic Outline	14
3.1.1.1. Substrate Scope - Alkenes	14
3.1.1.2. Sideproduct Studies	16
3.1.1.3. KIE Studies	19
3.1.1.4. Substrate Scope - Tertiary Amines	20
3.1.1.5. Imine Studies	21
3.1.1.6. Imine Intermediate Kinetics	24
3.1.1.7. Mechanistic Proposal	25
3.1.2. Investigations into the Kinetic Modelling	27
3.1.2.1. Initial Rate Experiments	28
3.1.2.2. K ₂ CO ₃ Studies	31
3.1.2.3. Induction Time Studies	34

Contents

3.1.2.4.	Kinetic Profiles	36
3.1.2.5.	Electronic Influence on Benzylic Amines	39
3.1.2.6.	Temperature Dependence of the Initial Rate	41
3.1.2.7.	Kinetic Modelling and Mechanistic Consequences	41
3.2.	Direct Alkylations using Alkylbromides	45
3.2.1.	Kinetic Profile Comparison	46
3.2.2.	Investigations into all Major Sideproducts	47
3.2.2.1.	Sideproduct I (14)	47
3.2.2.2.	Sideproduct II (15)	49
3.2.2.3.	Sideproduct III (16)	50
3.2.2.4.	Sideproduct IV (17)	53
3.2.2.5.	Sideproduct Overview	55
3.2.3.	Optimisation of Reaction Conditions	56
3.3.	Conclusions	58
4.	Experimental	60
4.1.	General Methods	60
4.2.	General Procedures	62
4.2.1.	General procedure I for C–H activation reactions	62
4.2.2.	General procedure II for C–H activation reactions	62
4.2.3.	General work-up procedure for C–H activation reactions	62
4.3.	Synthetic Procedures	62
4.3.1.	Substrate Scope - Alkenes	62
4.3.1.1.	Hex-1-ene	63
4.3.1.2.	Styrene	64
4.3.1.3.	Cyclohexene	64
4.3.2.	Synthesis of Imines	65
4.3.2.1.	N-(3-methylpyridin-2-yl)-1-phenylmethanimine (10)	65
4.3.2.2.	3-methyl-N-(1-phenylheptylidene)-2-pyridinamine (11)	66
4.3.3.	Substrate Scope - Alkylbromides	66
4.3.3.1.	N-(1-phenylheptyl)-3-methylpyridin-2-amine (2)	66
4.3.3.2.	3-methyl-N-(1-phenylpentyl)pyridin-2-amine (9)	67
4.3.4.	Synthesis of Sideproduct 1	67
4.3.4.1.	N-(1,2-diphenylethyl)-3-methylpyridin-2-amine (14)	67
4.4.	Screening Experiments	68
4.4.1.	General Procedure	68
4.4.2.	Isolation of Sideproduct 2	68
4.4.2.1.	N-benzyl-N-(3-methylpyridin-2-yl)heptanamide (15)	68
4.5.	Kinetic Experiments	69
4.5.1.	General Procedure	69
4.5.2.	Kinetic Profiles	70
4.5.2.1.	Kinetic Profile Comparison	70

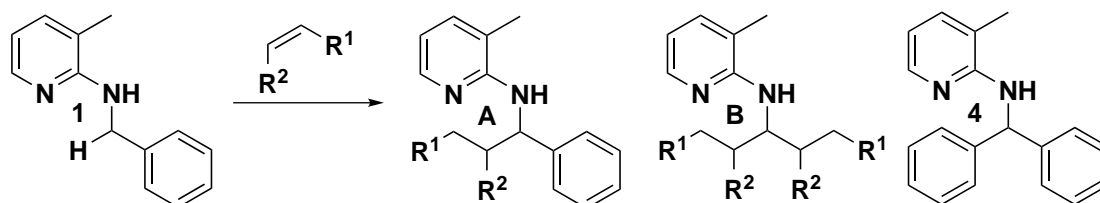
Contents

4.5.2.2. Kinetic Profile using Alkenes with K_2CO_3 in Catalytic Amounts	70
4.5.3. Kinetic Model - Alkene Alkylation	71
4.5.4. KIE Studies	71
4.5.4.1. KIE of Benzylic C–H	71
4.5.4.2. KIE of N–H	71
4.5.5. Electronic Influence on Benzylic Amines	72
4.5.6. Temperature Dependence of the Initial Rate	72
4.5.7. Induction Time Studies	73
4.6. Mechanistic Experiments	74
4.6.1. General Procedure	74
4.6.2. Sideproduct Experiment - Alkene	74
4.6.3. Substrate Scope - Tertiary Amines	75
4.6.4. Imine Experiments	75
4.6.5. K_2CO_3 in Catalytic Amounts	77
4.6.6. Sideproduct Experiments - Alkylbromide	77
4.6.6.1. Sideproduct I (14)	78
4.6.6.2. Sideproduct II (15)	78
4.6.6.3. Sideproduct III (16)	78
4.6.6.4. Sideproduct IV (17)	78
5. Data Evaluation and Mathematical Derivations	80
5.1. General Remarks	80
5.2. Direct Alkylations using Alkenes	80
5.2.1. Investigations into the Mechanistic Outline	80
5.2.1.1. KIE Studies	80
5.2.1.2. Imine Intermediate Kinetics	83
5.2.2. Investigations into the Kinetic Modelling	94
5.2.2.1. Initial Rate Experiments	94
5.2.2.2. K_2CO_3 Studies	97
5.2.2.3. Kinetic Profile with K_2CO_3 in Stoichiometric Amounts	105
5.2.2.4. Electronic Influence on Benzylic Amines	110
5.2.2.5. Temperature Dependence of the Initial Rate	110
5.2.2.6. Kinetic Modelling	117
5.3. Direct Alkylations using Alkylbromides	122
5.3.1. Kinetic Profile Comparison	122
5.3.2. Investigations into all Major Sideproducts	123
A. Appendices	130
A.1. Direct Alkylations using Alkenes	130
A.1.1. Investigations into the Mechanistic Outline	130
A.1.1.1. KIE Studies	130
A.1.1.2. Imine Intermediate Kinetics	130

Contents

A.1.2. Investigations into the Kinetic Modelling	130
A.1.2.1. Initial Rate Experiments	130
A.1.2.2. K_2CO_3 Studies	136
A.1.2.3. Kinetic Profiles	136
A.1.2.4. Electronic Influence on Benzylic Amines	136
A.1.2.5. Temperature Dependence of the Initial Rate	139
A.2. Direct Alkylations using Alkylbromides	141
A.2.1. Kinetic Profile Comparison	141
A.2.2. Investigations into all Major Sideproducts	141
A.2.3. Optimisation of Reaction Conditions	141

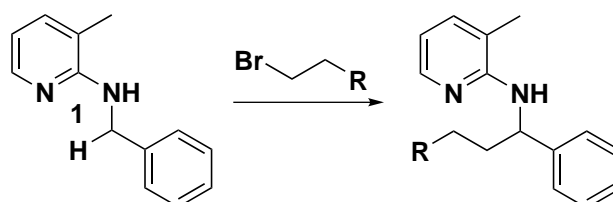
1. General Synthetic Schemes



Compound A	Yield	Compound B	Yield	Yield of 4
2 ($R^1 = n\text{-but}$, $R^2 = \text{H}$)	61 %	3 ($R = n\text{-but}$, $R^2 = \text{H}$)	8 %	6 %
5 ($R^1 = \text{Ph}$, $R^2 = \text{H}$)	58 % ^a	6 ($R^1 = \text{Ph}$, $R^2 = \text{H}$)	n.i.	n.i.
7 ($R^1 = R^2 = -(\text{CH}_2)_4-$)	39 % ^b	8 ($R^1 = R^2 = -(\text{CH}_2)_4-$)	3 %	7 %

^aGC purity 88 %.

^b32 % of **1** were recovered.

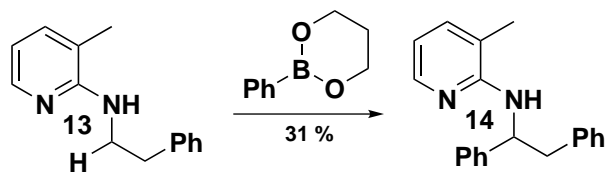
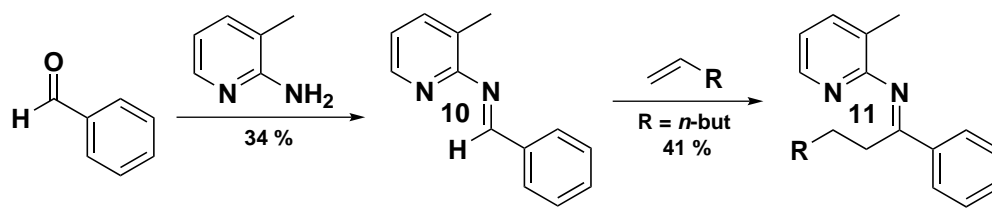


Product	Product yield
2 ($R = n\text{-but}$)	50 % ^a
9 ($R = \text{Et}$)	50 % ^b

^aGC purity 89 %.

^bGC purity 76 %.

1. General Synthetic Schemes

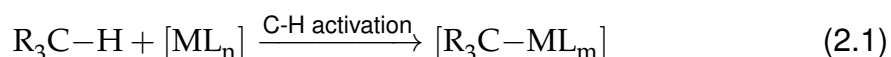


2. Introduction

In recent years the development of catalytic C–H activation methods to selectively functionalise organic molecules at unsubstituted carbon atoms has emerged tremendously.^{1–13} Especially, C–H activation of sp²-hybridised C–H bonds is quite common and well established in the field by now.^{14–20} On the other hand, C–H activation of sp³-hybridised C–H bonds still remains difficult and is therefore of special interest.^{21–25} In order to gain a better understanding of these reactions and overcome the difficulties detailed mechanistic investigations are important. They provide insight into the intrinsic problems and indicate in which step of the catalytic cycle optimisation is necessary. A very useful and general method to achieve catalytic C–H activation is cyclometalation which employs the aid of a nearby coordinating group to direct the catalyst selectively to one specific C–H bond to be activated and functionalised.^{26–32} In recent years, several useful methods for the C–H activation of benzylic C(sp³)–H bonds directed by 3-substituted pyridin-2-yls including Ru(0)-catalysed arylation employing arylboronates³³ and Ru(II)-catalysed arylation of benzylic amines with aryl halides³⁴, among others, have been developed. The Rh(I)-catalysed direct alkylation of benzylic amines using either alkylbromides or alkenes had also been investigated before but several unresolved questions and open ends remained.³⁵

2.1. C–H Activation

At present, the term C–H activation is ambiguous in literature. From a general perspective it can simply be defined as the weakening or energetic excitation of a C–H bond.³⁶ Alternatively, a more restrictive definition is that C–H activation refers to the formation of metal-carbon bonds from unreactive C–H bonds and transition metal complexes (cf. Equation 2.1).³⁷



The second definition reflects the field of C–H activation better since most of the research that had been carried out focusses on the aid of transition metal catalysis. However, in recent years so called metal-free C–H activation reactions^{38,39}, which usually are radical coupling reactions or are organocatalytic, have emerged and so, since it is still a young and developing research field, its boundaries are fluxional and a more general definition like the first one is becoming more appropriate.

2. Introduction

In this thesis the focus lies on C–H activations in metal-catalysed reactions so the term C–H activation can be defined according to the second definition. Figure 2.1 shows the most important reaction mechanisms for C–H activations under metal catalysis.⁴⁰

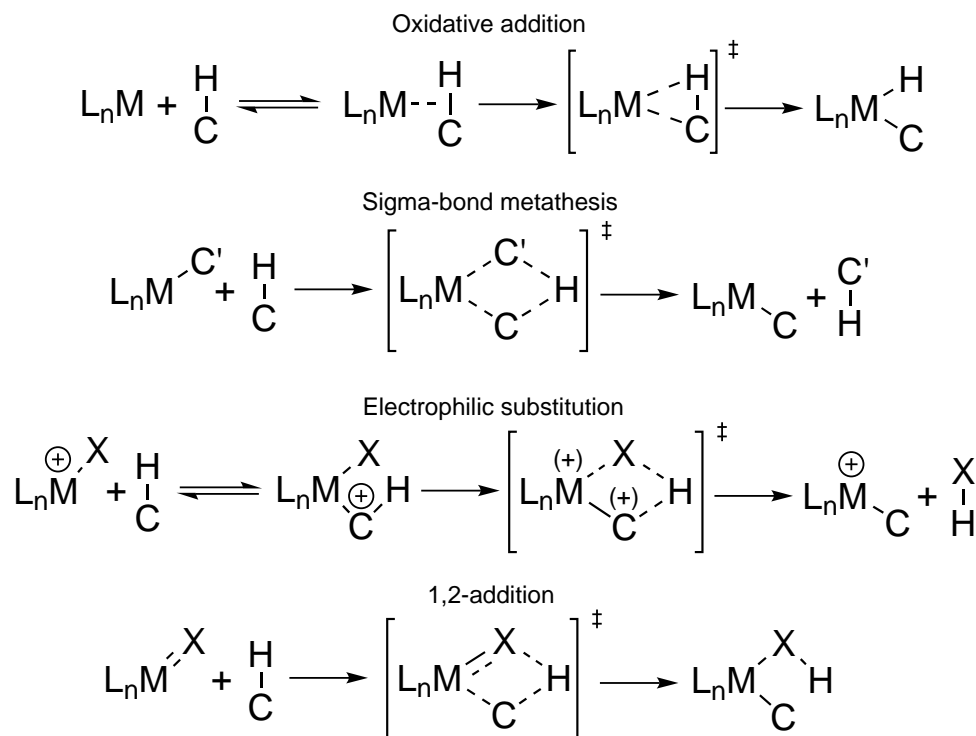


Figure 2.1.: Most important reaction mechanisms for C–H activations under metal catalysis.⁴⁰

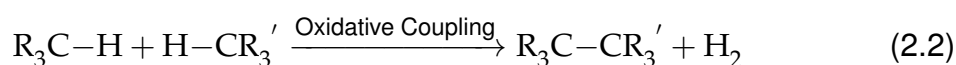
From these 4 mechanisms for C–H activations oxidative addition is the most common and therefore also the most important one. In general, it is accepted that in the C–H activation by oxidative addition the metal first coordinates to the C–H bond itself to form an agostic complex and then breaks the bond to form both a new C–M and a new M–H bond. This mechanism is especially typical for low-valent, electron-rich late transition metals like Ru(0) or Rh(I).⁴⁰ It should be noted that in C–H activation reactions the true C–H activation is only one step in the reaction mechanism of a transformation and additional steps are required to reach the ultimate reaction product. Therefore, in order to develop effective transformations all the other steps are equally important and also need to be investigated in great detail.

The great appeal of C–H activation reactions is the fact that almost any organic molecule contains at least one C–H bond which might be intended to be functionalised in order to create new organic molecules with structural diversity. Since most

2. Introduction

organic compounds not only contain one but naturally many C–H bonds intrinsic selectivity issues arise. In order to selectively address and functionalise one specific C–H bond in a certain reaction in the presence of many others there must be a discriminating element making specifically this C–H bond more reactive, i.e. making the free enthalpy of activation in the reaction pathway to functionalise it sufficiently lower compared to the others. This is the reason why the C–H activation of sp^2 -hybridised C–H bonds is more established by now since selectivity, especially in aromatic heterocycles, is achieved more easily and on many occasions arises from the intrinsic electronic properties of the starting material. A very general concept to achieve selectivity in C–H activation reactions of systems not possessing a high enough intrinsic difference in reactivity is cyclometalation, which is explained in more detail in the next section.

In addition, C–H activation reactions are potentially very attractive from an atom economic point of view. In traditional metal-catalysed cross coupling reactions usually two prefunctionalised carbon atoms are bonded together generating considerable waste molecules from the functional groups of the starting materials. In an ideal C–H activation reaction, a so-called oxidative coupling reaction or cross-dehydrogenative coupling^a, the carbon atoms of two C–H bonds are bonded together formally generating only H_2 as waste material^{15,21,41–43} (cf. Equation 2.2). This type of reaction potentially is the most atom economic transformation besides addition reactions^b and it obviates the need for prefunctionalisation further increasing efficiency and reducing waste generation.



However, there are several aspects of C–H activation reactions that are not ideal by now and need further significant research efforts. On many occasions, especially in the C–H activation of sp^3 -hybridised C–H bonds, harsh reaction conditions are required significantly limiting the synthetic potential and the efficiency of the transformations. In addition, high catalyst and co-catalyst loadings are often required for acceptable conversions decreasing the atom efficiency of the transformations.

2.2. Cyclometalation

In general, cyclometalation can be defined as the formation of a metallacycle, i.e. a ring containing at least one metal atom, from an organic molecule by forming at least one new metal-carbon bond.²⁶ In a specific reaction it refers to the formation

^aThe two terms are sometimes used synonymous in literature and strictly distinguished on other occasions.

^bIdeal addition reactions have an atom economy of 100 %.

2. Introduction

of a metallacycle from the starting material to be functionalised in the transformation. Usually, the aid of a coordinating group in proximity to the carbon atom to be bonded to the metal in the organic molecule is employed.²⁹ Selectivity arises from the fact that the formation of one specific metallacycle is thermodynamically, kinetically or both thermodynamically and kinetically preferred compared to others. Some molecules might carry an intrinsic so-called directing group which is the second coordination centre to the metal in the metallacycle. However, many molecules do not carry such a group and hence the introduction of a directing group is required in order to apply this method for C–H activation reactions (cf. Figure 2.2).

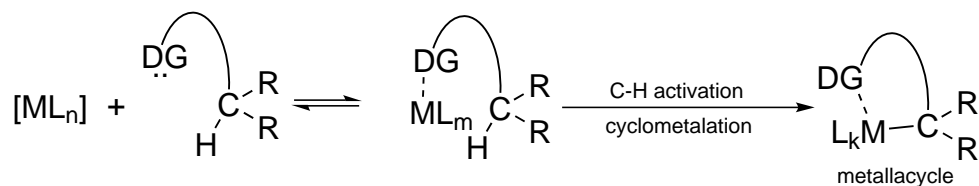


Figure 2.2.: General scheme of cyclometalation in C–H activation reactions.³⁵

The chelation effect is responsible for both an entropic and a kinetic advantage with respect to selectivity. Initial coordination to the directing group keeps the metal centre in close proximity to the C–H bond to be broken and functionalised. Selectivity potentially arises from both the thermodynamic and the kinetic preference of one specific ring size of the metallacycle.

There are several drawbacks of this approach. Substrates not intrinsically carrying a suitable directing group need to be transformed in additional synthetic steps to a suitable starting material for a C–H activation reaction. However, substrates intrinsically carrying a suitable directing group may effectively allow one C–H activation reaction but subsequent functionalisations by C–H activation at different sites of the molecule may not be effective and hence may require the derivatisation of the intrinsic directing group to prevent misdirection. Therefore, while the approach of cyclometalation is very useful to make specific C–H activation reactions more feasible and eases detailed mechanistic studies of these reactions as well, it also diminishes the atom economy of the process and potentially leads to the production of more waste materials. Overall, some of the benefits of C–H activation reactions are therefore lost by employing cyclometalation.

2.3. Direct C–H Alkylation

Direct C–H alkylation reactions are C–H activation reactions formally substituting a C–H group for an alkyl group. Therefore, a substrate is required which donates the alkyl group to be introduced. The most commonly employed alkylating agents in

2. Introduction

such transformations are alkyl (pseudo)halides and alkenes. The general reaction outline of classical direct C–H alkylation reactions is depicted in Figure 2.3.

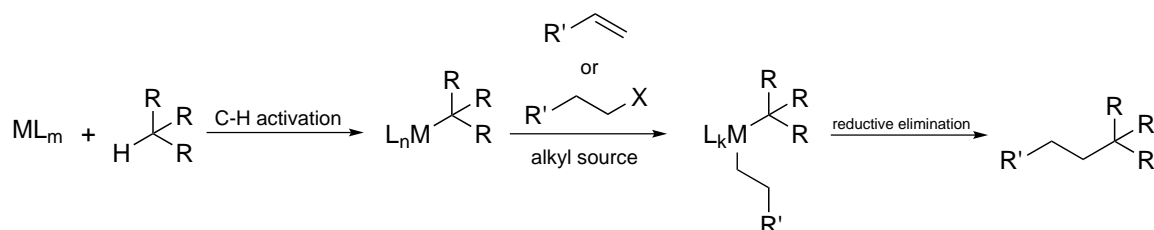


Figure 2.3.: General scheme of classical direct C–H alkylation reactions.

Classically, after both the substrate and the alkylating agent are bound to the metal centre, the alkyl group is transferred to the carbon atom by reductive elimination to form a new C–C bond and therefore the alkylated product. Depending on the alkylating agent used the alkyl complex is formed by different mechanisms. In the case of alkyl (pseudo)halides the most common mechanistic pathway is through oxidative addition of the metal centre into the C–X bond of the (pseudo)halide. Alkenes usually form a π -complex and then the alkene is inserted into a M–H bond to form the corresponding metal alkyl complex.

Recently, a Pd-catalysed direct C–H alkylation reaction was published in which a $C(sp^3)$ –H group is alkylated and a new $C(sp^3)$ – $C(sp^3)$ bond is generated (cf. Figure 2.4).⁴⁴

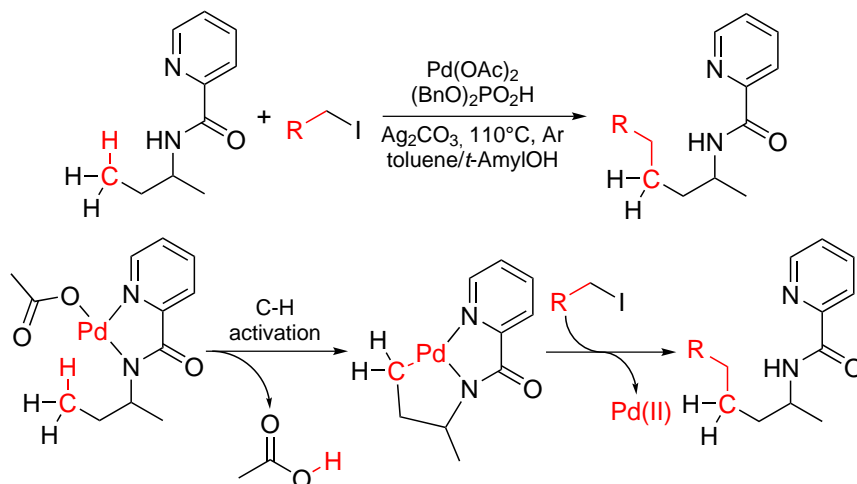


Figure 2.4.: Pd-catalysed direct C–H alkylation reaction of a γ - $C(sp^3)$ –H group of alkyl picolinamides using alkyl iodides.⁴⁴

In this direct C–H alkylation reaction a picolinamide directing group is used to se-

2. Introduction

lectively alkylate the C–H in γ -position relative to the picolinamide. Therefore, the concept of cyclometalation is applied to make this reaction feasible. Interestingly, the directing group itself can chelate to Pd(II) having potentially two coordinating groups and this type of directing group is therefore called a bidentate directing group⁹. Therefore, the cyclometalation forms a second ring and hence is actually an annulation. It should be noted that no detailed mechanistic investigations have been carried out but it is proposed that after the cyclometalative C–H activation the alkyl iodide, which is used as alkylating agent, is bonded to Pd by oxidative addition. The resulting intermediate would undergo reductive elimination to form the direct C–H alkylation product.⁴⁴ This literature example nicely illustrates both the concept of cyclometalation and direct C–H alkylation reactions on a very rare example of a C(sp³)–C(sp³) coupling by a C(sp³)–H activation pathway.

2.4. C–H Activation Reactions of Benzylic Amines

In this thesis the Rh(I)-catalysed direct C–H alkylation of benzylic amines directed by 3-substituted pyridin-2-yls, a removable directing group³³, is investigated in detail from both a mechanistic and a kinetic point of view. Before the previous research on the specific system under investigation is summarised, a short overview on other transformations using this type of substrate is given.

In 2013 a Ru-catalysed arylation of 3-substituted pyridin-2-yls using boronic acid esters was reported.³³ The substituent in the 3-position of the directing group was shown to be crucial for high conversions and this was rationalised on the basis of a computational study which showed that only with a substituent in the 3-position of the directing group the molecule would prefer a conformation in which the pyridine nitrogen atom and the benzylic methylene group are in spatial proximity and aligned favourably for the C–H activation. The general mechanistic outline of this transformation is shown in Figure 2.5.

The reaction is proposed to proceed by cyclometalative C–H activation, transmetalation of the aryl boronic acid ester and reductive elimination to form the final product. Tertiary benzylic amines and also homobenzylic amines are arylated under these conditions as well but with lower efficiency and slower reactions.³³

In 2013 again, Ru-catalysed arylations of 3-substituted pyridin-2-yls using either aryl chlorides or aryl bromides were reported.³⁴ In these protocols the formation of the corresponding imines of both the starting material and the product were observed under the reaction conditions. Therefore, it was considered that the reaction might proceed over the corresponding imines but there was not enough evidence supporting this hypothesis so the reaction was proposed to proceed over the amine intermediates, which is the straightforward mechanistic proposal. The proposed general mechanistic outline is therefore very similar to the mechanism proposed for the previous reaction. The only difference is that C–H activation is proposed to occur via the concerted metalation deprotonation mechanism (cf. Figure 2.6),

2. Introduction

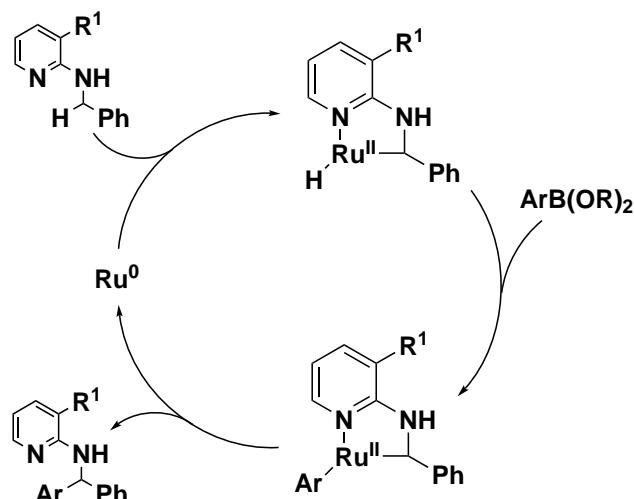


Figure 2.5.: Ru-catalysed direct C–H arylation reaction of benzylic amines using aryl boronic acid esters directed by 3-substituted pyridin-2-yls.³³

which could formally be viewed as a special form of the electrophilic substitution mechanism for C–H activation (cf. Figure 2.1). The only evidence which really supported the imine mechanism was the fact that tertiary benzylic amines were not arylated under these reaction conditions. However, proposing that the reaction proceeds over the corresponding imines needs more evidence than only this single hint.

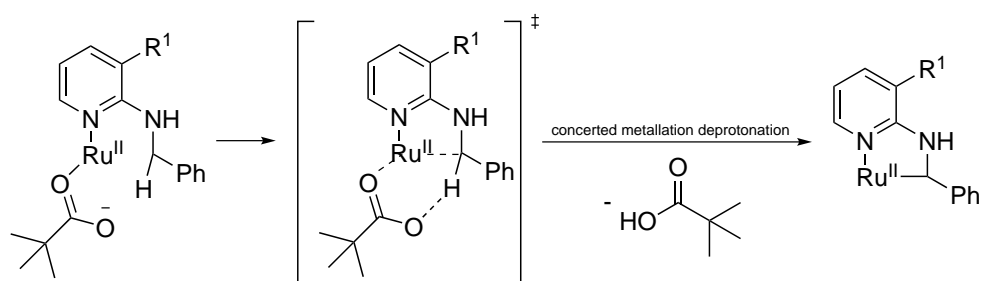


Figure 2.6.: C–H activation by concerted metallation deprotonation in the Ru(II)-catalysed direct C–H arylation reaction of benzylic amines using aryl halides directed by 3-substituted pyridin-2-yls.³⁴

Already in 1998, the Ru-catalysed direct C–H alkylation of benzylic amine **1** using alkenes was reported.⁴⁵ This very short paper demonstrates the substrate scope with respect to alkenes and one mechanistic experiment indicating that electron-donating groups on the phenyl group of the benzylic amine react prefer-

2. Introduction

entially to form the corresponding alkylation product. The general reaction outline is proposed to occur via the most straightforward route, i.e. cyclometalative C–H activation followed by insertion of the alkene into the Ru–H bond and reductive elimination to form the reaction product (cf. Figure 2.7), and hence via amine intermediates.⁴⁵

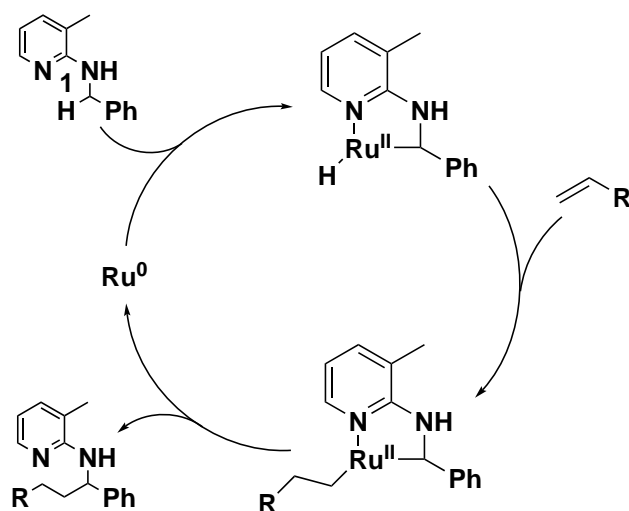


Figure 2.7.: Ru-catalysed direct C–H alkylation reaction of benzylic amine **1** using alkenes directed by 3-substituted pyridin-2-yls.⁴⁵

2.5. Starting Point in Direct Alkylation Reactions of Benzylic Amines

This section briefly summarises the previous research on Rh(I)-catalysed direct C–H alkylation reactions of benzylic amines that has been carried out and forms the basis of this thesis.³⁵

2.5.1. Direct Alkylation of Benzylic Amines with Alkylbromides

The initial goal of this project was to achieve direct alkylation of benzylic amines employing alkylbromides as alkylating agents using a removable directing group like 3-substituted pyridin-2-yls.³³ Intensive screenings revealed the reaction conditions depicted in Figure 2.8, which give low to moderate yields of the corresponding alkylation product depending on the alkylbromide used.

After the development of these reaction conditions the substrate scope with respect to alkylbromides was investigated. The focus was to use not only primary

2. Introduction

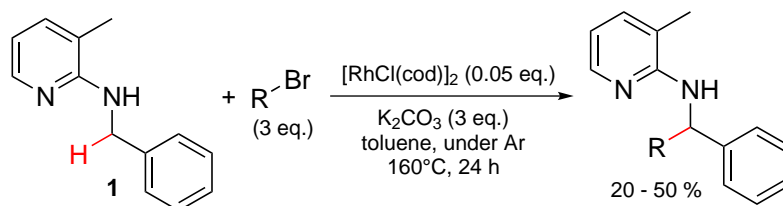


Figure 2.8.: Conditions for direct alkylation of benzylic amines with alkyl bromides.

but also secondary alkyl bromides. Direct alkylation of **1** with 2-bromobutane resulted in alkylation in the terminal instead of the secondary position and therefore the same product was formed as with 1-bromobutane (cf. Figure 2.9).

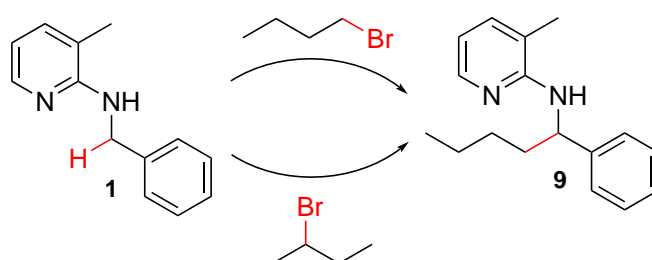


Figure 2.9.: Both primary and secondary alkyl bromides yield the same alkylation product.

Since β -H eliminations are common in transition metal alkyl complexes^{46–49} the hypothesis is that the initially formed metal alkyl complex is able to undergo β -H elimination potentially followed by insertion to isomerise to the more stable primary alkyl ligand (cf. Figure 2.10).

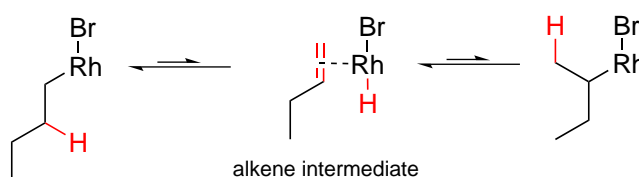


Figure 2.10.: The secondary alkyl complex is proposed to isomerise to the primary alkyl complex by β -H elimination followed by insertion.

Therefore, the corresponding alkene is an intermediate in this reaction and it was envisioned that direct alkylation using alkenes should therefore be possible under the same reaction conditions. Initial experiments using either hex-1-ene or styrene

2. Introduction

resulted in the formation of the corresponding alkylation products. In addition, in experiments using either 1-bromododecane or 1-bromo-2-phenylethane the corresponding alkenes could be detected in low amounts by means of GC/MS in the reaction mixture. In the absence of $[\text{RhCl}(\text{cod})]_2$ no alkene formation was observed confirming a crucial role of the catalyst and excluding simple thermal elimination.

A kinetic profile comparison for the alkylation using either 1-bromohexane or hex-1-ene under the same reaction conditions showed that the reaction using alkenes is significantly faster indicating that in the alkylbromide reaction one of the additional steps that have to occur is turnover-limiting and that in the alkene reaction a different step is turnover-limiting.

2.5.2. Direct Alkylation of Benzylic Amines with Alkenes

The alkylation of **1** using alkenes catalysed by $\text{Ru}(0)$ was already reported in literature.⁴⁵ However, there have not yet been any published reports using $\text{Rh}(I)$ catalysis or contributions dedicated to detailed mechanistic investigations of such a transformation. Since the reactions using alkylbromides and alkenes proceed most likely through the same reaction mechanism the reaction using alkenes, which is the simpler reaction, was investigated in more detail in order to learn more about the reaction using alkylbromides as well.

Initial investigations revealed the significant formation of two sideproducts which are presumably formed by C-C activations⁵⁰⁻⁵² (cf. Figure 2.11). Investigations into the formation of the alkylation product **2** and these two sideproducts could show that the formation of both **2** and **4** is in principle reversible under the reaction conditions. Experiments showing whether the formation of **3** is reversible as well had not been performed. In addition, the method of initial rates was applied

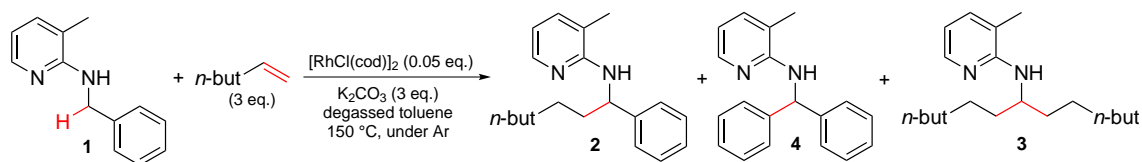


Figure 2.11.: Direct alkylation of **1** using hex-1-ene resulted in formation of side-products **3** and **4**.

to determine the partial reaction orders with respect to all starting materials. The partial reaction order with respect to **1** was shown to be 1 over the whole concentration region investigated and the partial reaction order with respect to hex-1-ene was shown to be 0 over the whole concentration region investigated. For both K_2CO_3 and $[\text{RhCl}(\text{cod})]_2$ more complex dependences were observed and in both cases there were concentration ranges identified showing first order dependence, respectively. However, the kinetic picture had not been fully revealed in that regard.

2.5.3. Motivation for Additional Investigations

On the basis of these previous results³⁵ the goals for this thesis were to further investigate the reaction mechanism of the direct alkylation reaction using alkenes because the initial rate experiments performed previously left some open questions and otherwise nothing was known about the mechanism, to further optimise the reaction conditions of the direct alkylation using alkylbromides because the yields were not satisfactory and the conditions were quite harsh and to perform further mechanistic studies on the alkylbromide reaction as well to gain further understanding of the reaction.

3. Results and Discussion

On the basis of the previously performed research³⁵ summarised before (vide supra) different aspects of the direct alkylation of benzylic amines using either alkenes or alkylbromides were investigated. The following chapter is split into two parts focussing in the first part on the reaction using alkenes and in the second part on the reaction using alkylbromides, respectively.

3.1. Direct Alkylations using Alkenes

3.1.1. Investigations into the Mechanistic Outline

The first aspect of the direct alkylation using alkenes that was investigated intensively was the mechanistic outline of this reaction i.e. the general mechanistic course that is followed. The goal was not to identify all elementary steps in the reaction mechanism since that is, by now, impossible without performing computational studies into the reaction mechanism. The goal was to identify schematically the most important steps in the reaction mechanism and therefore also the most important intermediates.

3.1.1.1. Substrate Scope - Alkenes

The optimised reaction conditions established in previous research efforts³⁵ were applied to perform the direct alkylation with different alkenes in order to investigate the substrate scope of this reaction. However, only a limited number of alkenes was investigated (cf. Table 3.1).

It should be noted that when styrene was used as alkene the main product (i.e. compound **5**) could not be separated from the sideproducts **4** and **6**, respectively, by means of flash chromatography (cf. Table 3.1, Entry 2). This is not surprising as these compounds are expected to have both a very similar polarity and show very similar interactions with both the stationary and the mobile phase. All alkenes used with additional functional groups did not show any considerable conversion to the corresponding alkylated products. One possible reason could be that the functional groups coordinate to the catalyst and maybe even form stable complexes, i.e. at least too stable for catalysis, by chelating through their functional groups and the double bond. It could be possible that alkenes with functional groups being further

3. Results and Discussion

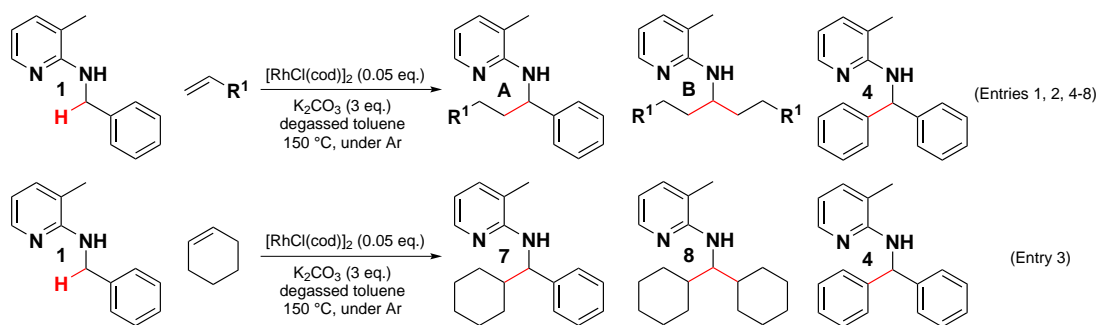


Table 3.1.: Results of the substrate scope investigation with respect to alkenes.

Entry	R^1	Alkene eq.	Time [h]	A^a	Yield of A	B^a	Yield of B	Yield of 4
1	<i>n</i> -but	3	3	2	61 %	3	8 %	6 %
2	Ph	3	12	5	58 % ^b	6	n.i.	n.i.
3	– ^c	12	24	7	39 % ^d	8	3 %	7 %
4	CO_2Me	3	3		<1 % conversion ^e			
5	CN	3	3		No product observed ^e			
6	OEt	3	3		No product observed ^e			
7	OAc	3	3		No product observed ^e			
8	OH	3	3		No product observed ^e			

^aCorresponding compound number.

^bGC purity 88 %.

^cSecond scheme.

^d32 % of **1** were recovered.

^eBased on GC and GC/MS analysis of the crude reaction mixture.

3. Results and Discussion

away from the double bond would be able to react in this alkylation reaction. However, this remains to be investigated in further experiments. Cyclohexene gives both the alkylation product **7** and the by-product **8** but reacts significantly slower being an alkene substituted on both sides of the double bond. In general, terminal alkenes bearing no additional functional group are expected to be converted to the corresponding alkylation product in this reaction.

3.1.1.2. Sideproduct Studies

It was already mentioned before that the formation of the sideproducts observed in the direct alkylation using alkenes had been investigated previously.³⁵ It could be shown that in the reaction using hex-1-ene the formation of both **2** and **4** is in principle reversible under the reaction conditions. In the course of this thesis it was investigated whether the formation of **3** is reversible as well. For the following discussion the results of all experiments investigating the formation of the sideproducts are given again (cf. Table 3.2).³⁵

Entries 1 and 2 show that the initial product **2** can be converted to the two sideproducts **3** and **4** by subjecting it to the reaction conditions. Without any alkene present (Table 3.2, Entry 3) compound **2** is even converted back to **1** showing that its formation is reversible under the reaction conditions. Entries 4 and 5 indicate that compound **4** can be converted to **2** under the reaction conditions showing that its formation is also reversible. Finally, mixing **3** and **4** in the absence of alkene leads to formation of **2** (Table 3.2, Entry 6). Overall, these experiments demonstrate that the formation of **3** and **4** starting from **2**, and also the formation of **2** from **1** is in principle reversible and that C–C bond cleavages by C–C activation reactions^{50–52} are occurring in the reaction mixture to a significant extent. Figure 3.1 illustrates the formation and interconversion of products **2**, **3**, and **4** from **1** in a very simplified way. As indicated in Figure 3.2 it is still unclear how H and Ph are exchanged in these interconversions (cf. Figure 3.1, unspecified residue X). However, it is proposed that the unspecified species X is most likely a Rh-complex which aids the exchange of H and Ph and vice versa.

Interestingly, no side-product deriving from bisalkylation of the benzylic position was detected in any experiment. One possible explanation is that formation of a quaternary carbon is simply disfavoured due to steric hindrance. Alternatively, if the alkylation does not occur on the amine substrate **1** but proceeds via an imine intermediate thereof, formation of a quaternary carbon is impossible. This can be considered as a first finding pointing towards an imine mechanism. In addition, in a similar system using imines with the same directing group and also employing Rh(I)-catalysis similar C–C activation reactions are already known.⁵³

3. Results and Discussion

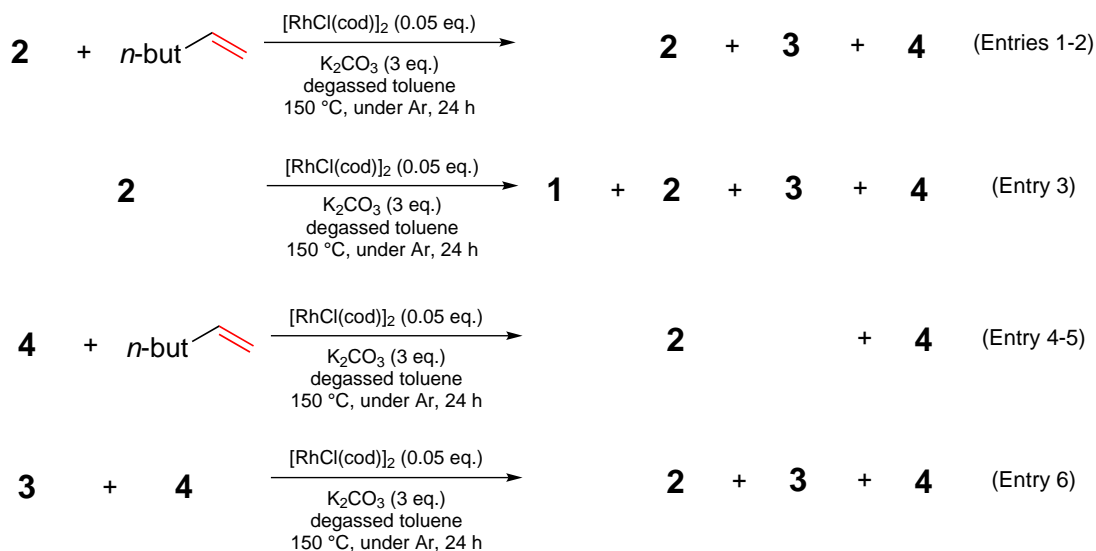


Table 3.2.: Results of the sideproduct studies of the direct alkylation using alkenes.

Entry	Starting Compound(s)	Hex-1-ene	Compound Amounts ^a			
			1	2	3	4
1	2 (1 eq.)	3 eq.	<0.1 %	62 %	11 %	5 %
2	2 (1 eq.)	6 eq.	<0.1 %	72 %	12 %	4 %
3	2 (1 eq.)	0 eq.	2 %	76 %	3 %	2 %
4	4 (1 eq.)	3 eq.	<0.1 %	4 %	<0.1 %	68 %
5	4 (1 eq.)	6 eq.	<0.1 %	6 %	<0.1 %	58 %
6	3 (0.5 eq.) + 4 (0.5 eq.) ^b	0 eq.	<0.1 %	1 %	46 %	42 %

^aDetermined at the end of the reaction, calibrated GC-Yields.

^bSum of amounts of 3 and 4 was considered as 1 eq.

3. Results and Discussion

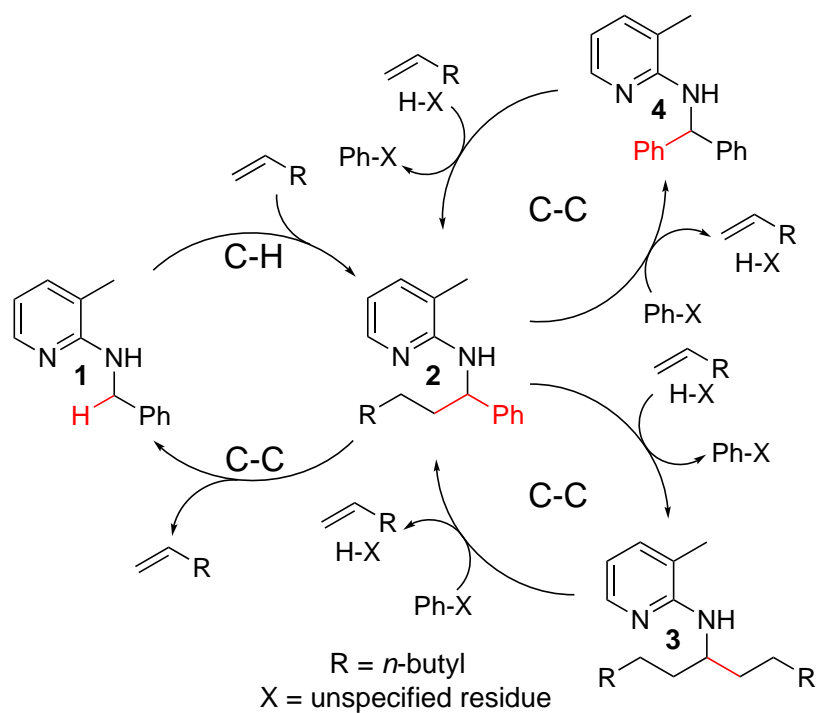


Figure 3.1.: Formation and interconversion of **1** and reaction products **2**, **3**, and **4** in the direct C–H alkylation using alkenes (C–H = C–H activation, C–C = C–C activation).

3. Results and Discussion

3.1.1.3. KIE Studies

In order to gain more information about the turnover-limiting step of the reaction KIE studies were conducted. In C–H activation reactions one major question is always whether the oxidative addition of the metal catalyst into the C–H bond is turnover-limiting. Therefore, in a first study the KIE of the benzylic C–H bonds was determined by measuring the initial rate of the reaction with the deuterated compound **1a** and comparing it to the initial rate determined for **1** under the same reaction conditions (cf. Figure 3.2).

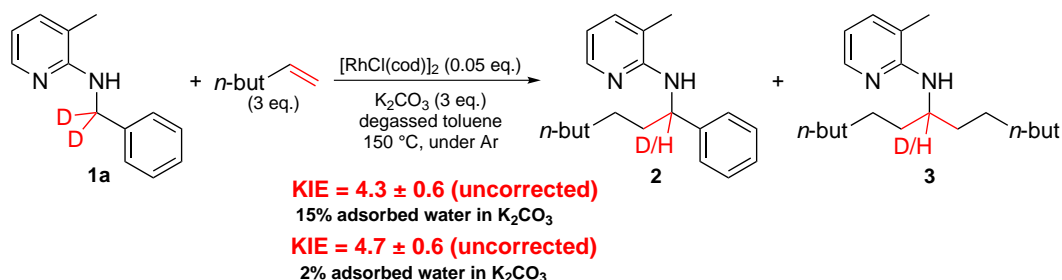


Figure 3.2.: Determination of the KIE of the benzylic C–H bonds in the direct C–H alkylation of **1** using hex-1-ene.

The large observed value indicates a primary KIE and suggests that the benzylic C–H bond is broken in the turnover-limiting step i.e. oxidative addition into the C–H bond is turnover-limiting. There are several things to be noticed. First, the KIE is independent of the adsorbed water content or the specific surface area of K₂CO₃.^a This is very important so that the result can be compared to the KIE study of the N–H bond (vide infra). Second there is significant H–D exchange observed in unreacted **1a** during the reaction. Actually, the H–D exchange is higher than the total amount of products formed (The corresponding values are found in the Appendices). This seems contradictory to the primary KIE observed because this would suggest a (compared to the overall reaction rate) fast and reversible C–H activation. However, it makes perfect sense if the reaction proceeds over the corresponding imine via a fast reversible amine to imine interconversion which would account for the H–D exchange observed. The consecutive oxidative addition into the sp²-hybridised C–H bond would then be turnover-limiting accounting for the large primary KIE observed.

In a second study the KIE of the N–H bond was determined (cf. Figure 3.3) in order to find out whether this hypothesis could be supported. The KIE was determined by comparing the initial reaction rate of deuterated compound **1b** and the

^aThe dependence of the initial reaction rate on both the adsorbed water content and the specific surface area of K₂CO₃ is demonstrated later.

3. Results and Discussion

initial rate obtained for the undeuterated compound **1** under the same reaction conditions. It should be noted that this is not an easy experiment to perform since the N–D readily exchanges with any H₂O that is introduced into the reaction mixture. The concomitant extent of H–D exchange has to be minimized in order to obtain a meaningful result.

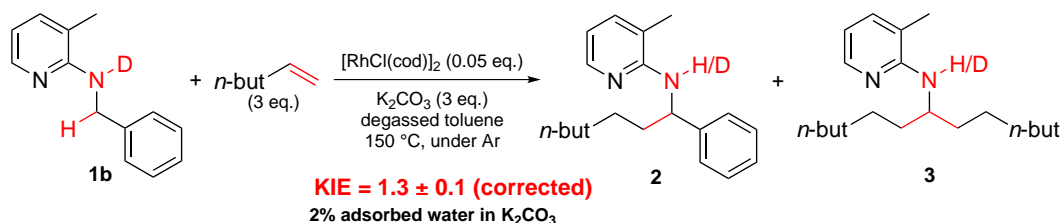


Figure 3.3.: Determination of the KIE of the N–H bond in the direct C–H alkylation of **1** using hex-1-ene.

Before the value is discussed it is important to mention that due to the adsorbed water introduced with K₂CO₃ the H–D exchange in this experiment series was high.^b Using K₂CO₃ with 2% of adsorbed water resulted in an H–D exchange low enough (even though still 56%) to determine the KIE reliably by correcting the observed initial rate (Details are discussed in Chapter 5). The small KIE value observed for the N–H bond indicates that the N–H bond is not broken in the turnover-limiting step excluding a mechanism where one of the benzylic C–H bonds and the N–H bond are broken simultaneously. In general, the absence of a (significant) KIE is not evidence that the corresponding bond is not broken in the turnover-limiting step. Since in this case a primary KIE was already observed for the benzylic C–H bonds, however, it could be concluded that the N–H bond is not broken in the turnover-limiting step. The observed value rather suggests a secondary KIE which would support the previously established hypothesis of a fast reversible imine formation prior to turnover-limiting oxidative addition into the C–H bond.

3.1.1.4. Substrate Scope - Tertiary Amines

The simplest experiment series to support or exclude an imine mechanism is to test whether tertiary benzylic amines are converted to the corresponding alkylated products under the reaction conditions (cf. Figure 3.4). If the formation of the corresponding products was observed at a similar rate as compared to secondary benzylic amines this would be evidence against an imine mechanism since the formation of the corresponding iminium ion is not expected to be occurring at a similar rate if possible at all. Of course, this experiment would not completely

^bThe H–D exchange in the deuterated amine was determined by means of transmission IR spectroscopy. Details are given in Chapter 5.

3. Results and Discussion

exclude an imine mechanism even if the corresponding alkylation products were formed at a similar rate because the reaction could theoretically occur then via a different mechanism. In neither experiment any alkylated products were observed even after 24 h of reaction time, again supporting the hypothesis of the reaction proceeding over the corresponding imines.

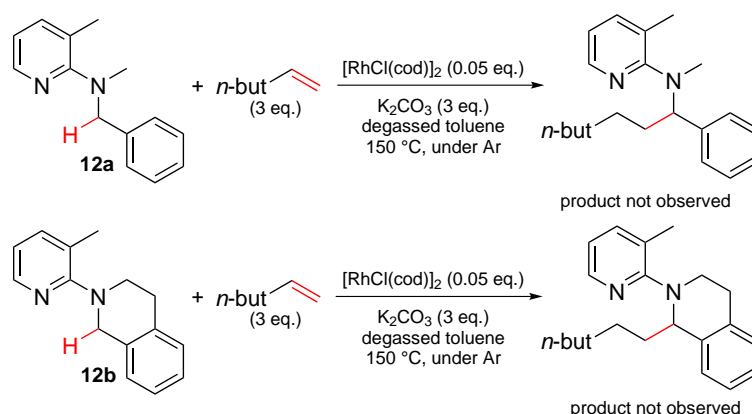


Figure 3.4.: Attempted alkylation of tertiary benzylic amines **12a** and **12b**.

3.1.1.5. Imine Studies

Based on the previous results the hypothesis is that amine **1** is converted to imine **10**, gets alkylated and the alkylated imine **11** is then converted back to alkylated amine **2** (cf. Figure 3.5). Of course, these interconversions would occur on a Rh-complex. It should be noted that a similar amine to imine oxidation prior to alkylation has been proposed previously in literature.⁵⁴ However, in that example the final reaction product is a ketone which is formed after hydrolysis of the imine so the amine to imine interconversion was not reversed.

It was hypothesised that if imines **10** and **11** were intermediates in the reaction they would be converted to the products of the reaction under the reaction conditions. Surprisingly, by using 1 eq. of **10** instead of **1** the reaction was significantly inhibited and only small amounts of the alkylated products **2** (about 1 %) and **11** (below 1 %) were observed after 2 h of reaction (cf. Figure 3.6). In addition, a small fraction of **10** was converted to the amine **1**. This result is rationalised by the imine **10** being a very strong ligand effectively coordinating multiple times to the catalytically active rhodium species thereby inhibiting the reaction. Therefore, crossover experiments were performed using 0.05 eq. of imines **10** and **11**, respectively, together with 1 eq. of amine **1d** as starting materials (cf. Figures 3.7 and 3.8).

In the first crossover experiment amine **1d** was alkylated in the presence of imine **10** which was completely converted to the alkylated amine **2**. In the second the

3. Results and Discussion

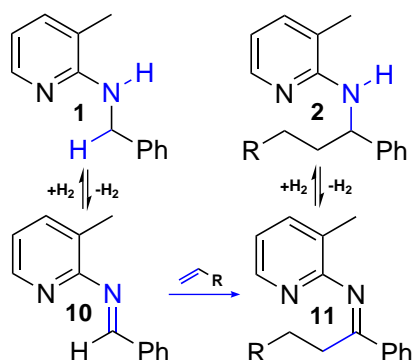
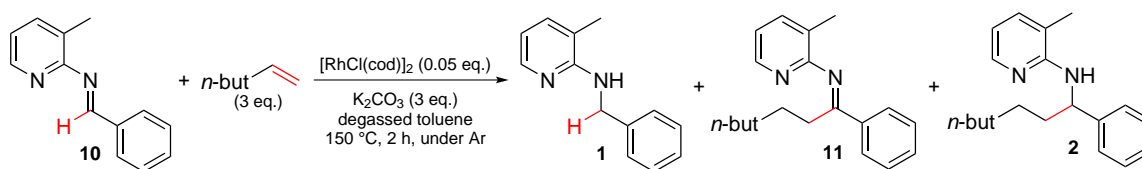


Figure 3.5.: Hypothetical general reaction course of the direct C–H alkylation of benzylic amine **1**.



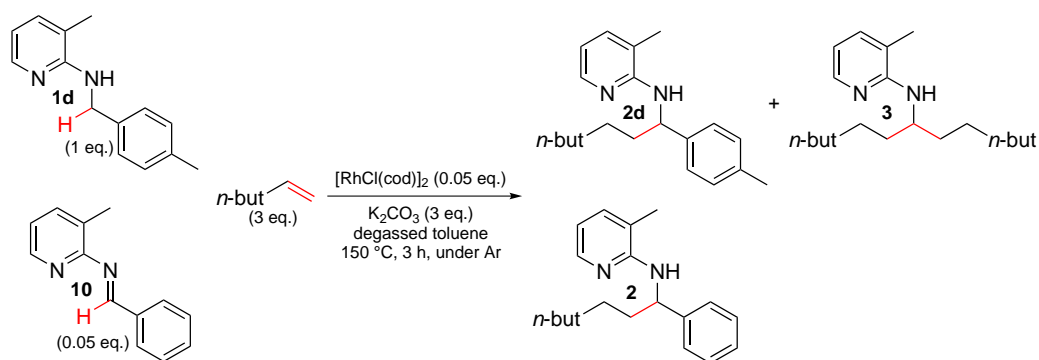
Product Amounts - Experiment 1			
10	1	11	2
25 % ^a	3 % ^b	1 % ^a	0.2 % ^b

^aBased on GC analysis with dodecane as internal standard assuming a conversion factor of 1.

^bGC yield.

Figure 3.6.: Subjecting imine **10** to the reaction conditions instead of amine **1** only leads to low conversion.

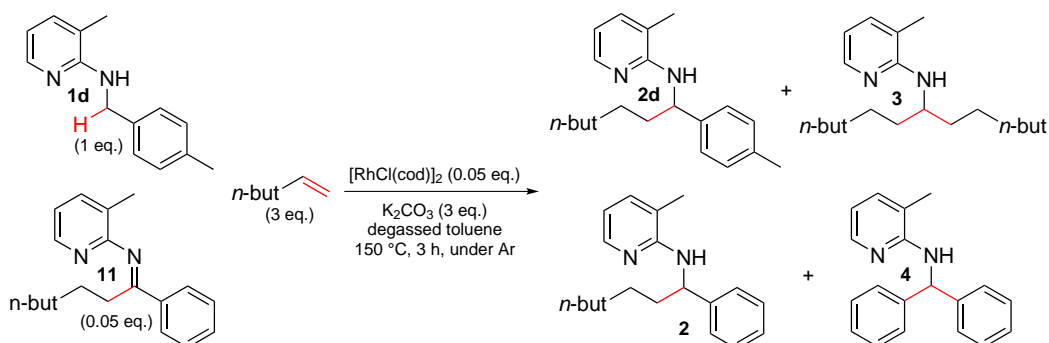
3. Results and Discussion



Product Amounts - Experiment 2					
10	1d	2d	2	3	
<0.1 % ^a	3 % ^a	95 % ^a	5 % ^b	6 % ^b	

^aBased on GC analysis with dodecane as internal standard assuming a conversion factor of 1.
^bGC yield.

Figure 3.7.: Crossover experiment investigating whether imine **10** is converted to the corresponding products of the direct C–H alkylation using hex-1-ene together with benzylic amine **1d**.



Product Amounts - Experiment 3					
11	1d	2d	2	3	4
<0.1 % ^a	4 % ^a	99 % ^a	2 % ^b	6 % ^b	1 % ^b

^aBased on GC analysis with dodecane as internal standard assuming a conversion factor of 1.
^bGC yield.

Figure 3.8.: Crossover experiment investigating whether imine **11** is converted to the corresponding products of the direct C–H alkylation using hex-1-ene together with benzylic amine **1d**.

3. Results and Discussion

same amine **1d** was reacted in presence of alkylated imine **11**. Full consumption of **11** was observed and it was converted to products **2** (2%), **4** (1%) and **3** (1%) with a total recovery of 80% (4% found from 5% used). These results show that both imine **10** and alkylated imine **11** are transformed to the corresponding amine products under the reaction conditions.

3.1.1.6. Imine Intermediate Kinetics

All previous experiments are in agreement with a reaction mechanism proceeding via the imines **10** and **11**. Still, a reaction mechanism where the alkylation takes place at the amine and the imines are formed in off-cycle reactions cannot be excluded yet. All three mechanistic scenarios depicted in Figure 3.9 are possible. Either imines **10** and **11** are formed as off-cycle products from **1** and **2**, respectively (Figure 3.9, Scenario 1) or the reaction mechanism is proceeding through imines **10** and **11** as intermediates with the alkylation taking place at the imine (Figure 3.9, Scenario 2). Scenario 3 is a combination of those two cases where both pathways occur at a similar rate.

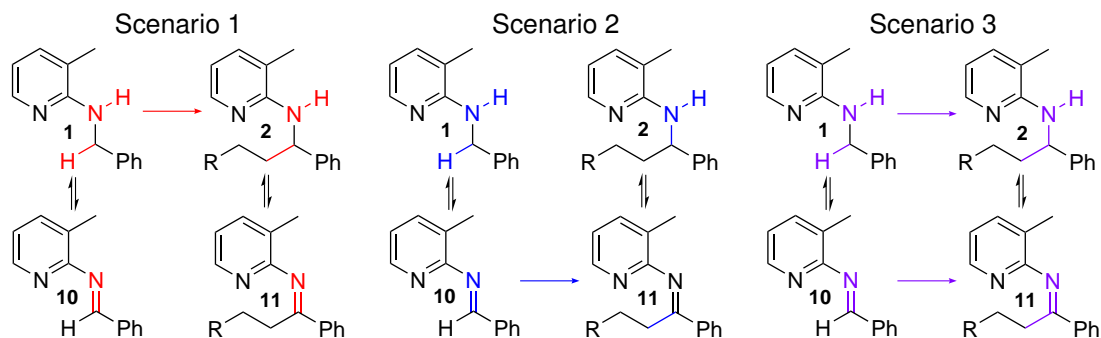


Figure 3.9.: Possible mechanistic scenarios for the direct C–H alkylation of benzylic amine **1** using alkenes. Schemes are not fully stoichiometrically balanced for simplicity.

To distinguish between scenarios 1 and 2 a method was developed based on simplified kinetic models. Since compounds **11** and **2** are interconvertible, the change of the ratio of these two compounds over time can deliver the desired information. If the ratio of the concentrations of **11** and **2** was decreasing over time in an initial reaction period it would mean that **11** is formed before **2** in the course of the reaction, supporting the imine mechanism. If the same ratio was increasing the opposite would be true. Similar methods to investigate reaction mechanisms are readily employed in the determination of biochemical reaction mechanisms.⁵⁵ The complete mathematical background of this method is given in Chapter 5 in order to keep the chemical discussion here concise. However, it is also shown there that

3. Results and Discussion

experimentally the third mechanistic scenario is very hard if not impossible to exclude by this method. The ratio of imine **11** to amine **2** over time was derived from the kinetic profile data using K_2CO_3 in stoichiometric amounts (cf. Figure 3.10).

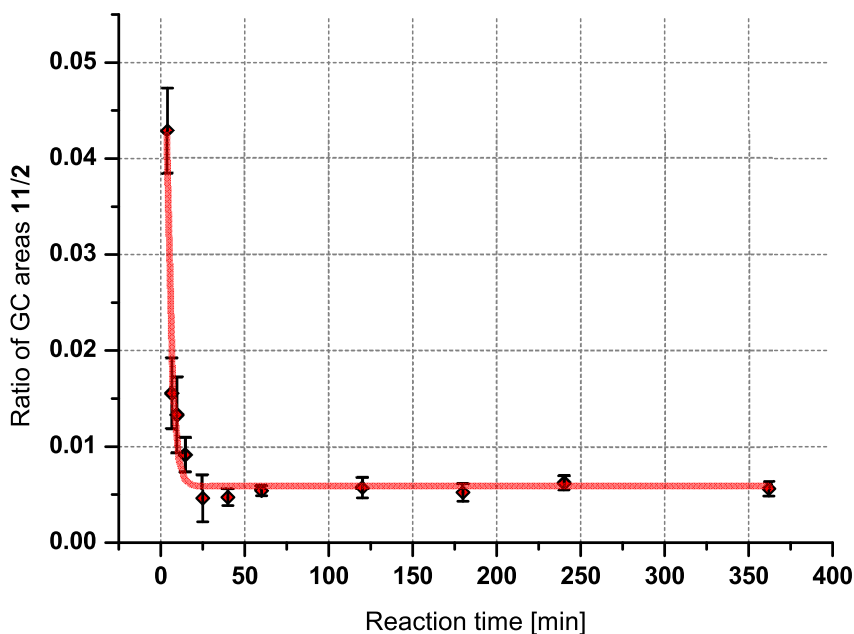


Figure 3.10.: Time course of the ratio of the GC areas under the peaks of imine **11** and amine **2**.

The decreasing ratio of imine **11** to amine **2** over time is in accordance to mechanistic scenario 2 (cf. Figure 3.9) where the alkylation occurs at the imine and not at the amine and excludes scenario 1. However, as already mentioned, mechanistic scenario 3, where both pathways occur at a similar rate at the same time, cannot be excluded. Since mechanistic scenario 2 is the significantly simpler explanation for all observations it is preferred over scenario 3. Either way the reaction would proceed (at least to a significant extent) over the corresponding imines **10** and **11** in the catalytic cycle.

3.1.1.7. Mechanistic Proposal

On the basis of the experimental results presented above the following general mechanistic outline for the direct C–H alkylation using alkenes is proposed (cf. Figure 3.11).

The catalytic cycle starts with coordination of **1** to a Rh-species (**I** in Figure 3.11) to form species **II**. Then, this amine-complex **II** is reversibly interconverted to the corresponding imine-complex **III** which is supported by the H–D exchange observed in unreacted **1** in the KIE studies of the benzylic C–H bond. It should be

3. Results and Discussion

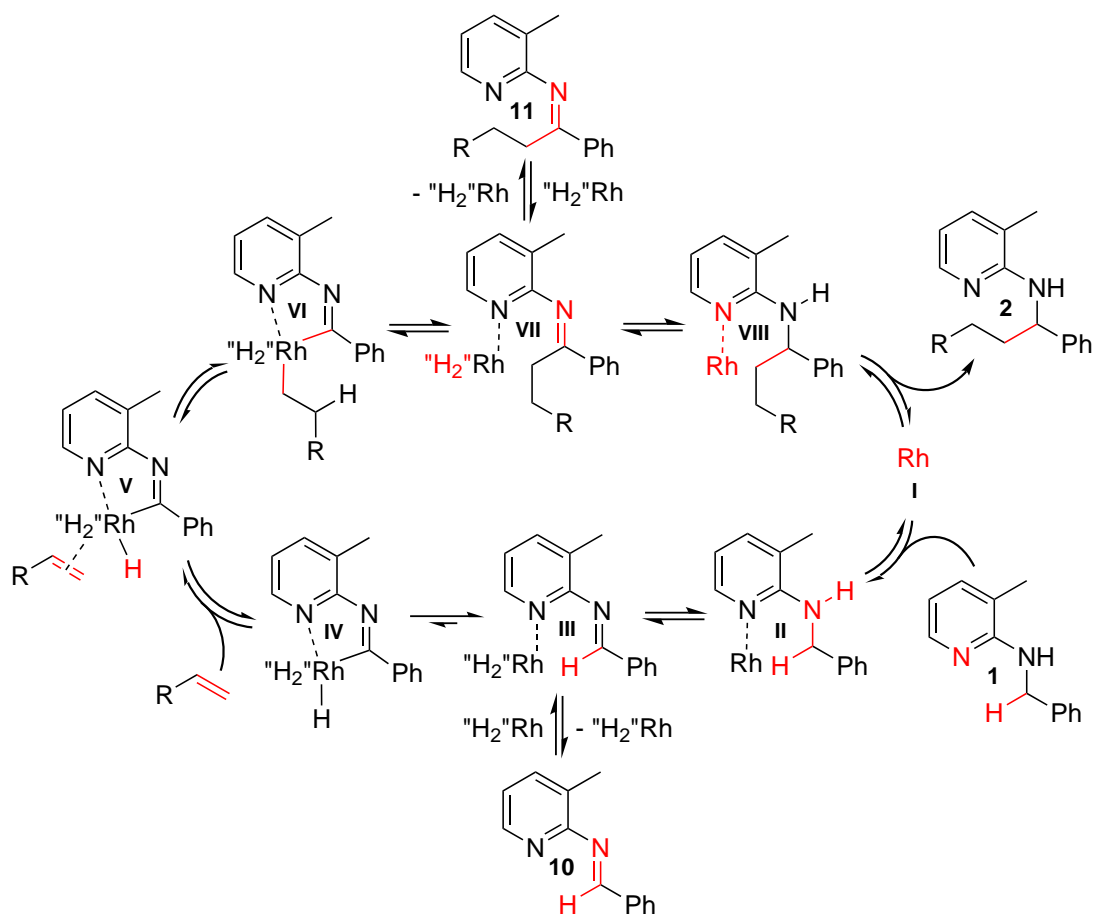


Figure 3.11.: Mechanistic proposal for the direct C–H alkylation of benzylic amines using alkenes. The turnover-limiting step is indicated by a significantly shorter forward reaction arrow. "H₂" emphasizes that it is not known how the two hydrogen atoms are bonded to the catalyst.

3. Results and Discussion

noted that this interconversion is simplified here and it is not expected to be a single step elementary reaction. Imine **10** can then be released from this complex (it can be detected in the reaction mixture) or it reacts in the turnover-limiting oxidative addition into the sp^2 -hybridised C–H bond to form a cyclometalated intermediate **IV** which is supported by the large KIE of about 4–5 observed for the benzylic C–H bond. Then, coordination of alkene to the Rh-centre is depicted in the proposed mechanistic outline (cf. Figure 3.11, Intermediate **V**). However, it should be noted that the alkene coordination may already take place at an earlier stage. This is only the latest stage when it has to occur. The insertion of the alkene into the Rh–H bond follows to form **VI** and reductive elimination yields a Rh-complex **VII** of the alkylated imine **11**. This imine can now be reversibly released (it can be detected in the reaction mixture) or it is converted to the alkylated amine coordinated to Rh (cf. Figure 3.11, Intermediate **VIII**), and the alkylated amine is released as the main product of the reaction. Again, the imine to amine interconversion is depicted only very simplified as before. Since the whole reaction is shown to be in principle reversible under the reaction conditions all mechanistic steps are also depicted to be reversible.

It should be noted that additional ligands coordinated to Rh were omitted since nothing is known about them on the basis of the performed experiments. In addition, it is not known how the two hydrogen atoms are bonded to the catalyst. If they were bonded directly to Rh the oxidative addition into the $C(sp^2)$ –H bond of the imine would result in a Rh(V) species which is not very common in literature but was reported on previous occasions, although on different complex systems.^{56–63} Alternatively, the interconversion of amine and imine could also proceed by transfer hydrogenations with a ligand on Rh. Transfer hydrogenations employing Rh-catalysis are quite common in literature.^{64–68}

Altogether, there are several important issues that remain open in this mechanistic investigation. First, almost nothing is known about the intermediate Rh-species involved in the catalytic cycle. Second the mechanism of the amine to imine interconversion is not known either. The last major unresolved issue is how the exchange between H and Ph in the interconversions of **2** and by-products **3** and **4** actually occurs. These points certainly need to be addressed in further studies in order to get more insight into the reaction mechanism.

3.1.2. Investigations into the Kinetic Modelling

The second aspect of the direct alkylation using alkenes that was investigated intensively were the kinetic characteristics of this reaction in order to make a detailed kinetic model of the reaction and to find out how the reaction rate is affected by temperature and electronic properties and in that way gain further mechanistic insight into the reaction.

3. Results and Discussion

3.1.2.1. Initial Rate Experiments

As mentioned before, the method of initial rates had been applied to determine the partial reaction orders with respect to all starting materials in the direct alkylation using alkenes already in a previous work.³⁵ However, for both K_2CO_3 and $[RhCl(cod)]_2$ the dependences showed changes in the partial reaction orders and the kinetic picture had not been fully revealed. Therefore, the old results are also included in this thesis together with new results in order to provide a complete picture with respect to the partial reaction orders of all the starting materials and all the data points can be found in the Appendices. The corresponding results are presented in Figure 3.12.

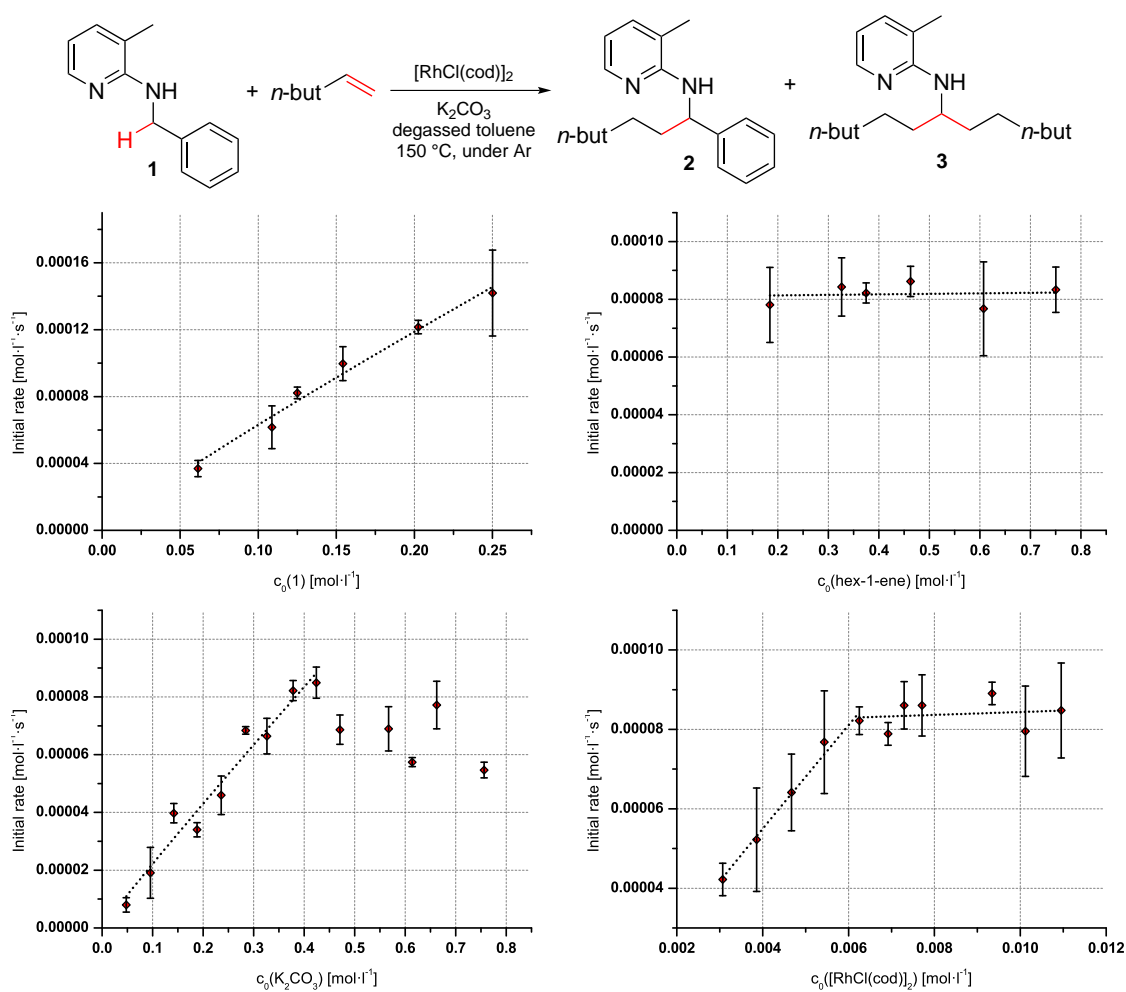


Figure 3.12.: Determination of the partial reaction orders for the direct C–H alkylation of **1** using hex-1-ene applying the method of initial rates.

From the results in Figure 3.12 the partial reaction orders with respect to both

3. Results and Discussion

1 and hex-1-ene over the whole concentration region investigated can easily be identified as 1 and 0, respectively. However, for K_2CO_3 and $[RhCl(cod)]_2$ there are changes in the partial reaction orders observed. The concentrations of both the Rh-catalyst and K_2CO_3 which were used for the determination of the kinetic profile are exactly at the transition between two partial reaction orders. At lower concentrations partial reaction orders of 1 are observed in both cases. Increasing the concentration of K_2CO_3 leads to no increase in the initial rate. Actually, a slight decrease is observed for higher K_2CO_3 concentrations. However, since the variability is rather high in that region the corresponding partial reaction order could not be determined reliably. Therefore, the partial reaction order with respect to K_2CO_3 at higher concentrations is assumed to be 0 (or at least near 0). In the case of $[RhCl(cod)]_2$ at high concentrations no decrease in the initial rate is observed and the partial reaction order is 0. It should be noted that from the dependence of the initial rate on the K_2CO_3 concentration it could be hypothesised that the phase transfer of K_2CO_3 is rate-limiting. However, since increasing the concentration of **1** up to a factor of 2 results in about a doubled initial rate even though the amount of K_2CO_3 is already in its 0th order region this can be excluded.

Since the common data point of all 4 experimental series is for both K_2CO_3 and $[RhCl(cod)]_2$ exactly at the transition between two partial reaction orders the empirical rate law cannot be directly deduced. There is either a change from an overall reaction order of 3 to 1 (Case 2, vide infra) or a change between two distinct rate laws having an overall reaction order of 2 (Case 1, vide infra). These two cases can be distinguished with a single experiment. Increasing the concentrations of both K_2CO_3 and $[RhCl(cod)]_2$ above those used in the standard experiment (i.e. $0.38 \text{ mol l}^{-1} K_2CO_3$ and $0.0063 \text{ mol l}^{-1} [RhCl(cod)]_2$) should lead to no increase in initial rate if a change in the overall reaction order from 3 to 1 occurs since the corresponding rate law would change from Equation 3.3 to Equation 3.4 in this case. If an increase in initial rate was observed, this would support a change between two rate laws having an overall reaction order of 2 (cf. Equations 3.1 and 3.2). However, it could not be unequivocally deduced which of the two equations (3.1 or 3.2) would be the rate limiting under the conditions of this experiment. Since in the corresponding experiment no increase in initial reaction rate was observed case 1 can be unequivocally excluded.

Case 1:

$$r_0 = k_{2,exp a} c_0(\mathbf{1}) c_0(K_2CO_3) \quad (3.1)$$

$$r_0 = k_{2,exp b} c_0(\mathbf{1}) c_0([RhCl(cod)]_2) \quad (3.2)$$

Case 2:

$$r_0 = k_{3,exp} c_0(\mathbf{1}) c_0([RhCl(cod)]_2) c_0(K_2CO_3) \quad (3.3)$$

$$r_0 = k_{1,exp} c_0(\mathbf{1}) \quad (3.4)$$

r_0 ... Initial reaction rate [$\text{mol l}^{-1} \text{ s}^{-1}$]

3. Results and Discussion

$k_{n,exp\ x}$... Empirical rate constant for an overall n^{th} reaction order^c [$\text{mol}^{1-n} \text{l}^{n-1} \text{s}^{-1}$]
 $c_0(X)$... Initial concentration of compound X [mol l^{-1}]

It was still unclear whether the observed plateaus in the initial rate dependences with respect to both K_2CO_3 and $[\text{RhCl}(\text{cod})]_2$ were independent from one another or not since neither of the two concentrations appear in the rate law in equation 3.4. In order to answer this question starting from a data point (cf. Figure 3.12, top left graph, the numerical value can be found in the Appendices) with a lower initial K_2CO_3 loading of 0.23 mol l^{-1} compared to 0.38 mol l^{-1} used in the standard experiment the concentration of $[\text{RhCl}(\text{cod})]_2$ was increased significantly ($0.0094 \text{ mol l}^{-1}$ as compared to $0.0063 \text{ mol l}^{-1}$ in the standard experiment). If the observed initial rate significantly increased in this experiment (compared to the experiment with an initial K_2CO_3 loading of 0.23 mol l^{-1} and an initial $[\text{RhCl}(\text{cod})]_2$ concentration of $0.0063 \text{ mol l}^{-1}$), the borderline concentration of $[\text{RhCl}(\text{cod})]_2$ would depend on the initial K_2CO_3 loading. If the observed initial rate did not change in this experiment, this would show that the borderline concentration of $[\text{RhCl}(\text{cod})]_2$ would be independent from the initial K_2CO_3 loading and hence the respective borderline concentrations of both K_2CO_3 and $[\text{RhCl}(\text{cod})]_2$ would not be mutually dependent. It was found that the initial reaction rate did not change in this additional experiment which is in accordance to the observed borderline concentrations not being mutually dependent.

The empirical rate law depending on the corresponding initial concentrations of K_2CO_3 and $[\text{RhCl}(\text{cod})]_2$ the reaction is performed can then be formulated as follows.

a) $c(\text{K}_2\text{CO}_3) < 0.38 \text{ mol l}^{-1}$ and $c([\text{RhCl}(\text{cod})]_2) < 0.0063 \text{ mol l}^{-1}$:

$$r_0 = k_{3,exp} c_0(\mathbf{1}) c_0([\text{RhCl}(\text{cod})]_2) c_0(\text{K}_2\text{CO}_3) \quad (3.5)$$

b) $c(\text{K}_2\text{CO}_3) \geq 0.38 \text{ mol l}^{-1}$ and $c([\text{RhCl}(\text{cod})]_2) < 0.0063 \text{ mol l}^{-1}$:

$$r_0 = k_{2,exp\ a} c_0(\mathbf{1}) c_0([\text{RhCl}(\text{cod})]_2) \quad (3.6)$$

c) $c(\text{K}_2\text{CO}_3) < 0.38 \text{ mol l}^{-1}$ and $c([\text{RhCl}(\text{cod})]_2) \geq 0.0063 \text{ mol l}^{-1}$:

$$r_0 = k_{2,exp\ b} c_0(\mathbf{1}) c_0(\text{K}_2\text{CO}_3) \quad (3.7)$$

d) $c(\text{K}_2\text{CO}_3) \geq 0.38 \text{ mol l}^{-1}$ and $c([\text{RhCl}(\text{cod})]_2) \geq 0.0063 \text{ mol l}^{-1}$:

$$r_0 = k_{1,exp} c_0(\mathbf{1}) \quad (3.8)$$

^cIn case of two or more different empirical rate constants of same overall reaction order x is used to distinguish between them.

3. Results and Discussion

A change in the overall reaction order could in general be explained by a change in the turnover-limiting step. However, a turnover-limiting step not involving any Rh-species is not very likely in this Rh-catalysed reaction. It should be emphasized that in this section the rate law was determined and interpreted solely from an empirical point of view and on the basis of the results presented so far the kinetic picture with respect to both K_2CO_3 and $[\text{RhCl}(\text{cod})]_2$ is still not clear.

3.1.2.2. K_2CO_3 Studies

In addition to the empirical rate law a very pronounced dependence of the initial rate on the adsorbed water content of K_2CO_3 was found, which is depicted in Figure 3.13 (dry toluene was used as solvent in these experiments). The higher the content of adsorbed water in the base, the higher was the initial reaction rate observed. This suggests that, in general, the presence of water speeds up the reaction. However, in experiments where toluene saturated with water at room temperature^d was used together with K_2CO_3 batches with 0, 2 or 15 m% adsorbed water, respectively, the initial reaction rate significantly dropped in each case. Actually, the observed initial reaction rates for all these three experiments were even lower compared to the experiment with completely dry K_2CO_3 and dry toluene, which showed the slowest reaction up to that point. It should be noted that the total amount of water dissolved in toluene saturated with water at 25 °C is about one order of magnitude lower than the amount of water introduced by the K_2CO_3 batches used. These observations clearly show that it is crucial that the water originates from K_2CO_3 . The difference between using adsorbed water and water already dissolved in toluene is that in the latter case the water is already present in solution from the beginning but in the former case a certain degree of heating is necessary to release it. Therefore, it is hypothesised, that the water present in solution from the very beginning may irreversibly react with the Rh-species in solution and deactivate the catalyst.

The presence of water being beneficial for C–H activation reactions (not including reactions employing water as solvent) is already known in some cases in literature.^{70–73} However, there has previously been no report on using a base effectively insoluble in the reaction solvent with superficially adsorbed water to increase the reaction rate. It was hypothesised that the water introduced into the reaction is partially dissolved into toluene when the reaction mixture is heated and as a consequence increases the solubility of K_2CO_3 in the reaction mixture which then results in an increased reaction rate. However, it could also influence other steps of the reaction.

In a further experiment it was investigated whether the water introduced by K_2CO_3 needs to be superficially adsorbed to increase the initial reaction rate or

^dThe water content in toluene saturated with H_2O at room temperature was determined to be about 500 ppm using Karl Fischer titration, which is in accordance to literature values at 30 °C.⁶⁹

3. Results and Discussion

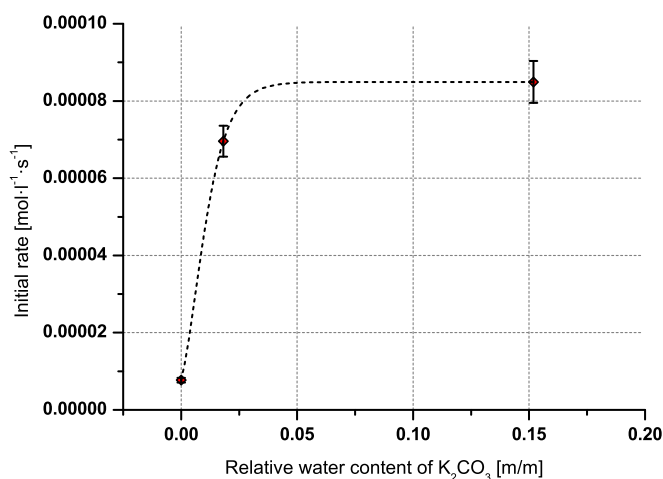


Figure 3.13.: Dependence of the initial reaction rate on the adsorbed water content of K_2CO_3 for the direct C–H alkylation of **1** using hex-1-ene.

K_2CO_3 with crystal water could also be used. Therefore, the reaction was carried out using $K_2CO_3 \cdot 1.5H_2O$ and a significantly lower initial rate compared to K_2CO_3 with a similar adsorbed water content. However, it was suspected that the reason for this result could also be the bigger particle size and the concomitant lower specific surface area of the sesquihydrate used. Therefore, the same experiment was repeated with comminuted $K_2CO_3 \cdot 1.5H_2O$ and a significant increase in the initial rate compared to the previous experiment was observed. However, the initial rate was still lower compared to the K_2CO_3 batches with superficially adsorbed water. So, it was decided to determine both the particle size distributions and the specific surface areas of all the K_2CO_3 batches used and observed a significant dependence of the initial rate of the reaction on the specific surface area of the base used. In the following two diagrams (Figure 3.14) the initial rates of the two experiments using $K_2CO_3 \cdot 1.5H_2O$ together with the initial rate using a base with a similar total water content of about 15 m% are shown as a function of the respective particle sizes and the respective specific surface areas. More details about the obtained particle size distributions and the adsorption isotherms are found in Chapter 5. It should be noted that since all the K_2CO_3 batches had a very low specific surface area the precision of the BET adsorption measurements was not very high. However, repetitive measurements with the lowest specific surface area batches showed that the relative error over several measurements did not exceed 10 %.

Several things should be noted at this point. The particle size of the batch with an adsorbed water content of about 15 m% is only slightly smaller compared to the comminuted $K_2CO_3 \cdot 1.5H_2O$ and the corresponding particle size distributions and distribution densities are also very similar (Details are given in Chapter 5). However, the initial reaction rates are significantly different. The big difference is better

3. Results and Discussion

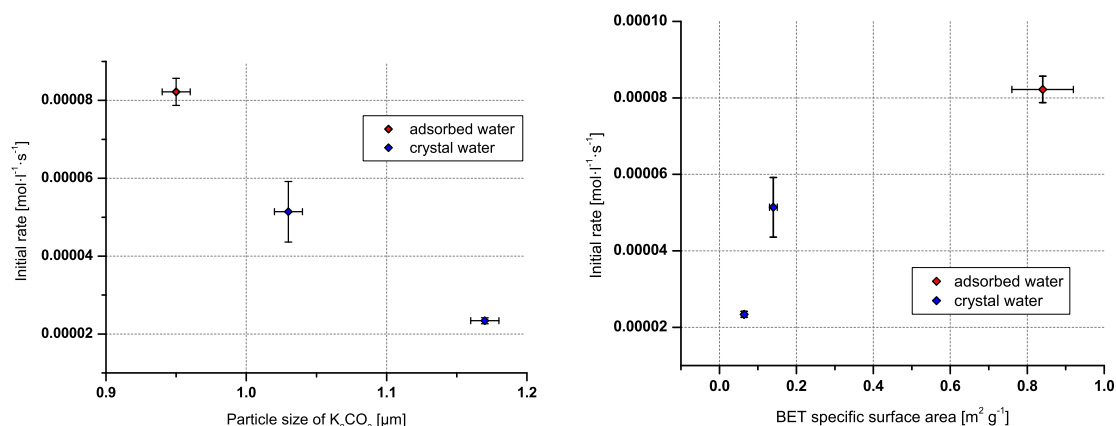


Figure 3.14.: Dependences of the initial reaction rate on the particle size and the BET specific surface area of K₂CO₃ for the direct C–H alkylation of **1** using hex-1-ene. Particle sizes given in this diagram are the medians determined from the respective particle size distribution densities.

understood on the basis of the BET specific surface areas. The K₂CO₃ batch with an adsorbed water content of about 15 m% has a significantly higher specific surface area compared to all the other batches although the particle size of the batch with an adsorbed water content of about 15 m% is significantly bigger compared to the batch with 2 m%. In addition, neither the particle size nor the specific surface area of the batch with 2 m% of adsorbed water did change when it was dried so the significantly lower initial rate with the dried base was not due to changes of the surface area during the drying process. On the basis of this data it cannot be unequivocally concluded whether it makes a difference if the water introduced with the base is adsorbed or crystal water. However, the significant difference in the specific surface areas between the batch with 15 m% of adsorbed water and the K₂CO₃ · 1.5 H₂O batches used could solely explain the big difference in the initial reaction rates that is observed. Therefore, it is hypothesised that K₂CO₃ · 1.5 H₂O with the same specific surface area would show, more or less, the same initial reaction rate as compared to the batch with 15 m% adsorbed water and hence it is expected that it does not matter whether the water introduced is superficially adsorbed or water of crystallisation.

Since K₂CO₃ is nearly insoluble in toluene^e and the reaction is therefore heterogeneous it will interact with other (dissolved) reactants or the solvent at its surface. This dependence can either be explained by the dissolution and phase transfer of K₂CO₃ to the reaction solvent or the transfer of the other reagents to the surface of K₂CO₃ having an influence on the overall reaction rate. In either case, the higher

^eThere has not yet been any report about the actual solubility of K₂CO₃ in toluene. In general, it is considered to be insoluble.

3. Results and Discussion

the specific surface of the K_2CO_3 batch used the faster the reaction is expected to occur. This explains the observed dependence of the initial reaction rate on the specific surface area of the base used.

It was also tested whether stirring has an influence on the initial reaction rate. Comparing the initial rates of experiments without stirring to the experiments with stirring showed that agitation increased the initial rate. From the results of the initial rate experiments without stirring so called stirring factors (abbreviated as SF, cf. Equations 3.9 and 3.10) were determined as ratios of the initial rates with stirring and without. The corresponding content of adsorbed water and the specific surface area of the K_2CO_3 batch used is given in brackets.

$$SF(2 \text{ m\% } H_2O, 0.4 \text{ m}^2\text{g}^{-1}) = 6 \pm 2 \quad (3.9)$$

$$SF(15 \text{ m\% } H_2O, 0.8 \text{ m}^2\text{g}^{-1}) = 1.7 \pm 0.2 \quad (3.10)$$

Interestingly, using K_2CO_3 with about 2 m% of adsorbed water and a lower specific surface area (i.e. $0.4 \text{ m}^2\text{g}^{-1}$) resulted in a much higher dependence on stirring (about 6 times faster with stirring) as was observed in experiments using K_2CO_3 with about 15 m% of adsorbed water and a higher specific surface area (i.e. $0.8 \text{ m}^2\text{g}^{-1}$, about 2 times faster with stirring). This experiment indicates that the reaction could be diffusion-controlled or diffusion-influenced.⁷⁴ It is not uncommon for a heterogeneous reaction that agitation significantly influences the reaction rate since transport problems are playing a major role as compared to homogeneous reactions.⁷⁵ However, even if this experiment shows an influence of stirring on the reaction rate the diffusion of reactants does not need to be rate-determining or turnover-limiting. In fact, it could be excluded that the diffusion of K_2CO_3 was turnover-limiting since experiments with double the amount of **1** showed also doubled initial rate without stirring.

Since the reaction is heterogeneous it is hypothesised that either the phase transfer of K_2CO_3 to the liquid phase or the phase transfer of a Rh-species in solution to the surface of K_2CO_3 has a major influence on the reaction rate which is also supported by the dependence on the particle size and surface area of K_2CO_3 . The reaction of K_2CO_3 and the Rh-catalyst could control the concentration of a Rh-carbonate species in solution which then catalyses the reaction and therefore has an influence on the overall reaction rate.

3.1.2.3. Induction Time Studies

On the basis of the previous results the role of K_2CO_3 is not clear. It was hypothesised that K_2CO_3 could serve as a heterogeneous catalyst for the reaction with the reaction taking place on the surface of K_2CO_3 . Alternatively, K_2CO_3 is dissolved to a very low extent and the dissolved K_2CO_3 then reacts with $[RhCl(cod)]_2$ to form the catalytically active species. In order answer this question the following experiments were designed (cf. Table 3.3, Entry 1). In the first experiment all the

3. Results and Discussion

starting materials of the direct alkylation were reacted for 10 min in the presence of dodecane as internal standard. The reaction was stopped and filtrated. The solid residue was reacted with **1** and hex-1-ene again, the filtrate was reacted as obtained after the filtration. In the filtrate the reaction continued at an even faster rate than before, the solid residue did not show any considerable catalytic activity. On the basis of this result additional experiments were performed where not all starting materials except $[\text{RhCl}(\text{cod})]_2$ and K_2CO_3 were heated together in the first 10 min. The results are summarised in Table 3.3.

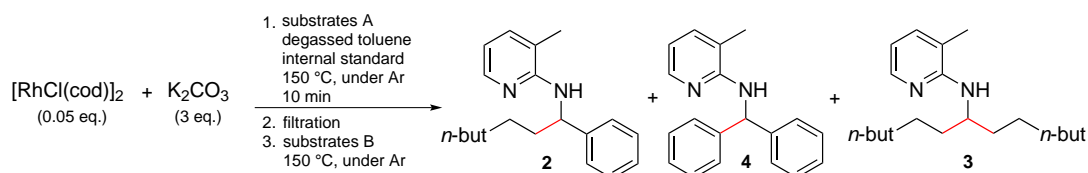


Table 3.3.: Results of the induction time studies of the direct alkylation using alkenes.

Entry	Substrates A	Substrates B	Rate ^a [10 ⁻⁵ mol l ⁻¹ s ⁻¹]	Compound Amounts ^b			
				1	2	3	4
1	1 (1 eq.) hex-1-ene (3 eq.)	-	20.3 ± 1.5	24 %	37 %	1.9 %	1.1 %
2	-	1 (1 eq.) hex-1-ene (3 eq.)	18.5 ± 1.1	15 %	67 %	4.6 %	1.7 %
3	1 (1 eq.) hex-1-ene (3 eq.)	hex-1-ene (3 eq.)	18.2 ± 0.5	17 %	43 %	3.6 %	0.7 %
4	hex-1-ene (3 eq.)	1 (1 eq.)	19.0 ± 0.8	7.0 %	68 %	3.5 %	2.2 %

^aAfter filtration of the reaction mixture in a time period of 6.61 min. Errors are determined over 3 GC measurements.

^bCalibrated GC-Yields determined after 2.05 h of reaction after filtration of the reaction mixture.

This experiment series is strong evidence against the hypothesis that K_2CO_3 could be a heterogeneous catalyst in this reaction because the reaction continued at an even faster rate than the reaction shows under the optimised reaction conditions in the initial reaction period [(19.0 ± 1.9) 10⁻⁵mol l⁻¹ s⁻¹ compared to (8.2 ± 0.3) 10⁻⁵mol l⁻¹ s⁻¹] after excess K_2CO_3 was removed by filtration and considerable catalytic activity was observed in all experiments. The experiments from entries 1 and 3 in Table 3.3, respectively, did not show comparable conversion to the reaction products than observed with stoichiometric amounts of K_2CO_3 after about 2 h of reaction time (cf. Kinetic Profile with K_2CO_3 in Stoichiometric Amounts) but since only single experiments were performed, it is not clear whether these results are significant. The experiments from entries 2 and 4 in Table 3.3, respectively, did show comparable conversion, although not full conversion. In addition, the amount of sideproducts **3** and **4** formed after filtration is lower compared to experiments under the optimised reaction conditions without filtration.

3. Results and Discussion

Besides the strong evidence against K_2CO_3 being a heterogeneous catalyst in this reaction these results implicate that K_2CO_3 is only needed in the beginning of the reaction. This suggests that there is an induction period. During this induction period K_2CO_3 reacts with $[RhCl(cod)]_2$ irreversibly to form the catalytically active species which then catalyses the direct alkylation reaction. This induction period should be observed when K_2CO_3 is used in lower amounts.

The significantly higher rate observed after the filtration suggests that excessive amounts of K_2CO_3 result in significant inhibition of the reaction rate. Coordination of additional carbonate ligands could result in catalytically less active or inactive species which could possibly explain this result. However, this needs to be investigated further in additional experiments in order to find more evidence for this hypothesis.

3.1.2.4. Kinetic Profiles

Kinetic Profile with K_2CO_3 in Stoichiometric Amounts The kinetic profile of the direct C–H alkylation using hex-1-ene had previously been determined.³⁵ However, in those experiments the conditions were not the same as compared to the initial rate experiments. Therefore, in order to justify the applicability of the method of initial rates the determination of the kinetic profile was repeated under the same reaction conditions that were used for the initial rate experiments (cf. Figure 3.15).

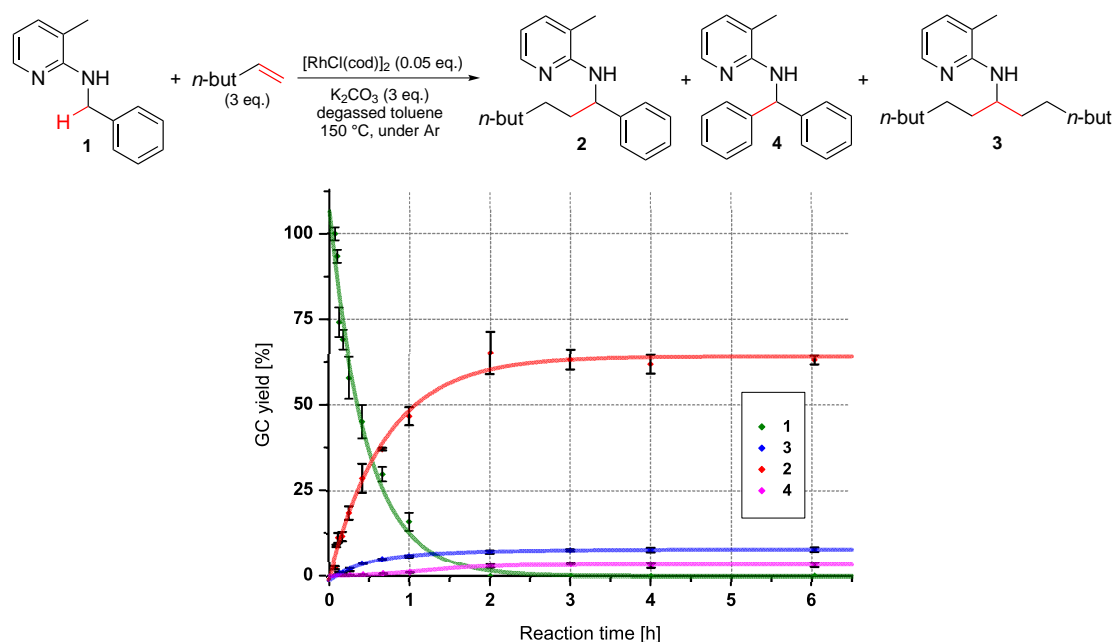


Figure 3.15.: Determination of the kinetic time course of the direct C–H alkylation of benzylic amine **1** using hex-1-ene.

3. Results and Discussion

There are some features to be noted. Firstly, the reaction is finished after 2 h and the amounts of **2**, **3** and **4** remain more or less constant thereafter. This can either be rationalized by inhibition or decomposition of the active catalyst under these conditions or by a reversible reaction between **2**, **3** and **4**. Secondly, both **2** and **3** are formed more or less from the beginning and, even though it was previously shown (*vide supra*) that there is in fact an induction period, it was not observable under these conditions, except for the time the reaction mixture needs to reach a constant temperature.^f This is very important as it allows to easily determine kinetic parameters by using the method of initial rates. It should be noted that for the formation of **4** there is an induction period observed.

Kinetic Profile with K₂CO₃ in Catalytic Amounts On the basis of previous results it should be possible to use K₂CO₃ in catalytic amounts in the reaction because it is not used up during the reaction. This was confirmed in first experiments using only 0.1 eq. K₂CO₃ in the reaction (cf. Figure 3.16). After 3 h only 1 % of **1** was formed. However, after 24 h the reaction was finished (cf. Figure 3.16).

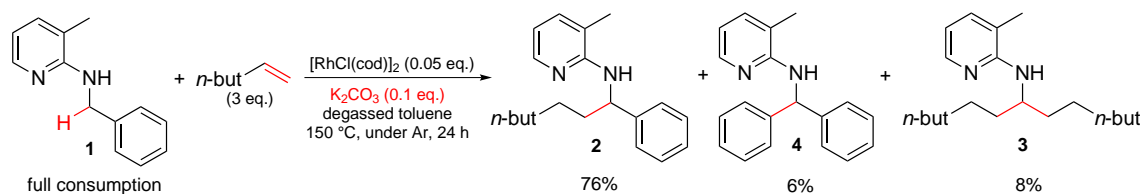


Figure 3.16.: Direct alkylation of **1** with hex-1-ene using K₂CO₃ in catalytic amounts.

These results are already indicative that under these reaction conditions a considerable induction period is observed as was suggested by previous results since after 3 h only 1 % of **1** is observed and then the reaction continues to proceed to full conversion after only 24 h i.e. after only the 8-fold reaction time the 90-fold total amount of reaction products is observed. Therefore, the kinetic profile of the reaction under these conditions was determined. However, this time only one experiment was performed with an internal standard being present in the reaction mixture from the beginning and stopping the reaction for every sample. After the sample was taken the reaction was continued again. The results are shown in Figure 3.17.

There are several points to be noted from this result. First, as predicted on the basis of previous experiments, a considerable induction period of at least 2 h is observed. After the induction period the reaction rate significantly increases until

^fAll consecutive reactions like multiple step catalytic processes have in fact an induction period for the formation of the final product. However, in many cases it is too short to be observed.

3. Results and Discussion

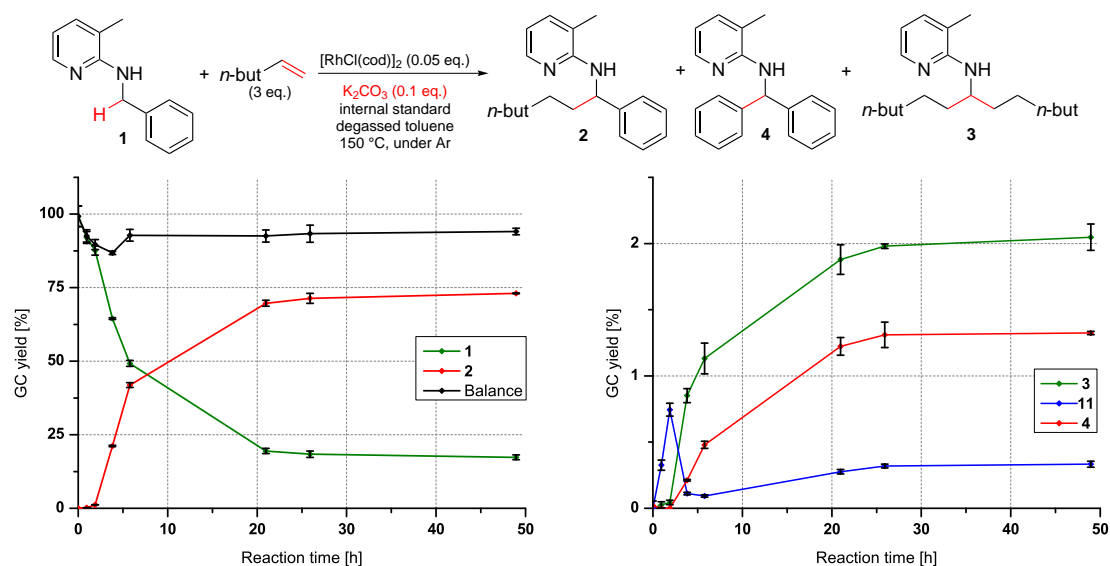


Figure 3.17.: Determination of the kinetic time course of the direct C–H alkylation of benzylic amine **1** with hex-1-ene using K_2CO_3 in catalytic amounts. Data points for the amount of alkylated imine **11** are obtained assuming a conversion factor of 1 and are not calibrated GC-yields.

73 % of **2** are formed while 17 % of **1** remain. So the yield of **2** is higher compared to experiments using K_2CO_3 in stoichiometric amounts besides the conversion being not full. Since this data is derived from one experiment only it is not clear how significant it is that the reaction does not reach full conversion after about 24 h like in the experiment before which was not stopped several times but only stopped and analysed after 24 h. In addition, significantly less of both **3** and **4** are formed under these conditions. Overall, the mass balance is also significantly better (over 90 % compared to about 80 % with stoichiometric K_2CO_3). Figure 3.18 shows the kinetic time course again focussing on the beginning of the reaction.

There are two very interesting features to be noticed from Figures 3.17 and 3.18. First, the mass balance is decreasing to 87 % in the beginning of the reaction and then it increases again quite sharply to about 93 % and stays more or less constant thereafter. This suggests that more of the material is converted into a chemical species which is not detectable by the means of GC analysis applied since no other significant peak is observed in the corresponding chromatograms. This chemical species is most likely a Rh-complex to which a considerable amount of the material is bound. After some time, however, the amount of bound material decreases again which indicates that the concentrations of Rh-complexes bonded to a benzylic amine decreases again and some of the material is released into the reaction mixture again. Second, the time course of **11** is strongly increasing at the beginning, shows a maximum and then decreases again. After reaching

3. Results and Discussion

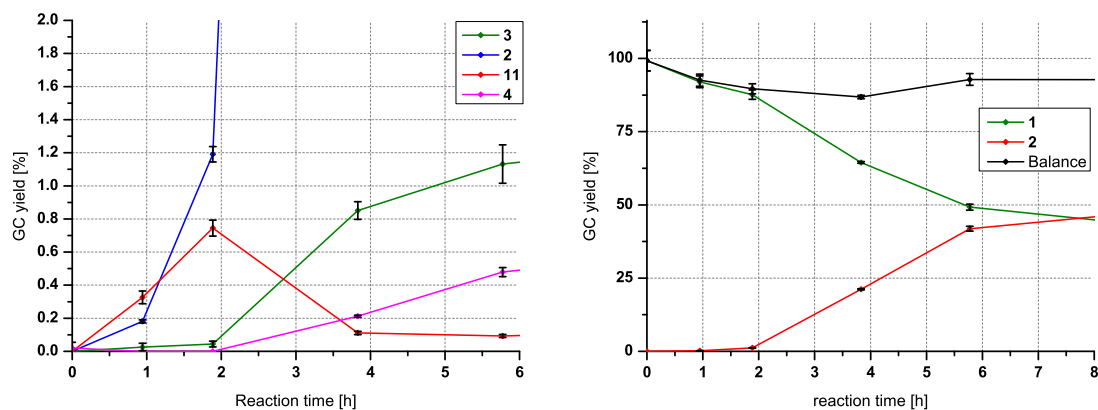


Figure 3.18.: Kinetic time course of the direct C–H alkylation of benzylic amine **1** with hex-1-ene using K_2CO_3 in catalytic amounts at the beginning of the reaction. Data points for the amount of **11** are obtained assuming a conversion factor of 1 and are not calibrated GC-yields.

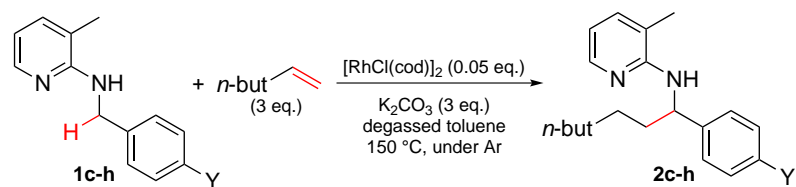
a minimum the amount of **11** is increasing again. This was not observed in the kinetic profile using stoichiometric K_2CO_3 . This suggests that under the conditions present at the very beginning the interconversion of **11** to **2** is slower and then significantly speeds up. From Figure 3.18 it can also be seen that at the very beginning more of the alkylated imine **11** than the alkylated amine **2** is present. This is in complete agreement to the previously established general mechanistic outline of this reaction that the reaction proceeds over the imine. In addition, the ratio of **11** to **2** shows the same general time course that is also observed in the kinetic profile using stoichiometric K_2CO_3 (cf. Figure 5.5).

3.1.2.5. Electronic Influence on Benzylic Amines

Another aspect of interest was the electronic influence of benzylic amines on the reaction. Therefore, a Hammett plot⁷⁶ was constructed from the initial rates of several benzylic amines **1c-h** (cf. Figure 3.19). The obtained initial rates were compared to the initial rate of the unsubstituted starting material **1**. Since the initial rates were determined by 1H -NMR analysis in these experiments the formation of by-product **3** could not be detected and quantified and was therefore not taken into account.

The reaction constant of -1.6 ± 0.2 indicates that the reaction is accelerated by electron-donating groups on the benzylic amine. This is in accordance to oxidative addition into the C–H bond being turnover-limiting as is also suggested by the KIE studies discussed earlier (vide supra). However, since the value of ρ is influenced by all steps prior to the turnover-limiting step the benzylic amine is involved in the reaction as well, the reaction constant ρ can only be interpreted on the basis of

3. Results and Discussion



Compound	Y
1c	OMe
1d	Me
1e	F
1f	Cl
1g	CO ₂ Me
1h	CF ₃

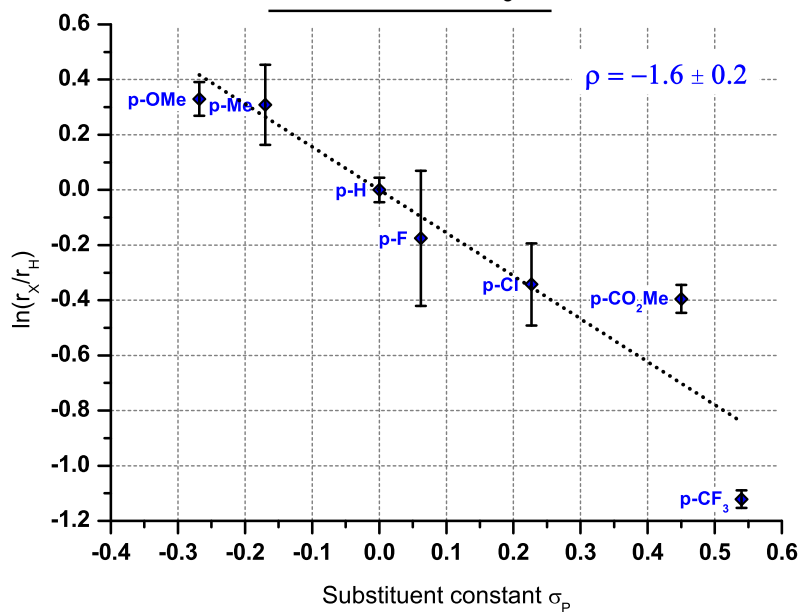


Figure 3.19.: Determination of the electronic influence of substituents in the benzyl group of benzylic amines on the reaction rate in the direct C–H alkylation using hex-1-ene.

3. Results and Discussion

a kinetic model of the reaction. A more detailed discussion and interpretation is given later (*vide infra*).

3.1.2.6. Temperature Dependence of the Initial Rate

It was also of interest to determine the temperature dependence of the reaction rate and hence the activation parameters of the reaction. In order to determine them the initial reaction rate at different temperatures was measured and the corresponding rate constants were derived. The activation parameters were then calculated on the basis of the Eyring equation.⁷⁷ The enthalpy of activation ΔH^\ddagger was found to be $(148.8 \pm 0.7) \text{ kJ mol}^{-1}$ or $(35.6 \pm 0.2) \text{ kcal mol}^{-1}$ and the entropy of activation ΔS^\ddagger was determined as $(81.4 \pm 1.4) \text{ J mol}^{-1} \text{ K}^{-1}$ or $(19.5 \pm 0.3) \text{ eu}$ based on the second order rate law. It should be noted that the high ΔH^\ddagger is the reason for the high temperature dependence of the reaction rate. In addition, the relatively large positive entropy of activation indicates that a significant degree of disorder has to be created prior to or in the turnover-limiting step. However, since this is a multi-step reaction and the turnover-limiting step is certainly not the first one an accurate interpretation is very difficult and can only be made on the basis of a kinetic model. Therefore, this is discussed together with the kinetic model later (*vide infra*).

3.1.2.7. Kinetic Modelling and Mechanistic Consequences

On the basis of all the experimental results for the direct alkylation using alkenes the following kinetic model is proposed (*cf.* Figure 3.20).

In general, this kinetic model is very vague with respect to the ligands on Rh because almost nothing is known on the basis of the experiments performed. There are two parts of this kinetic model, the reaction of K_2CO_3 and a Rh-species in solution, denoted as [Rh], to form the catalytically active species, denoted formally as $[\text{RhCO}_3]$, and the catalytic cycle for the direct alkylation of **1** using hex-1-ene to form the corresponding alkylated product **2**. In the reaction of K_2CO_3 and a Rh-species $\text{K}_2\text{CO}_3(\text{s})$ is proposed to be dissolved into the reaction mixture to a very small extent since K_2CO_3 is almost insoluble in toluene.⁹ The very small dissolved portion $\text{K}_2\text{CO}_3(\text{sol})$ immediately reacts irreversibly with [Rh], an unspecified Rh-species present in solution which is (formally) derived from the $[\text{RhCl}(\text{cod})_2]$ complex used as catalyst precursor in this reaction, to form the catalytically active $[\text{RhCO}_3]$. This reaction is also the reason for the induction period. As long as the reaction between [Rh] and $\text{K}_2\text{CO}_3(\text{sol})$ is not finished, the concentration of catalytically active $[\text{RhCO}_3]$ is increasing over time and therefore an increasing overall reaction rate is observed. In the simplified catalytic cycle $[\text{RhCO}_3]$ is assumed to be in equilibrium with both $[\text{Rh}\cdot\mathbf{1}\cdot\text{CO}_3]$ and $[\text{Rh}-\mathbf{1}\cdot\text{CO}_3]$. However, $[\text{RhCO}_3]$ is proposed to be the resting state and the concentrations of both $[\text{Rh}\cdot\mathbf{1}\cdot\text{CO}_3]$ and

⁹There is no literature report about the actual solubility of K_2CO_3 in toluene.

3. Results and Discussion

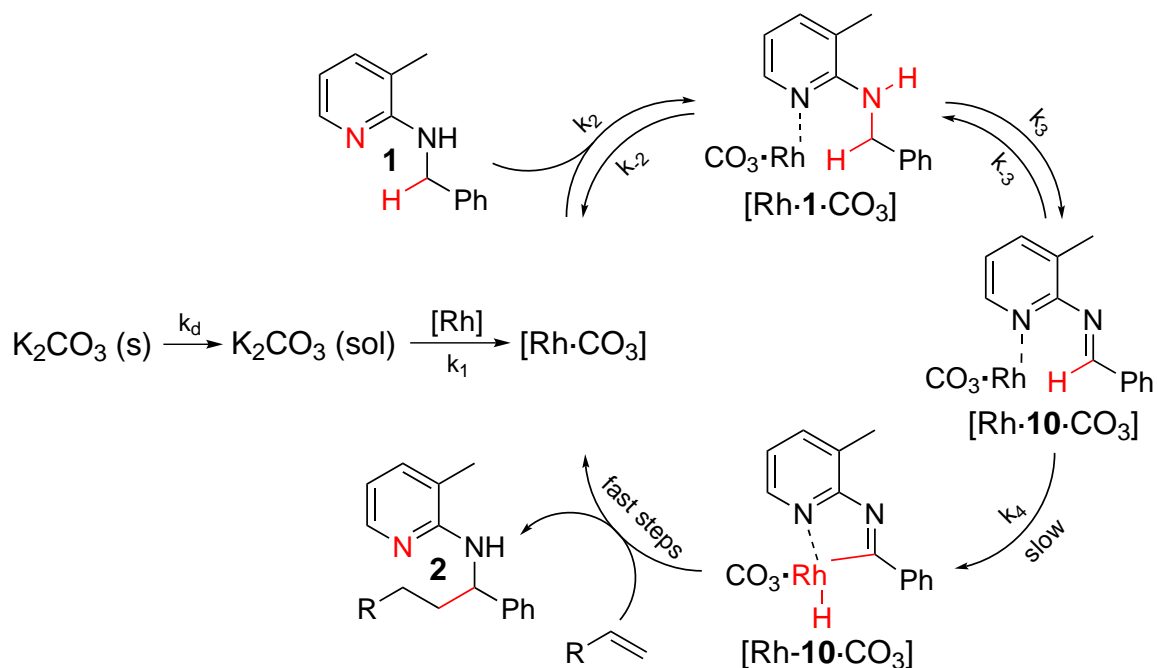


Figure 3.20.: Proposed simplified kinetic model for the direct C–H alkylation of benzylic amines using alkenes. Equations are neither stoichiometrically balanced nor balanced with respect to total charge for clarity.

3. Results and Discussion

[Rh–1·CO₃] are considered to be very small compared to the concentration of [RhCO₃] during the reaction. The turnover-limiting step is proposed to be the oxidative addition into the C(sp²)–H bond. On the basis of this proposed kinetic model the dependence of [RhCO₃] on time during the induction period can be described with the following equation.^h

$$c([RhCO_3])(t) = \frac{D M S}{\delta} c_s c_0(K_2CO_3) t \quad (3.11)$$

t ... Time during the induction period [s]

D ... Diffusion coefficient of K₂CO₃ dissolved in toluene [m² s⁻¹]

δ ... Thin static solvent layer (Solvent adheres tightly to the surface) [m]

c_s ... Saturation concentration of K₂CO₃ in solution [mol l⁻¹]

M ... Molar mass of K₂CO₃ [g mol⁻¹]

S ... Specific surface of K₂CO₃ [m² g⁻¹]

c₀(K₂CO₃) ... Initial molar loading of K₂CO₃ in the reaction [mol l⁻¹]

The concentration of the catalytically active species increases linearly over the induction period until all of the initial catalyst precursor [RhCl(cod)₂] is converted to catalytically active [RhCO₃]. It should be noted that due to simplifications in the derivation this equation is only valid when K₂CO₃ is used in excess and the total amount of K₂CO₃ that is dissolved and bound is negligible to the total amount of K₂CO₃ used in the beginning. After the induction period, the reaction follows the following rate law (at least in an initial reaction period).

$$r = k_4 K_3 K_2 c([RhCO_3]) c_0(\mathbf{1}) = 2 k_4 K_3 K_2 c_0([RhCl(cod)]_2) c_0(\mathbf{1}) \quad (3.12)$$

Now it must be determined whether the obtained kinetic model is in agreement to the experimental results. To begin with, the first order dependence on both [RhCl(cod)₂] and **1** is in principle correctly predicted. The rate would be first order with respect to **1** over a wide concentration region which is in accordance to the experimental results and also the first order dependence on [RhCl(cod)₂] when the initial concentration is decreased is correctly described. Now, when only the concentration of [RhCl(cod)₂] is increased the zeroth order dependence can be explained without further assumptions in the kinetic model since then it is proposed that the induction time is not over and not all of the [RhCl(cod)₂] is converted to the catalytically active species. The constant initial rate with increasing initial [RhCl(cod)₂] concentration results because the reaction has not reached a period of constant rate under these conditions and is still in the induction period. The same explanation applies for the apparently observed first order dependence on K₂CO₃ which is strictly speaking not a first order dependence but rather a prolonged induction period combined with formally the wrong method under these conditions

^hThe detailed mathematical derivation is found in Chapter 5.

3. Results and Discussion

to determine the initial rate. The mathematic reasoning why such a dependence is observed is found in Chapter 5. In addition, the zeroth order dependence which is observed when the initial K_2CO_3 loading is increased is also easily explained by this kinetic model because under these conditions the induction period is already over and no additional $[\text{RhCl}(\text{cod})_2]$ is left anymore which could be converted to $[\text{RhCO}_3]$. Therefore, under these conditions a zeroth order dependence of the initial rate on K_2CO_3 is evident.

However, there is one experiment which cannot be explained by this kinetic model without further ado. When both $[\text{RhCl}(\text{cod})_2]$ and K_2CO_3 are increased the proposed kinetic model would predict an increased initial rate, which is not observed. In this experiment the initial rate remains unchanged. This could be explained if $[\text{RhCO}_3]$ exceeded its solubility limit under these conditions.

The strength of this kinetic model lies in the fact that it can easily qualitatively explain the additional dependences of the initial rate that were observed. First, it can qualitatively explain why adsorbed H_2O on K_2CO_3 would show a significant increase in the reaction rate. The introduced water will be partially dissolved into the reaction mixture resulting in a higher solubility of K_2CO_3 in the reaction mixture and therefore in an increased saturation concentration c_s of K_2CO_3 . According to equation 3.11 an increased c_s also means an increased rate in the induction period and therefore a decreased induction time which directly results in an increased reaction rate by the method used to determine it. Second, the dependence on the specific surface of K_2CO_3 is directly evident from equation 3.11. Third, the dependence of the initial reaction rate on stirring can also be easily explained since no stirring would result in an increase of the thickness of the static solvent layer δ resulting in an increased induction time.

It should be noted that such a kinetic behaviour of heterogeneous solids, which are widely used in the field of metal-catalysed coupling reactions, has not been reported on many occasions for similar transformations and is therefore not well studied by now. A similar kinetic description of solubilisation of one reactant has been reported in solid-liquid phase transfer catalysis.⁷⁸ The experimental results presented in this thesis are therefore of great interest. In addition, studies on the influence of particle size or specific surface area and water content of the heterogeneous base in C–H activation reactions have not been performed so far. Thus, these results will be of significant interest for future research in this field since in many cases of metal-catalysed direct functionalisations heterogeneous bases or other heterogeneous components are used. It would be surprising if this transformation would be unique in showing such a significant dependence on the above mentioned parameters. These results obtained raise for example the question whether differences in screening results with different bases (e.g. K_2CO_3 versus Cs_2CO_3) really stem from the different counter ions or are rather an effect of particle size and surface area. Therefore, these parameters have to be considered in future studies when such reactions are optimised and should also be taken into account as possible explanation for observed induction periods.

3. Results and Discussion

Now, the observed KIE can be interpreted on the basis of the proposed kinetic model. The large KIE of about 4–5 with respect to the benzylic C–H bond is mainly explained by the oxidative addition into the C–H bond of the imine being the turnover-limiting step. However, there may also be an EIE influencing K_3 since the interconversion of amine to imine also involves breaking the benzylic C–H bond. This EIE, however, is not expected to be dominant. The observed small KIE of 1.3 with respect to the N–H bond of the amine is also suggested to be originated from an EIE influencing K_3 since the corresponding N–H bond is broken in this step.

In addition, the observed electronic influence on the reaction rate can also be interpreted on the basis of the proposed kinetic model. The reaction constant of -1.6 obtained from the Hammett plot with respect to functional groups on the amine phenyl group mainly comes from the oxidative addition into the C–H bond which is expected to be accelerated by electron-donating groups on the amine. Even though the reaction constant for complex reactions is the sum of all reaction constants prior to and in the rate-determining or the turnover-limiting step, all reaction constants of earlier steps are not expected to have significant influence on the overall reaction constant or are expected to cancel each other out in this reaction.

An interpretation of the activation parameters is not very simple because not much is known about the exact nature of the Rh-complexes in the catalytic cycle by now. The large enthalpy of activation suggests that high energy transition states are involved in the course of the catalytic cycle. The entropy of activation suggests that a significant degree of disorder is created in the course of the catalytic cycle until the turnover-limiting step or in it but since not much is known as of the exact nature of the intermediates and all the elementary steps in the catalytic cycle an interpretation is almost impossible and therefore omitted here.

3.2. Direct Alkylations using Alkylbromides

On the basis of previous experiments not much was known about the direct alkylation of benzylic amines using alkylbromides. It was known that several sideproducts are formed in significant amounts in this reaction making this reaction not very efficient but these sideproducts had not been identified before. Therefore, the goal was first to identify all the major sideproducts of the reaction and then find reaction conditions which are both more selective for the direct alkylation product and which also form it more quickly since the reaction conditions used so far are quite harsh with respect to temperature and catalyst loading and the reaction still proceeds only quite slowly.

3.2.1. Kinetic Profile Comparison

It was already previously mentioned that it was observed that alkenes react significantly faster than alkylbromides with **1** to give the corresponding alkylated products. This was already investigated in previous experiments by comparing the kinetic time course of both reactions under comparable reaction conditions.³⁵ However, this comparison was not performed under the optimised reaction conditions using degassed toluene. Therefore, the kinetic profile determination was repeated in order to determine the influence of using degassed solvent also for the direct alkylation reaction using alkylbromides. The kinetic time course of the reaction was followed for 6 h (cf. Figure 3.21).

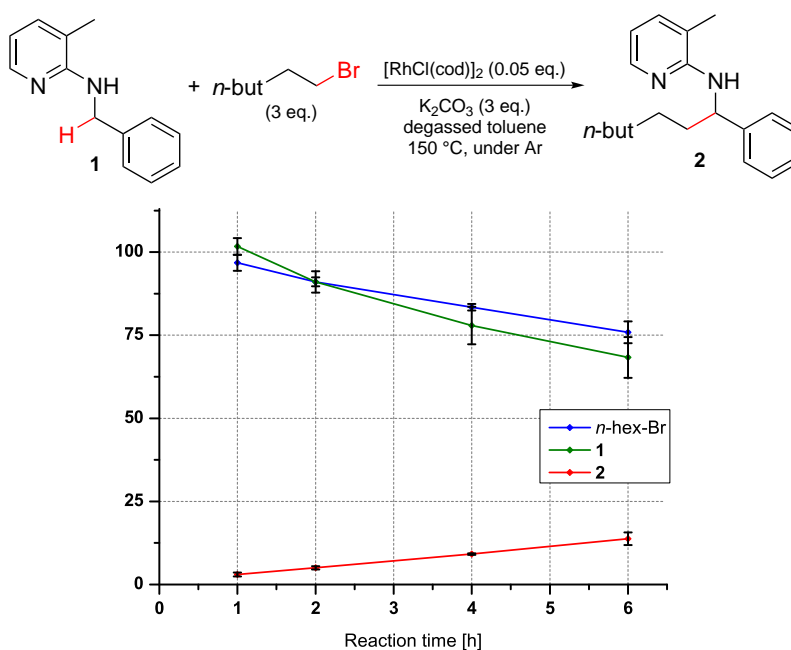


Figure 3.21.: Determination of the kinetic time course of the direct C–H alkylation of benzylic amine **1** using 1-bromohexane. 100 % equals 3 eq. for 1-bromohexane.

While the reaction using alkenes was finished after 2 h (vide supra), the reaction with alkylbromides was not even near completion and still in the initial reaction period (i.e. the product showed still linear increase over time). Details about the calculated linear regression for the formation of **2** are given in Chapter 5. Since the reaction is significantly slower with alkylbromides than with alkenes, one of the steps in which the alkylbromide is involved in the reaction is most likely turnover-limiting, as was already established in previous investigations.³⁵ It is therefore hypothesised that oxidative addition of Rh into the C–Br bond is turnover-limiting. However, this remains to be proven in this transformation by further experiments.

3. Results and Discussion

It should be noted that the formation of both **3** and **4** was observed but in significantly lower amounts (i.e. amounts significantly below 1 %) compared to the amounts observed in the direct alkylation using alkenes. In addition, the formation of three additional sideproducts was observed in significant amounts (i.e. amounts bigger than 1 %). These sideproducts had to be identified first in order to investigate their formation.

3.2.2. Investigations into all Major Sideproducts

The first step of a mechanistic investigation always is the identification of all the products of a reaction. It was already mentioned that in the experiments to determine the kinetic profile of the direct alkylation of **1** using 1-bromohexane besides **3** and **4**, which were only detected in low amounts (i.e. amounts significantly below 1 %), 3 additional sideproducts were observed in amounts bigger than 1 %. The first step towards the identification of these sideproducts was the detailed investigation of the mass spectra of these compounds obtained from GC/MS analysis. The process of identification and experiments investigating the formation of the corresponding sideproduct are outlined below separately for each compound.

3.2.2.1. Sideproduct I (14)

The first sideproduct observed had a molecular ion with an m/z of 288. On the basis of the fragmentation pattern observed in the MS the following structure was proposed for sideproduct II (cf. Figure 3.22).

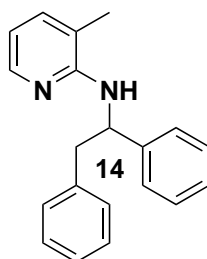


Figure 3.22.: Structure of sideproduct I in the direct alkylation with alkylbromides.

This compound was already known in literature and it was synthesised according to a literature procedure.³³ Sideproduct I could indeed be identified to be this compound. By looking at this sideproduct the question arises where the benzyl group that has been added to **1** originates from. The first and most obvious hypothesis was that it could come from the solvent toluene. An alternative hypothesis was that the phenyl group originates from a different molecule of **1** and the additional carbon atom would probably come from the alkylbromide used. In order to test

3. Results and Discussion

these hypotheses two experiments were performed. In the first experiment **1d** was subjected to the reaction conditions instead of **1** (cf. Figure 3.23).

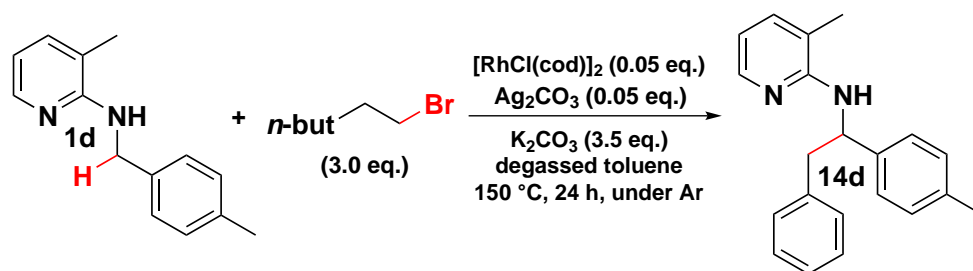


Figure 3.23.: First experiment to investigate the formation of **14** in the direct alkylation of **1** using alkylbromides by subjecting benzylic amine **1d** to the reaction conditions.

If the corresponding sideproduct was benzylated only (Sideproduct with m/z 302) this would support the hypothesis that the sideproduct is formed in a reaction with toluene. A sideproduct with an additional methyl group on the new benzylic group (Sideproduct with m/z 316) would support the second hypothesis. The reaction mixture was analysed with GC/MS. The corresponding sideproduct formed under these conditions had an m/z of 302 supporting the hypothesis that the additional benzyl group originates from toluene. In a second experiment the reaction was carried out with **1** as starting material but in d_8 -toluene (cf. Figure 3.24).

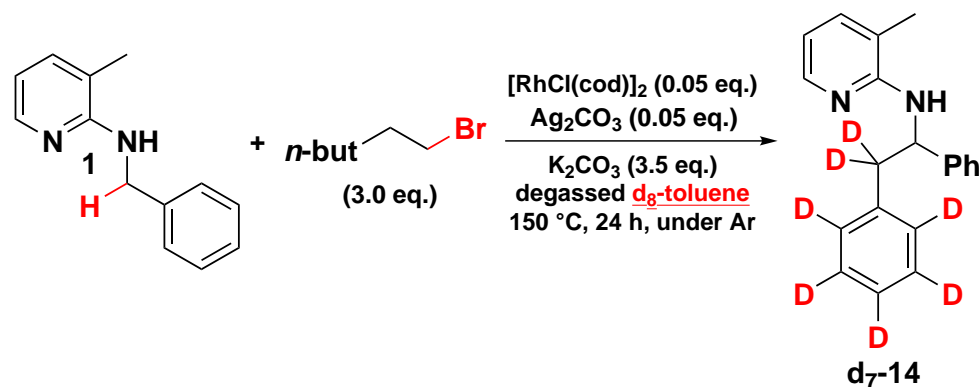


Figure 3.24.: Second experiment to investigate the formation of **14** in the direct alkylation of **1** using alkylbromides.

Again, the reaction mixture was analysed by means of GC/MS. The sideproduct formed had more or less the same retention time but had a molecular ion with an m/z of 295 instead of 288. The most significant observation in that regard was the

3. Results and Discussion

absence of significant m/z 288 signal at the retention time of **14**. This is strong evidence that the benzyl group originates from toluene. It should be noted that the formation of this sideproduct is of great interest since the corresponding reaction is an oxidative coupling^{15,21,41–43} between two $C(sp^3)-H$ centres (cf. Figure 3.25), a coupling which is not very common in literature by now and of great interest because of its high synthetic potential.

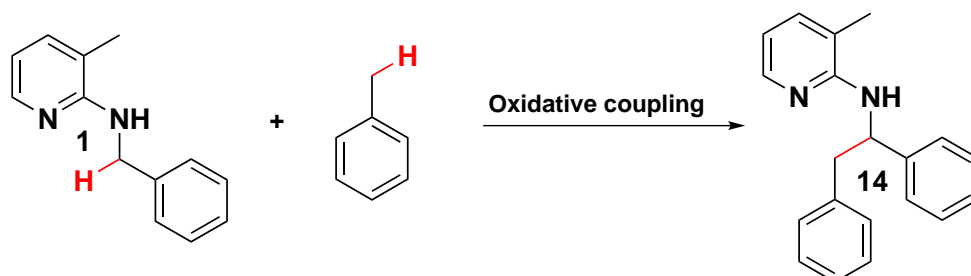


Figure 3.25.: The formation of **14** is an oxidative coupling between **1** and toluene.

The high appeal of such a transformation is the potentially very high atom economy which can be exceeded only by an addition reaction. Oxidative couplings employing toluene as benzylation agent are known in literature⁷⁹ but are not very common yet and therefore of great interest. Hence, steering the reaction conditions towards the predominant formation of **14** starting from **1** and toluene could be a potentially highly attractive follow up project to develop a synthetically very useful reaction.

3.2.2.2. Sideproduct II (**15**)

The second sideproduct observed had a molecular ion with an m/z of 310. On the basis of both the molecular ion and the fragmentation pattern it was suggested that this sideproduct could contain two additional methylene groups compared to the main product of the reaction (m/z of **2** is 282) which would account for the difference of 28 mass units. Alternatively, the additional mass units could be explained by a carbonyl group CO. It was decided to isolate sideproduct II from the reaction. In order to do that, several reaction mixtures obtained from the screening experiments carried out were pooled and worked up together in order to have a substantial amount of this by-product. Sideproduct 2 was isolated by flash chromatography, fully characterised and identified to be compound **15** (cf. Figure 3.26).

The first thing that strikes out about this sideproduct being observed under the reaction conditions is that except H_2O introduced with K_2CO_3 and residual H_2O introduced together with other starting materials and of course K_2CO_3 itself no oxygen is introduced into the reaction mixture. Residual O_2 is not expected to be

3. Results and Discussion

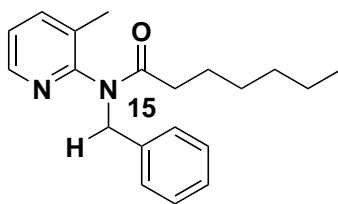


Figure 3.26.: Structure of sideproduct II in the direct alkylation with alkylbromides.

enough to account for the significant amounts (usually several percent) of compound **15** observed. Both the incorporation of oxygen from H₂O and from K₂CO₃ are potentially very interesting reactions. In addition, the carbon chain is elongated by one carbon atom compared to the alkylbromide used in the reaction. In order to gain some information about the formation of this sideproduct the origin of the additional carbon atom, which is bonded to oxygen, was investigated. It was hypothesised that this carbon atom could either originate from K₂CO₃ or it could originate from the alkylbromide used. Therefore, one experiment was performed using labelled K₂¹³CO₃ in order to investigate whether the ¹³C would be incorporated into the sideproduct (cf. Figure 3.27).

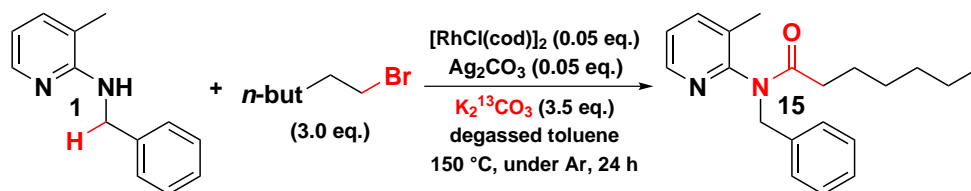


Figure 3.27.: Experiment to investigate the origin of the additional carbon atom in the formation of **15** in the direct alkylation of **1** using alkylbromides.

The resulting reaction mixture was analysed by means of GC/MS analysis. According to the obtained mass spectrum of compound **15** there was no significant incorporation of ¹³C observed. This is evidence against the hypothesis that the additional carbon atom originates from K₂CO₃. The origin of the oxygen atom was not investigated in the course of this thesis but would be a very interesting follow-up experiment to perform.

3.2.2.3. Sideproduct III (16)

The third sideproduct observed had a molecular ion with an m/z of 268. On the basis of the fragmentation pattern observed, which was in principle the same as in other linearly alkylated benzylic amines like **2**, the following structure was proposed for sideproduct III (cf. Figure 3.28).

3. Results and Discussion

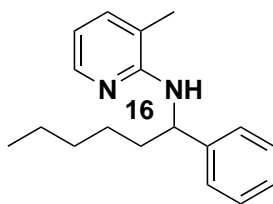


Figure 3.28.: Structure of sideproduct III in the direct alkylation with alkylbromides.

In order to identify this sideproduct it was synthesised by performing the direct alkylation of **1** with 1-bromopentane and the main product present in the resulting crude reaction mixture was used as reference for both GC and GC/MS analysis (cf. Figure 3.29). In addition, the corresponding sideproduct formed in this experiment was compared to **9** which was previously synthesised and fully characterised using the direct alkylation of **1** with 1-bromobutane.

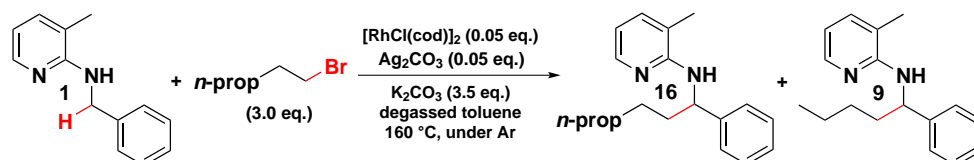


Figure 3.29.: Experiment to confirm the structure of sideproduct III in the direct alkylation of **1** using alkylbromides.

Both comparisons showed that the third sideproduct indeed is the alkylated benzylic amine with an alkyl group which is shorter by one carbon atom. Therefore, the proposed structure for sideproduct III (cf. Figure 3.28) is correct. The formation of **16** is mechanistically potentially very interesting because the formation of a similar sideproduct has not been reported in literature by now. However, its formation is unfavourable from a practical point of view since the main product of the reaction **2** is completely inseparable from **16** by means of flash chromatography. Alternative purification methods are also potentially very difficult considering the very similar properties expected from both **2** and **16** and may also not be generally applied for the purification of different alkylation products. As would be expected, it was also recognised that alkylation products obtained from previous direct alkylation experiments using alkylbromides which were purified by flash chromatography were indeed a mixture of the main product of the alkylation together with the corresponding sideproduct having a carbon chain shorter by one carbon atom. Therefore, in order to make the direct alkylation of **1** using alkylbromides a practically useful transformation the formation of significant amounts of this sideproduct need to be avoided. However, from a mechanistic point of view the formation of **16** is of high

3. Results and Discussion

interest since, as already mentioned before, a sideproduct like that has never been observed.

Now having identified the 3 additional sideproducts observed in the direct alkylation of **1** using alkylbromides the data from the kinetic profile of the reaction using 1-bromohexane was reviewed in order to obtain the kinetic time course of the formation of **14**, **15** and **16**, respectively. In addition, the selectivity of the main product **2** with respect to the formation of all other sideproducts was also determined and plotted over time (cf. Figure 3.30).

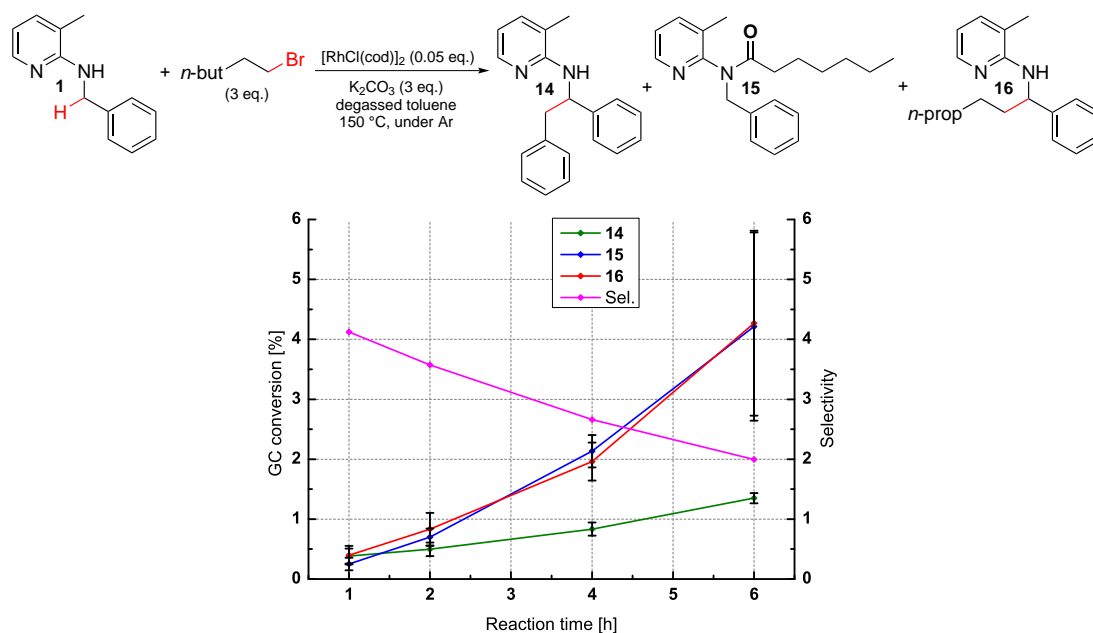


Figure 3.30.: Determination of the kinetic time course of the sideproducts **14**, **15** and **16** in the direct C–H alkylation of **1** using 1-bromohexane.

It should be noted that the formation of sideproducts **15** and **16** shows basically the same kinetic profile. This is confirmed by a high correlation observed between the corresponding data points (cf. Chapter 5 for details). Additionally, in the majority of the screening experiments it is observed that sideproducts **15** and **16** are formed in almost equal amounts. This indicates that the formation of both **15** and **16** could also be chemically correlated. From a chemical point of view this seems plausible since sideproduct **16** has one carbon atom less in the newly attached alkyl chain and sideproduct **15** has one additional carbon atom in the newly attached group. Therefore, it is suggested that this additional carbon atom originates from 1-bromohexane which is converted to a pentyl group, which then reacts in the alkylation of **1** to form sideproduct **16**. However, too little is known about the formation of these sideproducts and therefore mechanistic proposals for their formation are omitted in this thesis. Further investigations in that regard have to be

3. Results and Discussion

performed.

In addition, from the kinetic time course of the sideproducts it can be seen that in the beginning the formation of **14**, **15** and **16**, respectively, is slower and the corresponding rates are increasing with time which is evident from the positive curvature in the corresponding curves. Therefore, as can also be seen from Figure 3.30, the initial selectivity for **2** is higher and then decreases as the reaction progresses. It should be noted that under these reaction conditions the selectivity for **2** is not very high i.e. from an initial value of about 4 it shows decreasing monotony meaning that at least 20 % of the converted material is found in one of the sideproducts formed and not in the main product of the reaction.

3.2.2.4. Sideproduct IV (17)

During the optimisation of the reaction conditions of the direct alkylation of **1** using alkylbromides it was observed that the addition of Et₃N significantly speeds up the reaction and also slightly improves the selectivity (vide infra). However, at the same time the addition of Et₃N resulted in the formation of an additional sideproduct, which had a molecular ion with an m/z of 226. On the basis of this result and the observed fragmentation of this sideproduct the following structure was proposed for it (cf. Figure 3.31).

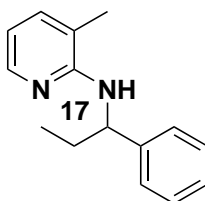


Figure 3.31.: Structure of sideproduct IV in the direct alkylation with alkylbromides when Et₃N is added.

In order to identify this sideproduct it was synthesised the same way as was **16** by performing the direct alkylation of **1** with 1-bromoethane and the main product present in the resulting crude reaction mixture was used as reference for both GC and GC/MS analysis (cf. Figure 3.32).

The comparison showed that the additional sideproduct indeed is the alkylated benzylic amine with an ethyl group. Therefore, the proposed structure for sideproduct IV (cf. Figure 3.31) is correct. It is proposed that the ethyl group originates from Et₃N since only when it was added was this sideproduct observed. Interestingly, when Bu₃N was used instead of Et₃N, neither the formation of **17** nor the formation of **9**, i.e. the butylated product, was observed. It was expected that at least some formation of **9** was observed. The reason could be the increased steric hindrance at the nitrogen atom when the ethyl groups are replaced by butyl groups

3. Results and Discussion

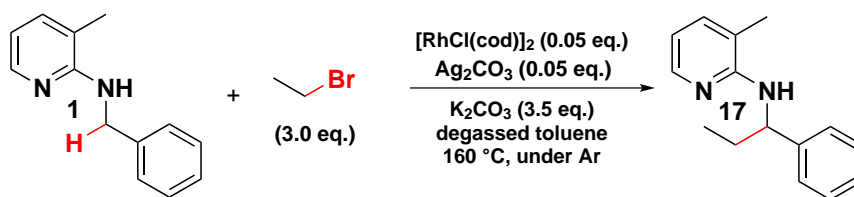


Figure 3.32.: Experiment to confirm the structure of sideproduct IV in the direct alkylation of **1** using alkylbromides when Et_3N is added.

but this needs to be investigated further. However, the reaction was accelerated to the same extent compared to experiments using Et_3N . This is a hint that the formation of an alkylation product from the alkyl chain on the amine and the observed acceleration of the reaction are independent from one another. In order to study the formation of **17** further, several experiments were performed to test under which conditions the formation of **17** is observed (cf. Figure 3.33).

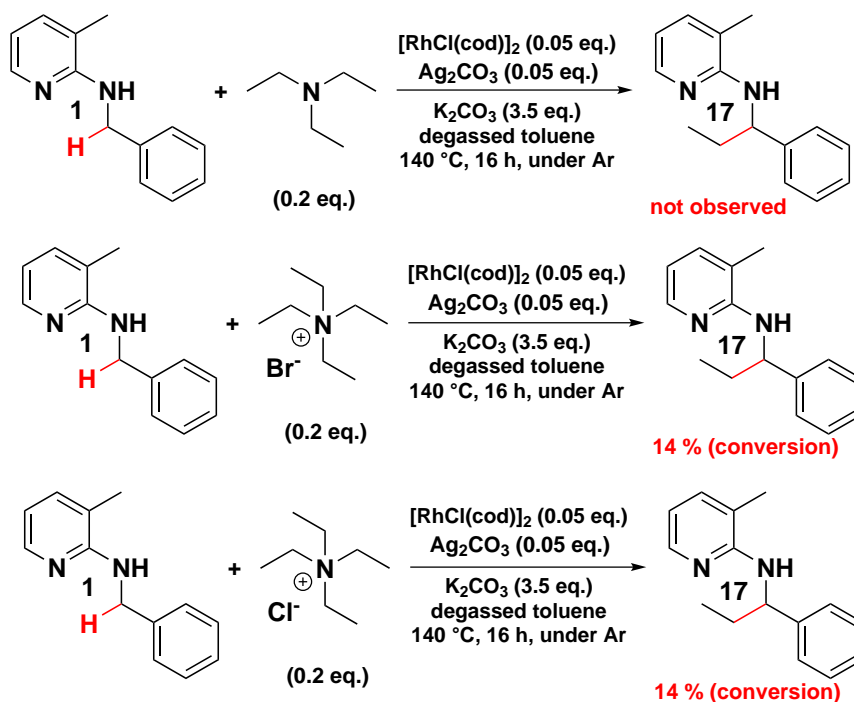


Figure 3.33.: Experiments to investigate the formation of **17** in the direct alkylation of **1** using alkylbromides when Et_3N is added. The conversion is determined relative to dodecane as internal standard assuming a conversion factor of 1.

From the first scheme in Figure 3.33 it can be seen that the formation of **17** is not

3. Results and Discussion

observed in the absence of 1-bromohexane. Therefore, it was hypothesised that Et_3N undergoes nucleophilic attack at the alkylbromide to form the corresponding quaternary ammonium salt which then reacts with **1** under the reaction conditions to form **17**. On the basis of this result, it was tested whether the formation of **17** was observed again when tetraethylammonium salts were used instead of Et_3N in the absence of 1-bromohexane (cf. Figure 3.33, second and third schemes). Under these conditions **17** was observed again supporting the established hypothesis. It should be noted that the presence of bromide is not required since the use of tetraethylammonium chloride resulted in the formation of the same amount of **17** compared to the experiment when tetraethylammonium bromide was used. Therefore, the formation of sideproduct **17** is rationalised on the basis of the following reaction course (cf. Figure 3.34).

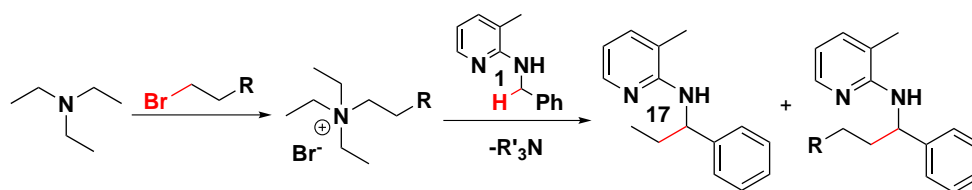


Figure 3.34.: General reaction course rationalising the formation of sideproduct **17** in the direct alkylation of **1** using alkylbromides in the presence of Et_3N .

Under the reaction conditions Et_3N reacts with the alkylbromide to form the corresponding quaternary ammonium salt which alkylates **1** to form sideproduct **17**. On the basis of the performed experiments, however, it is not fully clear whether the formation of quaternary ammonium salts and their role as alkylating agents is responsible for the significant increase in the reaction rate observed. This needs to be studied in further experiments. In addition, the alkylation of **1** using quaternary ammonium salts is potentially interesting both mechanistically and synthetically because the use of tetraalkylammonium salts as alkylation reagents in metal-catalysed transformations has not been reported yet and therefore needs further investigation.

3.2.2.5. Sideproduct Overview

To summarise, in the direct alkylation of **1** using 1-bromohexane to form **2** the formation of several sideproducts in significant amounts is observed (cf. Figure 3.35). Therefore, the reaction conditions need to be optimised in order to achieve higher selectivity for the formation of **2** especially with respect to the formation of sideproducts **16** and **17** because they are potentially hard to separate from **2** by means of flash chromatography.

3. Results and Discussion

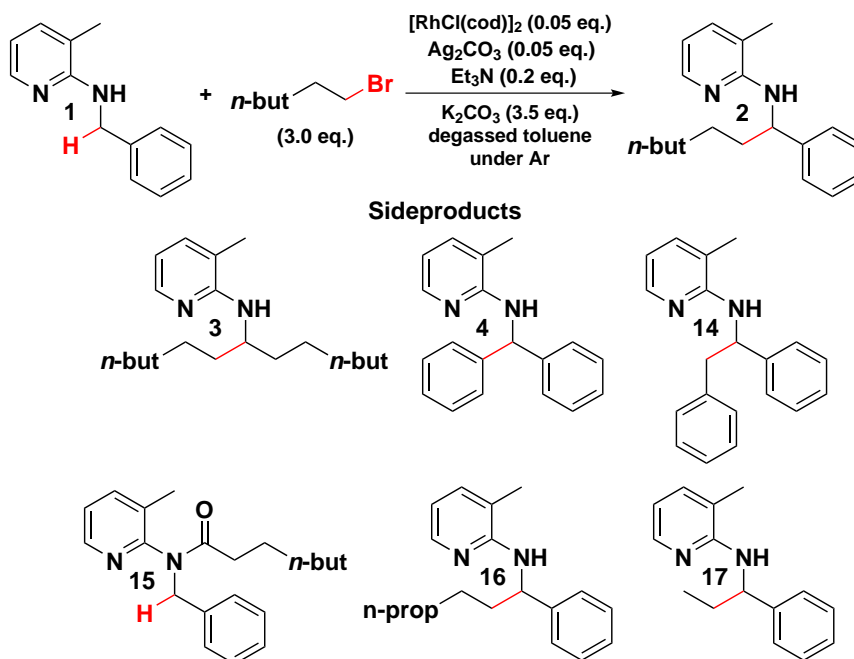


Figure 3.35.: Sideproducts observed in the direct C–H alkylation of **1** using 1-bromohexane.

3.2.3. Optimisation of Reaction Conditions

There were two goals for the optimisation of the reaction conditions of direct C–H alkylation of **1** using 1-bromohexane (cf. Figure 3.36). The first goal was to accelerate the reaction in order to carry it out at lower temperatures. The second, and even more important, goal was to increase the selectivity for the formation of the main product **2** with respect to the sideproducts formed under the reaction conditions (vide supra) in order to develop a synthetically useful transformation. The primary goal in this regard was to increase selectivity with respect to the formation of **16**. All the screening results are given in the Appendix.

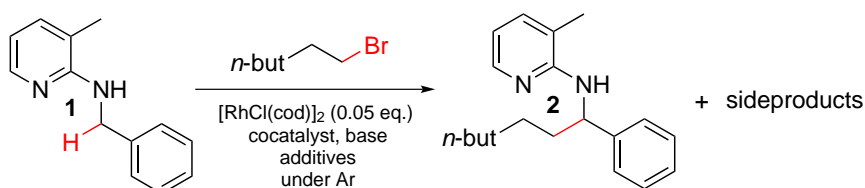


Figure 3.36.: Scheme of the screening experiments carried out to optimise the direct alkylation of **1** using 1-bromohexane.

3. Results and Discussion

The first major improvement in the reaction rate was observed by the addition of 0.05 eq. Ag_2CO_3 to the reaction. Then the reaction was already finished after 16 h at 160 °C (61 % of **2**, overall selectivityⁱ of 2.6) compared to finished after 24 h only without the addition of Ag_2CO_3 (57 % of **2**, overall selectivity of 4.1). However, the selectivity decreased upon the addition of Ag_2CO_3 . Unfortunately, when the temperature was reduced to 150 °C selectivity especially with respect to **16** decreased further (48 % of **2**, overall selectivity of 1.5 after 24 h). However, using completely dry K_2CO_3 improved the situation slightly (55 % of **2**, overall selectivity of 2.2 after 24 h) again.

The second major improvement was the addition of Et_3N to the reaction. Using 0.1 eq. of Et_3N resulted in the reaction being already finished after 16 h at 150 °C (57 % of **2**, overall selectivity of 3.1) and also the selectivity was improved even though the formation of **17** was now observed as well. It was decided to reduce the reaction temperature to 140 °C and 0.2 eq. of Et_3N turned out to be ideal (49 % of **2** with remaining 14 % of **1**, overall selectivity of 2.6 after 16 h).

In further screenings at 140 °C different solvents and solvent mixtures were used. The use of a mixture of toluene/dioxane 4:1 showed a slightly faster reaction (53 % of **2** with remaining 4 % of **1**, overall selectivity of 2.7 after 16 h). It was also tried to add ligands to increase both the selectivity and the rate. The addition of 0.2 eq. cod still using toluene as solvent showed significantly improved selectivity and slightly higher reaction rate (56 % of **2** with remaining 7 % of **1**, overall selectivity of 5.0 after 16 h).

Finally, the addition of secondary alcohols like cyclohexanol, cyclopentanol and 2-propanol gave very promising results with respect to the selectivity while lowering the reaction rate significantly. The best and most promising result was obtained with toluene/dioxane 4:1 as solvent and with the addition of 0.2 eq. cod and 1 eq. of 2-propanol (32 % of **2** with remaining 41 % of **1**, overall selectivity of 10.2 after 16 h). The selectivity was by far the best observed up to that point. In addition, the selectivity with respect to the formation of **16** was over 100. Therefore, it was thought that these conditions could easily be adapted slightly to reach full conversion while still keeping a high selectivity. However, when the reaction was heated for 24 h under the same conditions the selectivity significantly deteriorated (39 % of **2** with remaining 26 % of **1**, overall selectivity of 5.9). Running the reaction for 72 h did not give full conversion but selectivity was even lower compared to the best conditions without using 2-propanol (45 % of **2** with remaining 13 % of **1**, overall selectivity of 3.6). Therefore, it was tried to increase the temperature to 150 °C (29 % of **2** with remaining 38 % of **1**, overall selectivity of 11.2 after 16 h) and 160 °C (31 % of **2** with remaining 36 % of **1**, overall selectivity of 10.1 after 16 h). Interestingly, the reaction showed a very unusual dependence on the temperature because the conversion was the same, the reaction rate was completely unaffected. In addition, when it was tried to perform the reaction at 130 °C conver-

ⁱSelectivity is defined as ratio of **2** and all other sideproducts formed.

3. Results and Discussion

sion was actually increased but the selectivity was completely lost (35 % of **2** with remaining 28 % of **1**, overall selectivity of 1.7 after 16 h).

Unfortunately, in the course of this thesis the goal to achieve selective formation of **2** in the direct C–H alkylation of **1** using 1-bromohexane was therefore not achieved. Further investigations are necessary to understand the role of secondary alcohols in the reaction. The problems are that it is not understood why secondary alcohols improve the selectivity, why the reaction is selective up to a certain point only and why the reaction shows a very uncommon temperature dependence in the presence of 2-propanol.

3.3. Conclusions

To conclude, the direct C–H alkylation reactions of benzylic amines using either alkenes or alkylbromides were investigated in detail. In the mechanistic and kinetic studies performed it was focussed on the investigation and understanding of the direct alkylation using alkenes.

First of all, in the direct C–H alkylation using alkenes a primary KIE was observed at the benzylic C–H together with a reversible H–D exchange which was higher than the total amount of products formed in the same experiments indicating that there are at least two distinct steps in which the corresponding C–H bonds are broken. Crossover experiments revealed that the imines **10** and **11** are converted to the corresponding products of the reaction, respectively. On the basis of a newly developed method the analysis of the kinetic time course of the ratio of alkylated imine **11** to product **2**, which showed a decreasing monotony, revealed that **11** is formed before **2** indicating that the reaction proceeds over the corresponding imines. The direct alkylation of a C(sp³)–H bond proceeds mechanistically via a C(sp²)–H activation pathway.

Second of all, initial rate experiments of the direct C–H alkylation using alkenes yielded the partial reaction orders with respect to all the starting materials. A formal partial reaction order of 1 was observed with respect to K₂CO₃ at lower molar loadings. Additional experiments revealed a significant initial rate increase when K₂CO₃ with adsorbed H₂O was used and a dependence of the initial reaction rate on the specific surface of the K₂CO₃ batch used. Furthermore, when K₂CO₃ was removed from the reaction mixture after an initial reaction period by filtration the reaction was shown to continue at an even higher rate showing that K₂CO₃ is only needed in the beginning of the reaction and using K₂CO₃ in catalytic amounts resulted in the formation of less sideproducts but a significantly slower reaction and a considerable induction period of the reaction was observed. A detailed kinetic model was established explaining both the induction period with respect to K₂CO₃ and the partial reaction orders observed. It could be shown that K₂CO₃ is first partially dissolved into the reaction mixture and then reacts irreversibly with the catalyst precursor to form the catalytically active species. The apparent partial

3. Results and Discussion

reaction order with respect to K_2CO_3 actually results from the induction period observed when lower molar K_2CO_3 loadings are used.

Third of all, in the direct C–H alkylation using alkylbromides 3 additional side-products were observed compared to the reaction using alkenes. Compound **14** was shown to be formed from the oxidative coupling reaction of **1** with toluene which is formally a $C(sp^3)–H$ $C(sp^3)–H$ coupling, a reaction which is not very common in literature by now. The formation of compounds **15** and **16** was shown to be most probably correlated. The generation of a sideproduct like **16** has not been reported by now in direct alkylations using alkylbromides and this reaction is therefore of great mechanistic interest. Also the formation of **15** is, at least from a mechanistic point of view, very interesting and needs further investigation. In addition, when Et_3N was added, the formation of **17** as additional sideproduct was observed which was shown to originate from alkylation of **1** via the corresponding quaternary ammonium salt formed in the reaction of Et_3N and the alkylbromide. The use of quaternary ammonium salts as alkylation agents in metal-catalysed transformations is not known in literature either. In the screening experiments to optimise the reaction conditions the reaction could be significantly accelerated by the addition of both Ag_2CO_3 and Et_3N . Selectivity was shown to be only significantly increased at low conversion upon the addition of secondary alcohols, the best result being obtained using 2-propanol. Selectivity was lost completely when the reaction was carried out for longer times and, interestingly, increasing the temperature did not increase conversion at all.

Overall, the general mechanistic outline for the direct alkylation using alkenes was established and a detailed kinetic model explaining both the observed induction period with respect to K_2CO_3 and the kinetics of the catalytic cycle was developed. Several interesting sideproducts were identified in the direct alkylation using alkylbromides opening the door for several potentially attractive follow-up studies.

4. Experimental

4.1. General Methods

In general, unless noted otherwise, chemicals were purchased from commercial suppliers and used without further purification. Compounds **1**³³, **1a**³³, **1c-h**³³, **12a**³³ and **12b**³³ were synthesised according to literature procedures. Cyclooctadiene rhodium chloride dimer [RhCl(cod)]₂ was generally handled in a glove box under argon. 1-Bromohexane was distilled under reduced pressure before use. Dry and degassed toluene was purchased from commercial suppliers and stored over molecular sieves in a glove box under argon. Other dry solvents were obtained by passing pre-dried material through a cartridge containing activated alumina (solvent dispensing system) and stored under nitrogen atmosphere until usage. Degassing of liquids was performed by 3 successive freeze-pump-thaw cycles.

Water contents of K₂CO₃ batches were determined by measuring the loss on heating of the corresponding solids by heating a sample to about 200 °C under medium vacuum (0.1 mbar) overnight assuming that only water was lost in the process. The same procedure was followed to obtain dry K₂CO₃. Amounts of K₂CO₃ used in reactions were calculated assuming the solid to be completely dry, unless noted otherwise.

Particle size distributions of K₂CO₃ batches were determined by laser diffraction on a Malvern Mastersizer 2000 together with a Scirocco 2000 dry powder dispersion unit. Measurements were performed in 4-fold repetition and the reported result is the average over all those 4 repetitions.

Nitrogen adsorption and desorption experiments of K₂CO₃ batches were performed at 77 K on a Micromeritics ASAP 2020. Sample size was chosen to provide at least 1 m² of total surface for the measurement. Degassing was performed at room temperature for 5 h directly before the adsorption and desorption measurements. Specific surface areas were determined from the obtained adsorption isotherms by the standard BET method.

¹H-NMR and ¹³C-NMR spectra were recorded on either a Bruker AC200 or a Bruker Avance 400, chemical shifts are reported in ppm, using Me₄Si as internal standard. NMR Signals were assigned according to Figure 4.1 with different aromatic ring systems marked as a, b and c, respectively, and numbers without labels assigned to the aliphatic molecule part.

4. Experimental

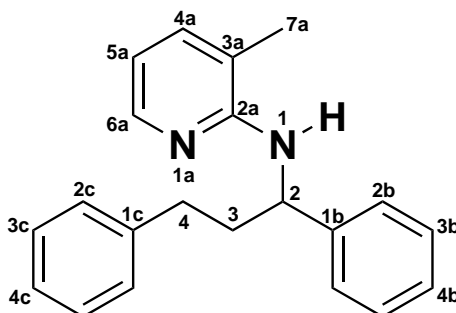


Figure 4.1.: NMR signal assignment scheme.

GC-MS was either performed on a Thermo Focus GC/ MS DSQ II (quadrupole, EI+) with a BGB5 capillary column (30 m x 0.32 mm, 1.0 μm film, achiral) or on a Thermo Trace 1300 GC/ MS ISQ LT (quadrupole, EI+) with a TR-5 capillary column (7 m x 0.32 mm, 0.25 μm film, achiral).

GC measurements were either carried out on a Thermo Focus GC using a BGB-5 capillary column (30 m x 0.32 mm, 1.0 μm film, achiral) with the following oven temperature program: 100 $^{\circ}\text{C}$ (2 min), 18 $^{\circ}\text{C min}^{-1}$, 280 $^{\circ}\text{C}$ (5 min) or on a Thermo Trace 1310 GC using a TR-5 MS capillary column (15 m x 0.25 mm, 1.0 μm film, achiral) with the following oven temperature program: 65 $^{\circ}\text{C}$ (0.85 min), 125 $^{\circ}\text{C min}^{-1}$ to 70 $^{\circ}\text{C}$, 100 $^{\circ}\text{C min}^{-1}$ to 115 $^{\circ}\text{C}$, 80 $^{\circ}\text{C min}^{-1}$ to 175 $^{\circ}\text{C}$, 50 $^{\circ}\text{C min}^{-1}$ to 195 $^{\circ}\text{C}$, 20 $^{\circ}\text{C min}^{-1}$ to 205 $^{\circ}\text{C}$, 50 $^{\circ}\text{C min}^{-1}$ to 300 $^{\circ}\text{C}$. GC yields were calculated by using the conversion factor of the corresponding compound relative to dodecane as internal standard, which was determined by calibration.

For TLC aluminium backed silica gel 60 with fluorescence indicator F254 was used. Column chromatography was performed on Silica 60 from Merck (40 μm –63 μm) unless noted otherwise. Flash chromatography, unless noted otherwise, was carried out on a Büchi SepacoreTM MPLC system.

Melting points were determined on an automated melting point system (BÜCHI Melting Point B-545) and are uncorrected.

IR measurements for quantification were carried out on a PerkinElmer Spectrum 400 in transmission mode using a ZnSe cuvette. ATR-IR measurements for characterisation were carried out on a PerkinElmer Spectrum 65. IR spectra were recorded as average over 16 spectra, the resolution of the recorded spectra was 4 cm^{-1} .

High-resolution mass spectrometry (HRMS) for literature-unknown compounds was performed by liquid chromatography in combination with hybrid ion trap and high-resolution time-of-flight mass spectrometry (LC-IT-TOF-MS) in only positive-

4. Experimental

ion detection mode with the recording of standard (MS) and tandem (MS/MS) spectra.

Karl Fischer titrations were carried out on a Mitsubishi CA-21 Moisture Meter using a stirring speed of 5.

4.2. General Procedures

4.2.1. General procedure I for C–H activation reactions

Solid and non-volatile liquid starting materials were placed in an oven-dried 8 ml vial with a septum screw cap and a magnetic stirring bar. The vial was evacuated and flushed with argon three times. Liquid starting materials and solvent were added via syringe through septum. Finally, the vial was closed with a fully covered solid Teflon-lined cap. The reaction mixture was heated in a reaction block at the desired temperature for the desired reaction time.

4.2.2. General procedure II for C–H activation reactions

Solid and non-volatile liquid starting materials except catalyst were placed in an oven-dried 8 ml vial with a fully covered solid Teflon-lined cap and a magnetic stirring bar under ambient atmosphere. The vial was transferred into a glove-box under argon. Catalyst, liquid starting materials and solvent were added inside the glove-box. Finally, the vial was closed and the reaction mixture was heated in a reaction block at the desired temperature for the desired reaction time.

4.2.3. General work-up procedure for C–H activation reactions

After cooling the reaction mixture to room temperature the solid material was removed by filtration and washed with CH_2Cl_2 . The combined organic filtrate was concentrated in vacuo and the resulting crude residue was purified by flash column chromatography (LP/EtOAc).

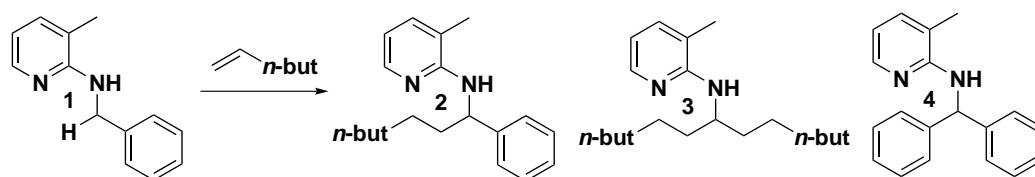
4.3. Synthetic Procedures

4.3.1. Substrate Scope - Alkenes

The experiments were performed on a 0.50 mmol scale with an initial concentration of 0.25 mol l^{-1} of **1** in the reaction mixture. K_2CO_3 with an adsorbed water content of 2 m%, a particle size median of $0.34 \mu\text{m}$ and a specific BET surface of $0.4 \text{ m}^2 \text{ g}^{-1}$ was used.

4. Experimental

4.3.1.1. Hex-1-ene



The reaction was carried out according to general procedure I with **1** (100 mg, 0.50 mmol, 1 eq.), hex-1-ene (127 mg, 1.5 mmol, 3 eq.), K_2CO_3 (209 mg, 1.5 mmol, 3 eq.) and $[RhCl(cod)]_2$ (12 mg, 0.025 mmol, 0.05 eq.) in dry and degassed toluene (2 ml). The reaction mixture was heated for 3 h at 150 °C. The general work-up procedure for C–H activation reactions was followed (LP/EtOAc 99:1) and the products **2** (61 %), **3** (9 %) and **4** (8 %) were isolated.

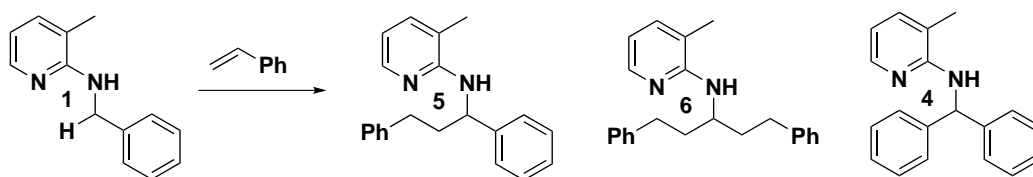
N-(1-phenylheptyl)-3-methylpyridin-2-amine (2) Colourless oil (87 mg, 61 %). 1H -NMR ($CDCl_3$, 200 MHz): δ = 0.85 (t, J = 6.9 Hz, 3 H, C[8]– H_3), 1.11–1.50 (m, 8 H, C[4–7]– H_2), 1.71–1.99 (m, 2 H, C[3]– H_2), 2.10 (s, 3 H, C[7a]– H_3), 4.36 (d, J = 7.4 Hz, 1 H, N[1]–H), 5.23 (q, J = 7.2 Hz, 1 H, C[2]–H), 6.45 (dd, J = 7.0, 5.1 Hz, 1 H, C[5a]–H), 7.12–7.43 (m, 6 H, C[5a]–H, C[2–4b]–H), 7.95 (dd, J = 5.0, 1.5 Hz, 1 H, C[6a]–H) ppm. ^{13}C -NMR ($CDCl_3$, 50 MHz): δ = 14.1 (q, C[8]), 17.1 (q, C[7a]), 22.6 (t, C[7]), 26.3 (t, C[6]), 29.3 (t, C[5]), 31.8 (t, C[4]), 37.6 (t, C[3]), 54.7 (d, C[2]), 112.5 (s, C[3a]), 116.2 (s, C[3a]), 126.5 (d, C[2b]), 126.7 (d, C[4b]), 128.4 (d, C[3b]), 136.8 (d, C[4a]), 144.6 (s, C[1b]), 145.5 (d, C[6a]), 156.1 (s, C[2a]) ppm. HRMS: calculated for $C_{19}H_{27}N_2$ [$M + H$] $^+$ 283.2169; found 283.2173.

N-(tridecan-7-yl)-3-methylpyridin-2-amine (3) Colourless oil (12 mg, 9 %). 1H -NMR ($CDCl_3$, 200 MHz): δ = 0.86 (t, J = 6.8 Hz, 3 H, C[8]– H_3), 1.11–1.70 (m, 20 H, C[3–7]– H_2), 2.05 (s, 3 H, C[7a]– H_3), 3.82 (d, J = 8.0 Hz, 1 H, N[1]–H), 4.22 (m, 1 H, C[2]–H), 6.44 (dd, J = 7.0, 5.1 Hz, 1 H, C[5a]–H), 7.17 (dd, J = 7.0 Hz, 1.0 Hz, 1 H, C[4a]–H), 7.98 (dd, J = 5.0, 1.5 Hz, 1 H, C[6a]–H) ppm. ^{13}C -NMR ($CDCl_3$, 50 MHz): δ = 14.1 (q, C[8]), 17.1 (q, C[7a]), 22.6 (t, C[7]), 25.7 (t, C[6]), 29.5 (t, C[5]), 31.9 (t, C[4]), 35.2 (t, C[3]), 50.1 (d, C[2]), 111.7 (d, C[5a]), 115.9 (s, C[3a]), 136.6 (d, C[4a]), 145.4 (d, C[6a]), 156.9 (s, C[2a]) ppm. HRMS: calculated for $C_{19}H_{35}N_2$ [$M + H$] $^+$ 291.2795; found 291.2786.

N-Benzhydryl-3-methylpyridin-2-amine (4) Colourless oil (8 mg, 6 %). Analytical data was in accordance to literature reports.³³ 1H -NMR ($CDCl_3$, 200 MHz): δ = 2.13 (s, 3 H, C[7a]– H_3), 4.65 (d, J = 6.8 Hz, 1 H, N[1]–H), 6.49–6.53 (m, 2 H, C[2]–H, C[5a]–H), 7.18–7.35 (m, 11 H, C[2–4b]–H, C[4a]–H), 7.95 (dd, J = 5.1, 1.4 Hz, 1 H, C[6a]–H) ppm.

4. Experimental

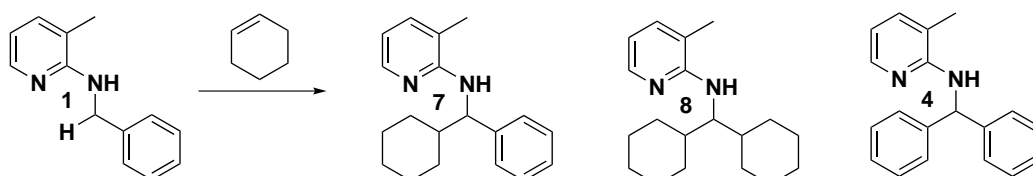
4.3.1.2. Styrene



The reaction was carried out according to general procedure I with **1** (100 mg, 0.50 mmol, 1 eq.), styrene (157 mg, 1.5 mmol, 3 eq.), K_2CO_3 (209 mg, 1.5 mmol, 3 eq.) and $[RhCl(cod)]_2$ (12 mg, 0.025 mmol, 0.05 eq.) in dry and degassed toluene (2 ml). The reaction mixture was heated for 12 h at 150 °C. The general work-up procedure for C–H activation reactions was followed (LP/EtOAc 99:1) and impure **5** (58 %) was obtained because it was inseparable from **4** and **6**, respectively.

N-(1,3-diphenylpropyl)-3-methylpyridin-2-amine (5) Colourless oil (89 mg, 58 %). GC purity: 88 %. 1H -NMR ($CDCl_3$, 200 MHz): δ = 2.00 (s, 3 H, C[7 a]–H₃), 2.23 (m, 2 H, C[3]–H₂), 2.69 (m, 2 H, C[4]–H₂), 4.35 (d, J = 7.7 Hz, 1 H, N[1]–H), 5.36 (q, J = 7.2 Hz, 1 H, C[2]–H), 6.45 (dd, J = 5.1 Hz, 7.2 Hz, 1 H, C[5 a]–H), 7.11–7.41 (m, 11 H, C[2–4b]–H & C[2–4c]–H & C[4 a]–H), 7.95 (dd, J = 5.0 Hz, J = 1.5 Hz, 1 H, C[6 a]–H) ppm. ^{13}C -NMR ($CDCl_3$, 50 MHz): δ = 17.0 (q, C[7a]), 32.8 (t, C[4]), 38.9 (t, C[3]), 54.6 (d, C[2]), 112.7 (d, C[5a]), 116.3 (s, C[3a]), 125.9 (d, C[4c]), 126.6 (d, C[4b]), 127.0 (d, C[2b]), 128.4 (d, C[2c]), 128.4 (d, C[3b]), 128.6 (d, C[3c]), 136.8 (d, C[4a]), 142.1 (s, C[1c]), 144.1 (s, C[1b]), 145.6 (d, C[6a]), 156.1 (s, C[2a]) ppm.

4.3.1.3. Cyclohexene



The reaction was carried out according to general procedure I with **1** (100 mg, 0.50 mmol, 1 eq.), cyclohexene (496 mg, 6.0 mmol, 12 eq.), K_2CO_3 (209 mg, 1.5 mmol, 3 eq.) and $[RhCl(cod)]_2$ (12 mg, 0.025 mmol, 0.05 eq.) in dry and degassed toluene (2 ml). The reaction mixture was heated for 24 h at 150 °C. The general work-up procedure for C–H activation reactions was followed (LP/EtOAc 99:1) and the products **7** (39 %), **8** (3 %) and **4** (7 %) together with unreacted **1** (32 %) were isolated.

4. Experimental

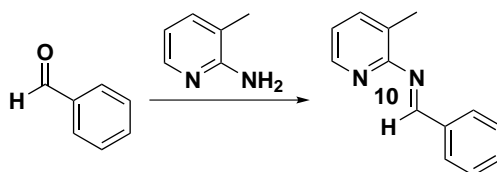
N-(cyclohexyl(phenyl)methyl)-3-methylpyridin-2-amine (7) Colourless solid (55 mg, 39%). mp = 107 °C–109 °C $^1\text{H-NMR}$ (CDCl_3 , 200 MHz): δ = 0.94–1.34 (m, 5 H, C[4–8]– H_{eq}), 1.45–1.98 (m, 6 H, C[3–8]– H_{ax}), 2.12 (s, 3 H, C[7a]– H_3), 4.50 (d, J = 8.2 Hz, 1 H, N[1]–H), 5.18 (m, 1 H, C[2]–H), 6.42 (dd, J = 7.0, 5.1 Hz, 1 H, C[5a]–H), 7.11–7.35 (m, 6 H, C[4a]–H, C[2–4b]–H), 7.92 (dd, J = 5.0, 1.5 Hz, 1 H, C[6a]–H) ppm. $^{13}\text{C-NMR}$ (CDCl_3 , 50 MHz): δ = 17.1 (q, C[7a]), 26.3 (t, C[6]), 26.4 (t, C[7]), 26.5 (t, C[5]), 29.5 (t, C[8]), 30.4 (t, C[4]), 44.1 (d, C[3]), 59.2 (d, C[2]), 112.4 (d, C[5a]), 116.0 (s, C[3a]), 126.5 (d, C[4b]), 127.1 (d, C[2b]), 128.1 (d, C[3b]), 136.7 (d, C[4a]), 143.4 (s, C[1b]), 145.6 (d, C[6a]), 156.4 (s, C[2a]) ppm. HRMS: calculated for $\text{C}_{19}\text{H}_{25}\text{N}_2$ [$\text{M} + \text{H}$] $^+$ 281.2012; found 281.2016.

N-(dicyclohexylmethyl)-3-methylpyridin-2-amine (8) Colourless oil (4 mg, 3%). $^1\text{H-NMR}$ (CDCl_3 , 200 MHz): δ = 0.93–1.30 (m, 10 H, C[4–8]– H_{eq}), 1.50–1.78 (m, 12 H, C[3–8]– H_{ax}), 2.09 (s, 3 H, C[7a]– H_3), 3.85 (d, J = 9.9 Hz, 1 H, N[1]–H), 4.13 (dt, J = 9.9, 6.4 Hz 1 H, C[2]–H), 6.41 (dd, J = 6.9, 5.1 Hz, 1 H, C[5a]–H), 7.17 (d, J = 6.9 Hz, 1 H, C[4a]–H), 7.94 (m, 1 H, C[6a]–H) ppm. $^{13}\text{C-NMR}$ (CDCl_3 , 50 MHz): δ = 17.2 (q, C[7a]), 26.5 (t, C[5], C[7]), 26.6 (t, C[6]), 28.1 (t, C[8]), 30.7 (t, C[4]), 39.9 (d, C[3]), 57.9 (d, C[2]), 111.3 (d, C[5a]), 115.1 (s, C[3a]), 136.6 (d, C[4a]), 145.3 (d, C[6a]), 158.0 (s, C[2a]) ppm. HRMS: calculated for $\text{C}_{19}\text{H}_{31}\text{N}_2$ [$\text{M} + \text{H}$] $^+$ 287.2482; found 287.2486.

N-Benzhydryl-3-methylpyridin-2-amine (4) Colourless oil (9.6 mg, 7%). Analytical data was in accordance to literature reports³³ and to previously reported data (vide supra).

4.3.2. Synthesis of Imines

4.3.2.1. N-(3-methylpyridin-2-yl)-1-phenylmethanimine (10)

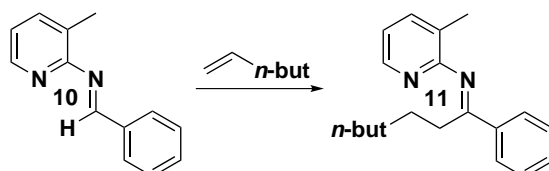


A procedure from literature⁸⁰ was followed to synthesise **10**. The reaction was carried out according to general procedure II with benzaldehyde (1.0 ml, 9.81 mmol, 1.1 eq.), 2-amino-3-methylpyridine (973 mg, 9.00 mmol, 1 eq.) and molecular sieves 4 Å (608 mg, 15 %[m/v]) in dry THF (4 ml). The reaction mixture was heated overnight at 70 °C. After cooling the reaction mixture to room temperature it was filtrated, washed with dry THF and concentrated in vacuo. The crude residue was purified by Kugelrohr distillation (120 °C, 0.23 mbar). Yellowish oil (592 mg,

4. Experimental

33%). Analytical data was in accordance to literature reports.⁸⁰ ¹H-NMR (CDCl₃, 200 MHz): δ = 2.47 (s, 3 H, C[7 a]–H₃), 7.09 (dd, J = 7.4, 4.7 Hz, 1 H, C[5 a]–H), 7.44–7.59 (m, 4 H, C[4 a]–H, C[3 –4b]–H), 7.98–8.06 (m, 2 H, C[2 b]–H), 8.32 (m, 1 H, C[6 a]–H), 9.09 (s, 1 H, C[2]–H) ppm.

4.3.2.2. 3-methyl-N-(1-phenylheptylidene)-2-pyridinamine (11)

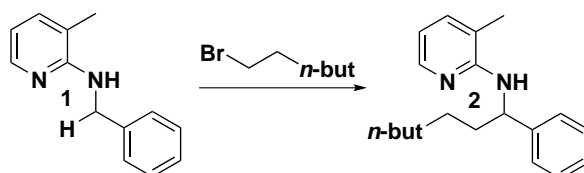


A procedure from literature⁸¹ was modified to synthesise **11**. The reaction was carried out according to general procedure II with **10** (74 mg, 0.38 mmol, 1 eq.), hex-1-ene (158 mg, 1.9 mmol, 5 eq.), dry K₂CO₃ (155 mg, 1.1 mmol, 3 eq.) and [RhCl(PPh₃)₃] (35 mg, 0.038 mmol, 0.1 eq.) in dry and degassed toluene (3 ml). The reaction mixture was heated for 3 h at 150 °C. The general work-up procedure for C–H activation reactions was followed (LP/CH₂Cl₂/Et₃N 97:2:1). Yellowish oil (43 mg, 41 %). ¹H-NMR (CD₂Cl₂, 200 MHz): δ = 0.79 (t, J = 7.1 Hz, 3 H, C[8]–H₃), 1.02–1.32 (m, 6 H, C[5 –7]–H₂), 1.39–1.62 (m, 2 H, C[4]–H₂), 2.13 (s, 3 H, C[7 a]–H₃), 2.63 (m, 2 H, C[3]–H₂), 6.96 (dd, J = 7.1, 5.0 Hz, 1 H, C[5 a]–H), 7.37–7.58 (m, 4 H, C[4 a]–H, C[3 –4b]–H), 7.92–8.08 (m, 2 H, C[2 b]–H), 8.25 (d, J = 4.2 Hz, 1 H, C[6 a]–H) ppm. ¹³C-NMR (CD₂Cl₂, 100 MHz): δ = 14.3 (q, C[8]), 17.7 (q, C[7a]), 22.9 (t, C[7]), 28.0 (t, C[6]), 29.8 (t, C[5]), 31.6 (t, C[4]), 31.7 (t, C[3]), 119.5 (d, C[5a]), 124.1 (s, C[3a]), 128.3 (d, C[3b]), 128.9 (d, C[2b]), 131.1 (d, C[4b]), 138.5 (d, C[4a]), 138.9 (s, C[1b]), 146.5 (d, C[6a]), 162.6 (s, C[2a]), 171.41 (s, C[2]) ppm. HRMS: calculated for C₁₉H₂₅N₂ [M + H]⁺ 281.2012; found 281.2002. IR (ATR): $\nu_{\text{C=N}}$ = 1635 cm⁻¹.

4.3.3. Substrate Scope - Alkylbromides

K₂CO₃ with an adsorbed water content of 2 m%, a particle size median of 0.34 μm and a specific BET surface of 0.4 m² g⁻¹ was used.

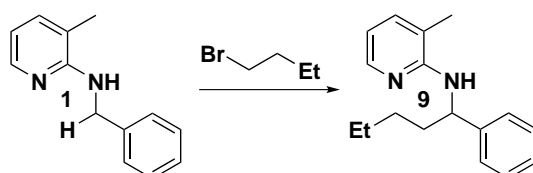
4.3.3.1. N-(1-phenylheptyl)-3-methylpyridin-2-amine (2)



4. Experimental

The reaction was carried out according to general procedure II with **1** (24.8 mg, 0.125 mmol, 1 eq.), 1-bromohexane (61.9 mg, 0.375 mmol, 3 eq.), K_2CO_3 (78 mg, 0.56 mmol, 4.5 eq.) and $[RhCl(cod)]_2$ (3 mg, 0.00625 mmol, 0.05 eq.) in dry and degassed toluene (1 ml). The reaction mixture was heated for 22 h at 160 °C. The general work-up procedure for C–H activation reactions was followed (LP/EtOAc 99:1). Sideproduct **16** could not be separated from **2**. Colourless oil (18 mg, 50%). GC purity: 89%. Analytical data was otherwise in accordance to what was mentioned earlier for **2**.

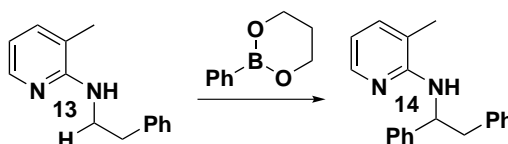
4.3.3.2. 3-methyl-N-(1-phenylpentyl)pyridin-2-amine (**9**)



The reaction was carried out according to general procedure I with **1** (100 mg, 0.50 mmol, 1 eq.), 1-bromobutane (206 mg, 1.50 mmol, 3 eq.), K_2CO_3 (208 mg, 1.50 mmol, 3 eq.) and $[RhCl(cod)]_2$ (12 mg, 0.025 mmol, 0.05 eq.) in dry toluene (2 ml). The reaction mixture was heated for 24 h at 160 °C. The general work-up procedure for C–H activation reactions was followed (LP/EtOAc 99:1). The side-product with an *n*-propyl instead of an *n*-butyl group could not be separated from **9**. Colourless oil (64 mg, 50%). GC purity: 76%. 1H -NMR ($CDCl_3$, 200 MHz): δ = 0.87 (t, J = 6.7 Hz, 3 H, C[6]–H₃), 1.16–1.49 (m, 4 H, C[4–5]–H₂), 1.71–1.99 (m, 2 H, C[3]–H₂), 2.10 (s, 3 H, C[7a]–H₃), 4.37 (d, J = 7.5 Hz, 1 H, N[1]–H), 5.23 (q, J = 7.4 Hz, 1 H, C[2]–H), 6.45 (dd, J = 7.1, 5.1 Hz, 1 H, C[5a]–H), 7.15–7.39 (m, 6 H, C[4a]–H, C[2–4b]–H), 7.95 (dd, J = 5.1, 1.4 Hz, 1H, C[6a]–H) ppm. ^{13}C -NMR ($CDCl_3$, 50 MHz): δ = 14.0 (q, C[6]), 17.1 (q, C[7a]), 22.7 (t, C[5]), 28.5 (t, C[4]), 37.3 (t, C[3]), 54.6 (d, C[2]), 112.5 (d, C[5a]), 116.1 (s, C[3a]), 126.5 (d, C[2b]), 126.7 (d, C[4b]), 128.4 (d, C[3b]), 136.7 (d, C[4a]), 144.6 (s, C[1b]), 145.6 (d, C[6a]), 156.2 (s, C[2a]) ppm. HRMS: calculated for $C_{17}H_{23}N_2$ [$M + H$]⁺ 255.1856; found 255.1853.

4.3.4. Synthesis of Sideproduct 1

4.3.4.1. N-(1,2-diphenylethyl)-3-methylpyridin-2-amine (**14**)

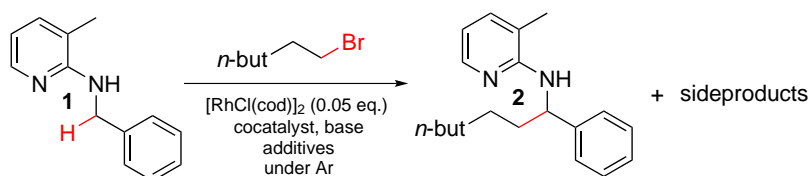


4. Experimental

A procedure from literature³³ was modified to synthesise **14**. The reaction was carried out according to general procedure I with **13** (74.9 mg, 0.353 mmol, 1 eq.), 2-phenyl-1,3,2-dioxaborinane (85.3 mg, 0.527 mmol, 1.5 eq.) and Ru₃CO₁₂ (11.3 mg, 0.0173 mmol, 0.05 eq.) in dry pinacolone (0.35 ml). The reaction mixture was heated overnight at 150 °C. Then, additional Ru₃CO₁₂ (13.0 mg, 0.0199 mmol, 0.058 eq.) was added and the reaction mixture was heated for 3 days at 140 °C. The general work-up procedure for C–H activation reactions was followed (LP/EtOAc 99:1 to 98:2). Brownish oil (32 mg, 31 %). Analytical data was in accordance to literature reports.³³ ¹H-NMR (CDCl₃, 200 MHz): δ = 2.03 (s, 3 H, C[7 a]–H₃), 3.19 (d, J = 6.7 Hz, 2 H, C[3]–H₂), 4.45 (d, J = 6.7 Hz, 1 H, N[1]–H), 5.52 (d, J = 6.7 Hz, 1 H, C[2]–H), 7.03-7.09 (m, 2 H, C[2 c]–H), 7.13-7.33 (m, 9 H, C[3–4c]–H, C[2–4b]–H, C[5 a]–H), 7.94 (m, 1 H, C[6 a]) ppm.

4.4. Screening Experiments

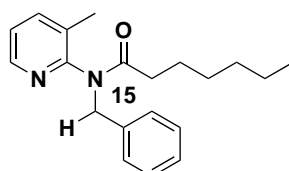
4.4.1. General Procedure



All experiments were carried out according to general procedure II for C–H activations. In all experiments, the concentration of **1** was 0.125 mol l⁻¹ and of [RhCl(cod)]₂ was 0.00625 mol l⁻¹ at the beginning. The reaction mixtures were stirred with 900 rpm on a Heidolph MR Hei-Standard magnetic stirrer. Quantifications were performed by means of GC analysis of the crude reaction mixtures using dodecane as internal standard which was added after stopping the reaction. All results are found in the Appendices.

4.4.2. Isolation of Sideproduct 2

4.4.2.1. N-benzyl-N-(3-methylpyridin-2-yl)heptanamide (**15**)



In order to isolate compound **15** several reaction mixtures from the screening experiments were pooled and worked up together. The general work-up procedure

4. Experimental

for C–H activation reactions was followed (LP/EtOAc 99:1 to 89:11 until **15** eluted). Yellow oil. The numbering of the aliphatic chain in **15** for the assignment of NMR-signals was inverted compared to Figure 4.1. ¹H-NMR (CDCl₃, 400 MHz): δ = 0.88 (t, J = 6.9 Hz, 3H, C[9]–H₃), 1.17-1.38 (m, 6H, C[8]–H₂, C[7]–H₂, C[6]–H₂), 1.66 (m, 2H, C[5]–H₂), 1.88-2.11 (m, 5H, C[4]–H₂, C[7 a]–H₃), 4.70 (d, J = 14 Hz, 1H, C[1]–H₂), 5.21 (d, J = 14 Hz, 1H, C[1]–H₂), 7.22-7.34 (m, 6H, C[5 a]–H, C[2–4b]–H), 7.59 (d, J = 7.3 Hz, 1H, C[4 a]–H), 8.47 (d, J = 3.8 Hz, 1H, C[6 a]–H) ppm. ¹³C-NMR (CDCl₃, 100 MHz): δ = 14.02 (q, C[9]), 17.06 (q, C[7a]), 22.43 (t, C[8]), 25.06 (t, C[7]), 28.97 (t, C[6]), 31.50 (t, C[5]), 34.34 (t, C[4]), 51.24 (d, C[1]), 123.37 (d, C[5a]), 127.35 (d, C[4b]), 128.26 (d, C[2b]), 129.25 (d, C[3b]), 131.70 (s, C[3a]), 137.13 (s, C[1b]), 140.04 (d, C[4a]), 147.62 (d, C[6a]), 153.97 (s, C[2a]), 172.71 (s, C[3]) ppm. HRMS: calculated for C₂₀H₂₇N₂O [M + H]⁺ 311.2118; found 311.2103.

4.5. Kinetic Experiments

All data points are found in the Appendices.

4.5.1. General Procedure

All experiments were performed in oven-dried 8 ml vials with a fully covered solid Teflon-lined cap and a magnetic stirring bar, unless noted otherwise. Unless stated otherwise, the reaction mixtures were heated in a pre-heated aluminium reaction block (150 °C) and the highest possible stirring rate (1400 rpm) on a Heidolph MR Hei-Standard was used. Time measurement was started immediately after placing the vials in the aluminium block. Unless noted otherwise, quantifications were performed by means of GC analysis of the crude reaction mixtures using dodecane as internal standard and based on calibration curves for compounds **1**, **2**, **3** and **4**, respectively, to determine their concentrations. Each kinetic experiment was performed in triplicate unless noted otherwise. GC measurements for quantifications were also performed in triplicate and the result for one sample was calculated as average over those 3 measurements and the corresponding error was calculated as standard deviation over those experiments. Given values are therefore averages over three experiments and the corresponding error is the standard deviation over those experiments.

General procedure II for C–H activations was followed. Unless noted otherwise, K₂CO₃ with an adsorbed water content of 15 m%, a particle size median of 0.95 μm and a specific BET surface of 0.8 m² g⁻¹ was used. For every individual experiment K₂CO₃ was placed in the vial. The vial was then transferred into a glove-box under argon. Cyclooctadiene rhodium chloride dimer (0.0313 mol l⁻¹ solution), benzylic

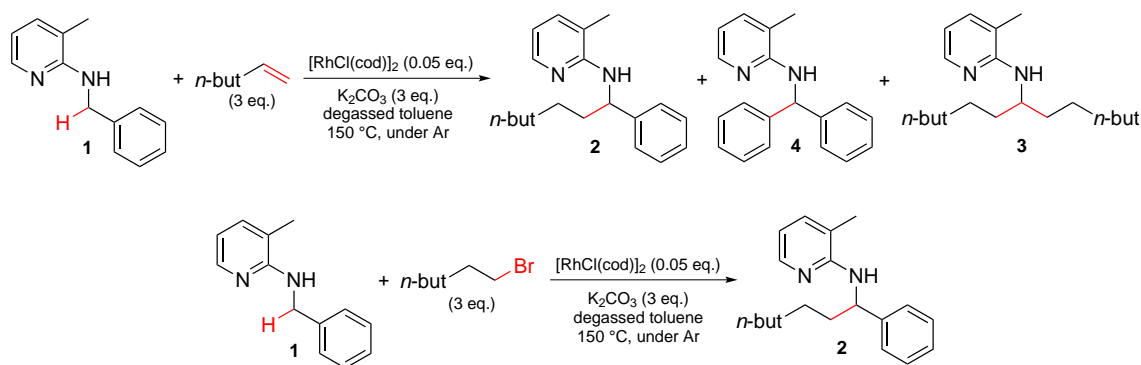
4. Experimental

amine derivative (0.625 mol l^{-1} solution), hex-1-ene (1.88 mol l^{-1} solution) and 1-bromohexane (1.88 mol l^{-1} solution) were added in solutions inside the glove-box and toluene as pure solvent was also added inside the glove-box. Reactions were stopped by immediately cooling them down to room temperature in a water bath.

Concentrations given for K_2CO_3 are not really concentrations since it is not completely dissolved in the reaction mixture. They can be viewed as molar loading with respect to the total reaction volume. In order to estimate the total reaction volume the volumes of all solutions and the pure solvent were assumed to be additive.

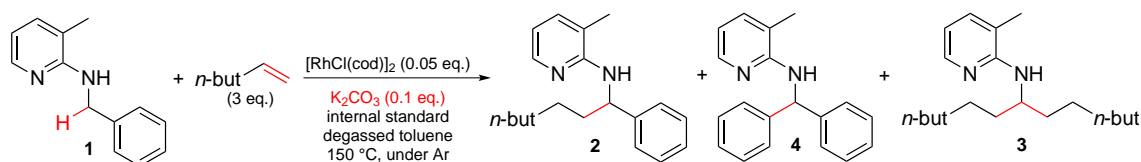
4.5.2. Kinetic Profiles

4.5.2.1. Kinetic Profile Comparison



All experiments were performed according to the general procedure for kinetic experiments.

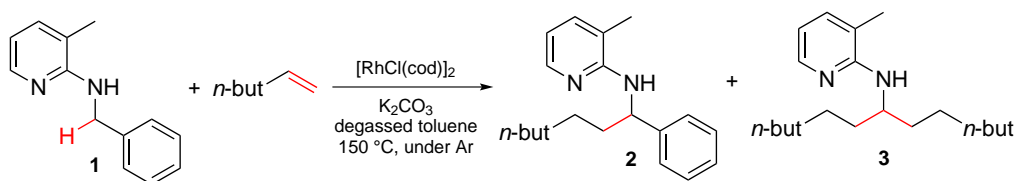
4.5.2.2. Kinetic Profile using Alkenes with K_2CO_3 in Catalytic Amounts



This experiment was performed according to the general procedure for kinetic experiments. K_2CO_3 with an adsorbed water content of 2 m%, a particle size median of $0.34 \mu\text{m}$ and a specific BET surface of $0.4 \text{ m}^2 \text{ g}^{-1}$ was used. Dodecane was added as internal standard during the reaction. In order to take samples the vial was opened inside a glove-box after stopping the reaction. The vial was closed again and the reaction was continued after taking each sample until the reaction did not proceed further.

4. Experimental

4.5.3. Kinetic Model - Alkene Alkylation

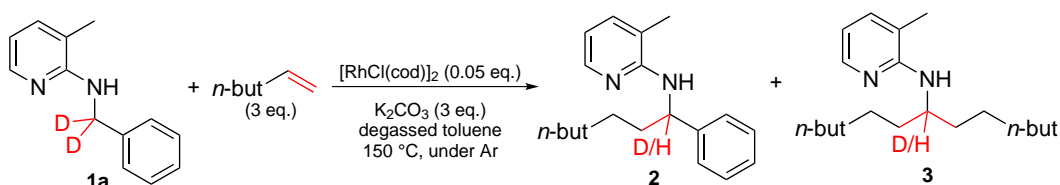


All experiments were performed according to the general procedure for kinetic experiments. All data points are found in the Appendices.

4.5.4. KIE Studies

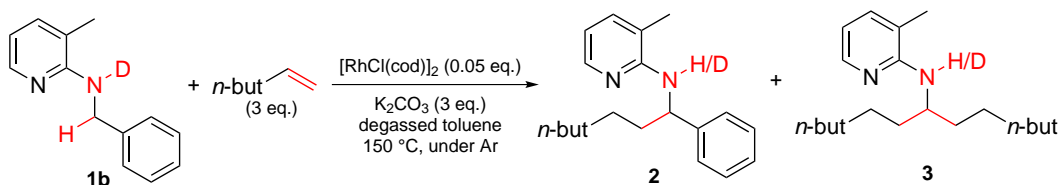
All experiments were performed according to the general procedure for kinetic experiments.

4.5.4.1. KIE of Benzylic C–H



The experiments were performed both with K_2CO_3 having an adsorbed water content of 15 m%, a particle size median of $0.95\ \mu\text{m}$ and a specific BET surface of $0.8\ \text{m}^2\ \text{g}^{-1}$ and with K_2CO_3 having an adsorbed water content of 2 m%, a particle size median of $0.34\ \mu\text{m}$ and a specific BET surface of $0.4\ \text{m}^2\ \text{g}^{-1}$. The deuterium content in the remaining unreacted starting material was determined by ^1H -NMR analysis of the crude residue after filtration of the reaction mixture and evaporation of the solvent.

4.5.4.2. KIE of N–H



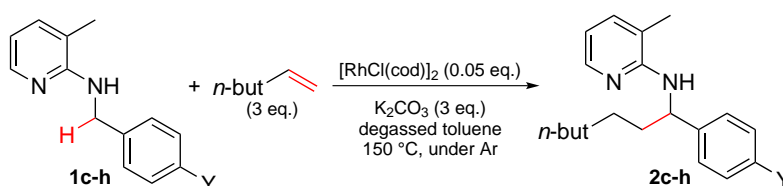
Compound **1b** was obtained by dissolving **1** in MeOD ($c = 0.21\ \text{mol l}^{-1}$) under an inert atmosphere of argon and letting the resulting solution stand for 1 h. The

4. Experimental

solvent was removed in vacuo and the deuterated compound **1b** was obtained with a typical deuterium content of 95%. IR (Transmission): $\nu = 2559 \text{ cm}^{-1}$.

K_2CO_3 with 2 m% adsorbed water, a particle size median of $0.34 \mu\text{m}$ and a specific BET surface of $0.4 \text{ m}^2 \text{ g}^{-1}$ was used. The deuterium content in the unreacted starting material was determined by IR analysis of the reaction mixture based on calibration curves for the N-H (3453 cm^{-1}) and the N-D (2559 cm^{-1}) bands of **1** and **1b**, respectively.

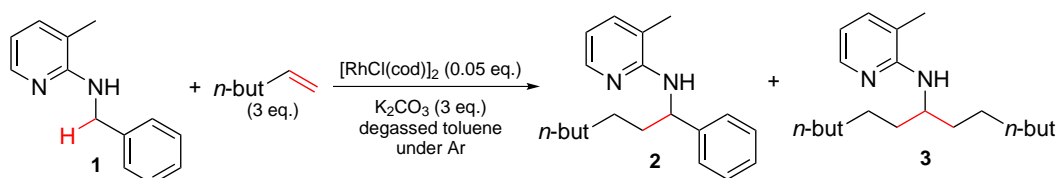
4.5.5. Electronic Influence on Benzylic Amines



Compound	Y
1c	OMe
1d	Me
1e	F
1f	Cl
1g	CO_2Me
1h	CF_3

All experiments were performed according to the general procedure for kinetic experiments. However, quantification of the reaction products was performed by $^1\text{H-NMR}$ analysis (400 MHz) of the crude residue in CDCl_3 after filtration of the reaction mixture and evaporation of the solvent with respect to DMSO as internal standard. In addition, for derivatives **1g** and **1h** ($\text{Y} = \text{CO}_2\text{Me}$ and CF_3 , respectively) the solubility in toluene was not high enough to prepare stock solutions with the same concentration as used for all other derivatives so these compounds were directly weighed as solids.

4.5.6. Temperature Dependence of the Initial Rate

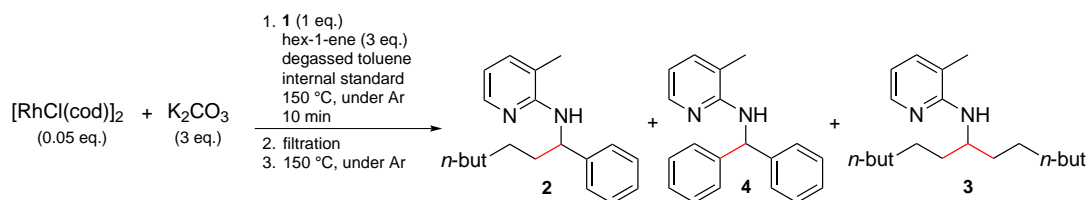


4. Experimental

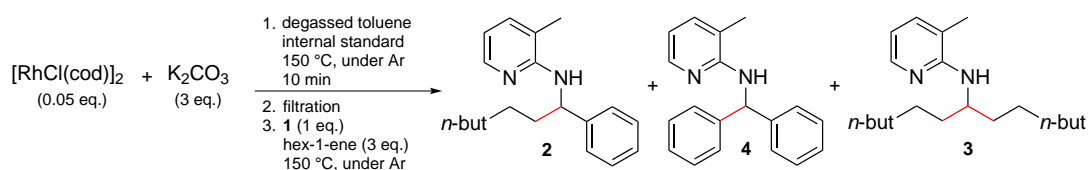
All experiments were performed according to the general procedure for kinetic experiments. However, reaction mixtures were placed in a pre-heated oil bath at the desired temperature in order to control the temperature of the reaction mixture more precisely. In addition, reaction mixtures were only stirred moderately (375 rpm, Heidolph MR Hei-Standard) in order to provide for proper stirring inside the oil bath as well.

4.5.7. Induction Time Studies

Experiments were performed according to the general procedure for kinetic experiments. K_2CO_3 with an adsorbed water content of 2 m%, a particle size median of $0.34 \mu\text{m}$ and a specific BET surface of $0.4 \text{ m}^2 \text{ g}^{-1}$ was used. Dodecane was added as internal standard during the reaction. In order to take samples the vial was opened inside a glove-box after stopping the reaction. The vial was closed again and the reaction was continued after taking each sample. Filtrations were performed using syringe filters with a pore size of $0.2 \mu\text{m}$.

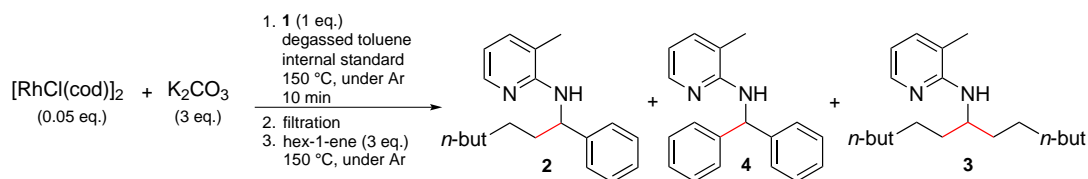


In the first experiment $[\text{RhCl}(\text{cod})]_2$, K_2CO_3 , hex-1-ene and **1** with dodecane as internal standard were reacted for 10 min at 150°C . After stopping the reaction the vial was transferred into a glove-box and the reaction mixture was filtrated into another vial charged with a stirring bar. The solid residue in the first vial was washed two times with 0.5 ml toluene and **1** (1 eq.) and hex-1-ene (3 eq.) with dodecane as internal standard were added. Both vials were heated again to 150°C to restart the reaction. Additional samples of both reaction mixtures were taken.

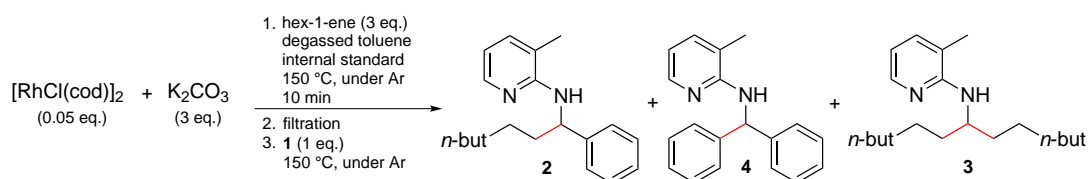


In the second experiment $[\text{RhCl}(\text{cod})]_2$ and K_2CO_3 were reacted for 10 min at 150°C . After stopping the reaction the vial was transferred into a glove-box. **1** (1 eq.), hex-1-ene (3 eq.) and dodecane as internal standard were added to the reaction mixture before filtration. The reaction mixture was filtrated into another vial charged with a stirring bar. The vial containing the filtrate was heated again to 150°C to restart the reaction. Additional samples of the reaction mixture were taken.

4. Experimental



In the third experiment $[\text{RhCl}(\text{cod})]_2$, K_2CO_3 and **1** with dodecane as internal standard were reacted for 10 min at 150 °C. After stopping the reaction the vial was transferred into a glove-box. Hex-1-ene (3 eq.) was added to the reaction mixture before filtration. The reaction mixture was filtrated into another vial charged with a stirring bar. The vial containing the filtrate was heated again to 150 °C to restart the reaction. Additional samples of the reaction mixture were taken.



In the fourth experiment $[\text{RhCl}(\text{cod})]_2$, K_2CO_3 and hex-1-ene were reacted for 10 min at 150 °C. After stopping the reaction the vial was transferred into a glove-box. **1** (1 eq.) and dodecane as internal standard were added to the reaction mixture before filtration. The reaction mixture was filtrated into another vial charged with a stirring bar. The vial containing the filtrate was heated again to 150 °C to restart the reaction. Additional samples of the reaction mixture were taken.

4.6. Mechanistic Experiments

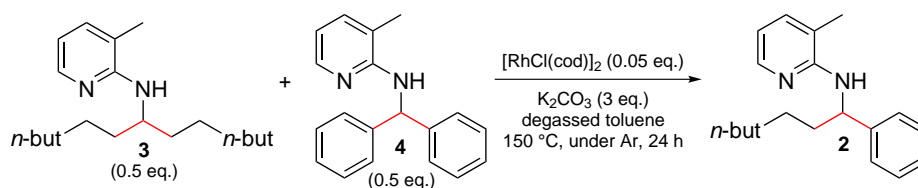
4.6.1. General Procedure

Unless noted otherwise, general procedure II for C–H activations was followed. Quantifications were performed by means of GC analysis of the crude reaction mixtures using dodecane as internal standard which was added after stopping the reaction. In all experiments 1 eq. was equal to a concentration of 0.125 mol l^{-1} in the reaction mixture, unless noted otherwise.

4.6.2. Sideproduct Experiment - Alkene

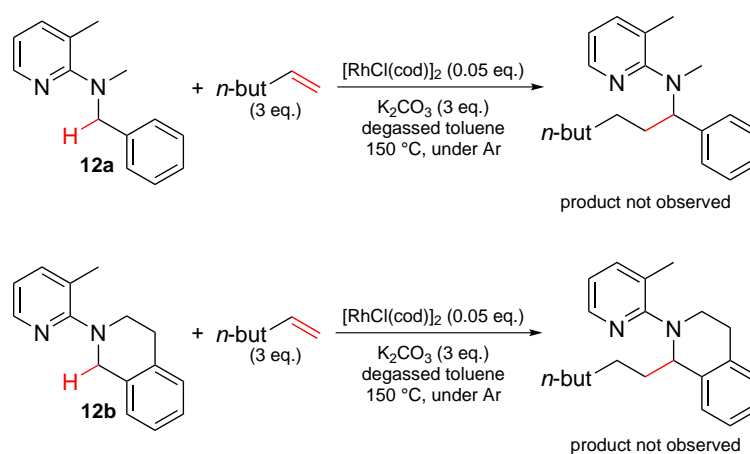
The experiment was performed on a 0.0625 mmol scale. K_2CO_3 with an adsorbed water content of 15 m%, a particle size median of $0.95 \mu\text{m}$ and a specific BET surface of $0.8 \text{ m}^2 \text{ g}^{-1}$ was used.

4. Experimental



Product Amounts			
1	2	3	4
<0.1 %	1 %	46 %	42 %

4.6.3. Substrate Scope - Tertiary Amines

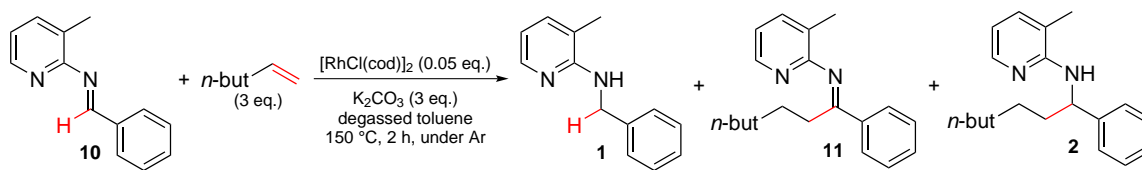


The experiments were performed on a 0.125 mmol scale. K_2CO_3 with an adsorbed water content of 2 m%, a particle size median of 0.34 μm and a specific BET surface of 0.4 $\text{m}^2 \text{g}^{-1}$ was used. In both experiments no conversion to any new product was observed neither after 3 nor after 24 h based on GC, GC/MS and TLC analysis.

4.6.4. Imine Experiments

The experiments were performed on a 0.0625 mmol scale. K_2CO_3 with an adsorbed water content of 2 m%, a particle size median of 0.34 μm and a specific BET surface of 0.4 $\text{m}^2 \text{g}^{-1}$ was used.

4. Experimental

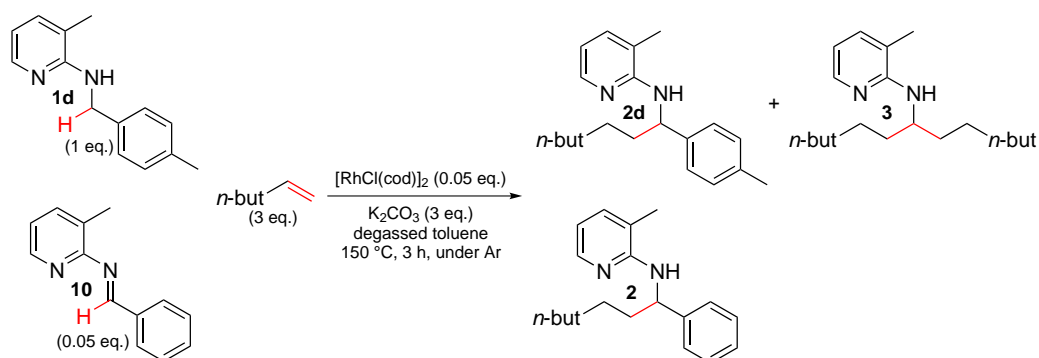


Product Amounts - Experiment 1

10	1	11	2
25 % ^a	3 % ^b	1 % ^a	0.2 % ^b

^aBased on GC analysis with dodecane as internal standard assuming a conversion factor of 1.

^bGC yield.



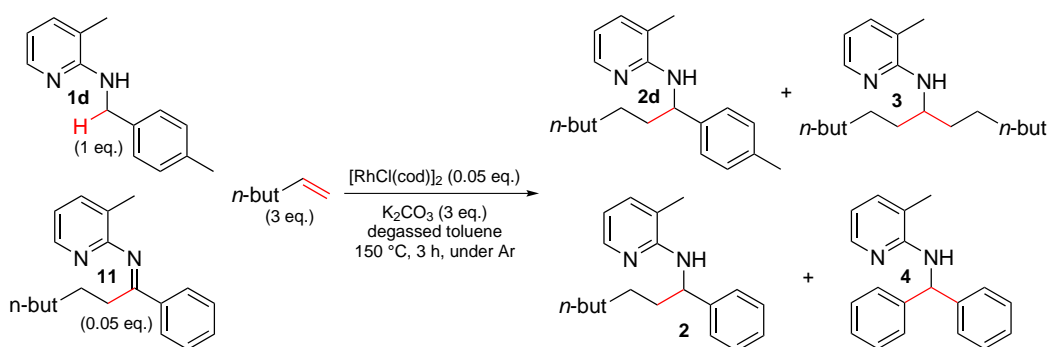
Product Amounts - Experiment 2

10	1d	2d	2	3
<0.1 % ^a	3 % ^a	95 % ^a	5 % ^b	6 % ^b

^aBased on GC analysis with dodecane as internal standard assuming a conversion factor of 1.

^bGC yield.

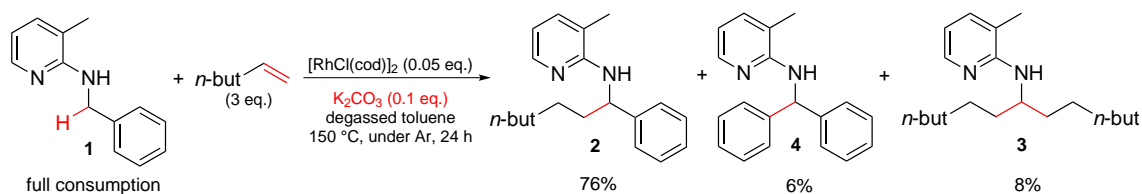
4. Experimental



Product Amounts - Experiment 3					
11	1d	2d	2	3	4
<0.1 % ^a	4 % ^a	99 % ^a	2 % ^b	6 % ^b	1 % ^b

^aBased on GC analysis with dodecane as internal standard assuming a conversion factor of 1.
^bGC yield.

4.6.5. K_2CO_3 in Catalytic Amounts



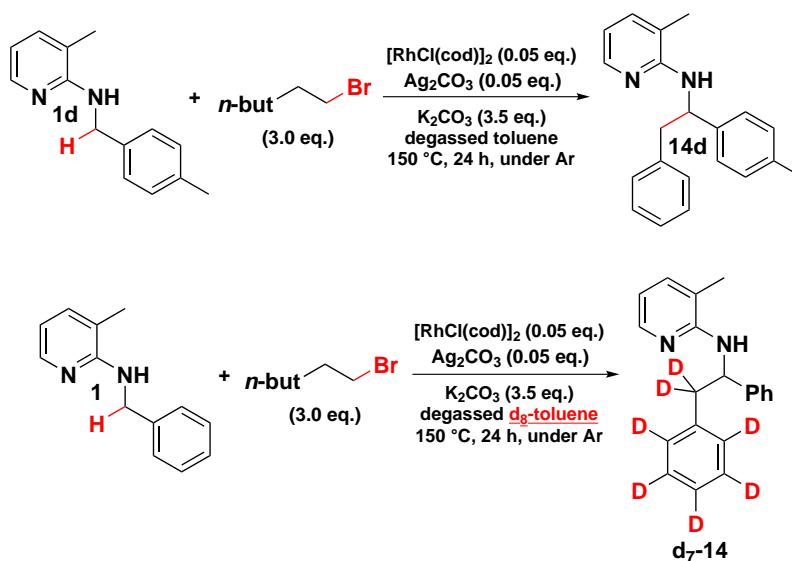
The experiment was performed on a 0.125 mmol scale. K_2CO_3 with an adsorbed water content of 2 m%, a particle size median of 0.34 μm and a specific BET surface of 0.4 $\text{m}^2 \text{g}^{-1}$ was used.

4.6.6. Sideproduct Experiments - Alkylbromide

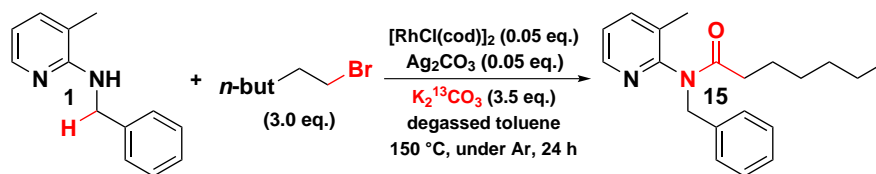
All experiments were carried out according to general procedure II for C–H activations. Experiments were performed on a 0.0625 mmol scale. In all experiments, the concentration of 1 was 0.125 mol l^{-1} and of $[\text{RhCl}(\text{cod})]_2$ was 0.00625 mol l^{-1} at the beginning. Quantifications were performed by means of GC analysis of the crude reaction mixtures using dodecane as internal standard which was added after stopping the reaction. Mass spectra of the reaction products were obtained by GC/MS analysis of the crude reaction mixtures.

4. Experimental

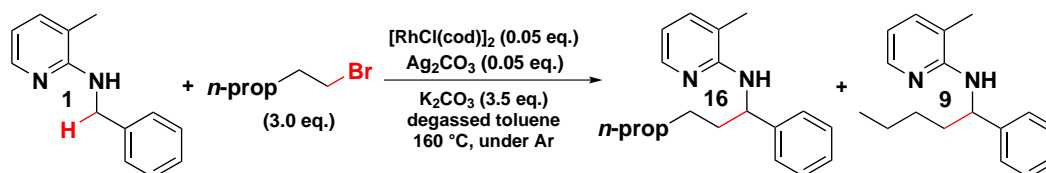
4.6.6.1. Sideproduct I (14)



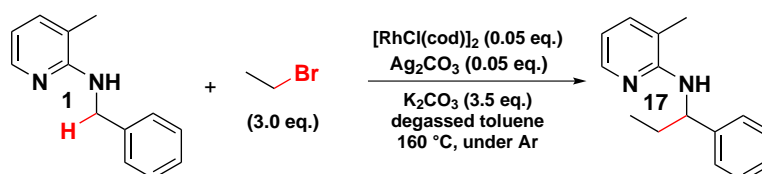
4.6.6.2. Sideproduct II (15)



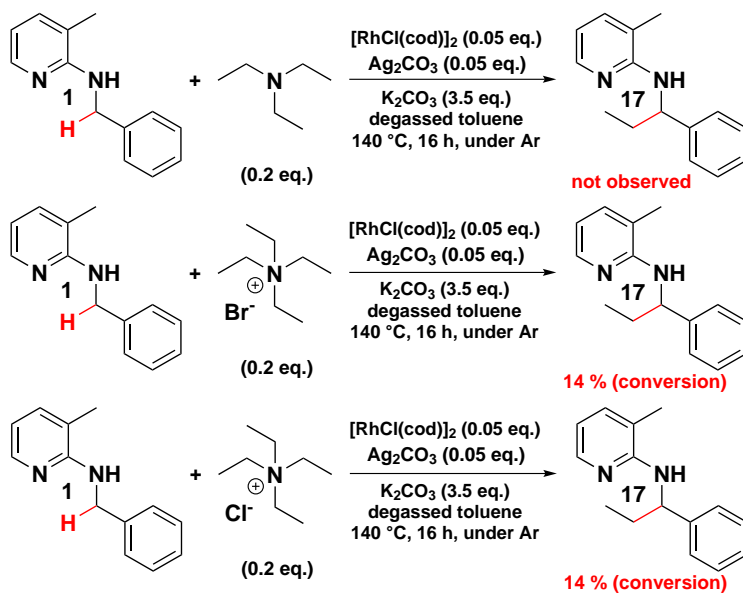
4.6.6.3. Sideproduct III (16)



4.6.6.4. Sideproduct IV (17)



4. Experimental



5. Data Evaluation and Mathematical Derivations

The following Chapter contains the evaluations of the experimental results and mathematical derivations for new methods that were applied in the course of this thesis and for the proposed kinetic model. The document structure is the same as in Chapter 3 in order to make it simpler to find the corresponding evaluations and calculations. However, in order to keep this Chapter concise the respective schemes of all the experiments are not given again.

5.1. General Remarks

Errors given for regression parameters are standard errors and not standard deviations. Numbers are rounded to the last given digit. Errors given for derived parameters are determined using error propagation.

5.2. Direct Alkylations using Alkenes

5.2.1. Investigations into the Mechanistic Outline

5.2.1.1. KIE Studies

Correction for H-D exchange during the reaction In this section the method used to correct the KIE determined by the initial rates of a reaction with both unlabelled and isotopically labelled starting materials is derived. First all the parameters used in the derivation are defined.

- r_H ... Initial rate of the reaction with unlabelled (H) starting material [$\text{mol l}^{-1} \text{s}^{-1}$]
- r_D ... Initial rate of the reaction with isotopically labelled (D) starting material [$\text{mol l}^{-1} \text{s}^{-1}$]
- r_{obs} ... Observed initial rate with mixture of isotopically labelled and unlabelled starting materials [$\text{mol l}^{-1} \text{s}^{-1}$]
- x_H ... Mole fraction of unlabelled starting material in the reaction mixture
- x_{Ha} ... Mole fraction of unlabelled starting material at the effective reaction start time

5. Data Evaluation and Mathematical Derivations

x_{He} ... Mole fraction of unlabelled starting material at the effective reaction end time

x_D ... Mole fraction of isotopically labelled starting material in the reaction mixture

t ... Reaction time [s]

t_a ... Effective start time of the reaction [s]

t_e ... Effective end time of the reaction [s]

c_{obs} ... Observed concentration of reaction product in the experiment [$mol\ l^{-1}$]

The general simplified approach is that the change of product concentration over time is a linear combination of product formed from unlabelled starting material and product formed from isotopically labelled starting material. If the corresponding rates for both unlabelled starting material and labelled starting material are assumed to be time-independent the reaction is assumed to be in a period of constant reaction rate i.e. the initial reaction period. In a general approach, however, the rates have to be assumed to be functions of time.

$$dc_{obs} = r_H x_H(t) dt + r_D x_D(t) dt \quad (5.1)$$

The following equation is assumed in order to eliminate one of the two mole fractions.

$$x_D(t) = 1 - x_H(t) \quad (5.2)$$

Equation 5.2 is substituted into Equation 5.1.

$$dc_{obs} = (r_H - r_D) x_H(t) dt + r_D dt \quad (5.3)$$

Integration of Equation 5.3 yields Equations 5.4 and 5.5 assuming the reaction is in the initial reaction period and the reaction rates are independent from time in that reaction period (i.e. the reaction is in the initial reaction period showing linear decrease and increase of starting materials and products, respectively).

$$c_{obs} = \int_{t_a}^{t_e} (r_H - r_D) x_H(t) dt + r_D (t_e - t_a) \quad (5.4)$$

$$r_{obs} = \frac{c_{obs}}{t_e - t_a} = r_D + \frac{r_H - r_D}{t_e - t_a} \int_{t_a}^{t_e} x_H(t) dt \quad (5.5)$$

This general formula allows determination of the true initial rate of the reaction with isotopically labelled starting material from the observed initial rate if the time dependence of the mole fraction of unlabelled starting material over the course of the reaction is known.

In an optimal case this time dependence can be measured directly with an in-situ method. Integration can then be performed with the usually applied approximative integration methods. However, when for any reason an in-situ method cannot be

5. Data Evaluation and Mathematical Derivations

used either a lot of additional experiments have to be performed to determine the time dependence of this mole fraction accurately or this time dependence needs to be simplified in order to reduce the number of necessary experiments. The simplest case would be to determine this mole fraction at the effective start of the reaction and at the end of the reaction and assuming linear time dependence in between. Besides being very simple this method also has the advantage that it is more likely to overestimate the true initial rate of the reaction with isotopically labelled starting material rather than underestimate it because the time dependence of the mole fraction is more likely to have a negative curvature. So, corrected KIE values are therefore estimated to be slightly lower by this method compared to KIE values corrected with the true time dependence of the mole fraction. Keeping this in mind is important to correctly interpret the obtained corrected KIE values.

In order to integrate Equation 5.5 a linear dependence of x_H on time is assumed. For this linear dependence x_{Ha} and x_{He} at the time points t_a and t_e , respectively, are known and therefore its analytical form can easily be derived by solving a system of two linear equations. The corresponding solution is given in equation 5.6.

$$x_H(t) = \frac{x_{He} - x_{Ha}}{t_e - t_a}t + \frac{x_{Ha}t_e - x_{He}t_a}{t_e - t_a} \quad (5.6)$$

From Equations 5.5 and 5.6 the integral can easily be determined and the equation can be solved for the initial rate of only the isotopically labelled starting material (cf. Equations 5.7-5.12).

$$r_{obs} = r_D + \frac{r_H - r_D}{t_e - t_a} \left[\frac{x_{He} - x_{Ha}}{2(t_e - t_a)}(t_e^2 - t_a^2) + \frac{x_{Ha}t_e - x_{He}t_a}{t_e - t_a}(t_e - t_a) \right] \quad (5.7)$$

$$r_{obs} = r_D + \frac{r_H - r_D}{t_e - t_a} \left[\frac{1}{2}(x_{He}t_e - x_{Ha}t_e + x_{He}t_a - x_{Ha}t_a) + x_{Ha}t_e - x_{He}t_a \right] \quad (5.8)$$

$$r_{obs} = r_D + \frac{r_H - r_D}{2(t_e - t_a)}(x_{He}t_e + x_{Ha}t_e - x_{He}t_a - x_{Ha}t_a) \quad (5.9)$$

$$r_{obs} = r_D + \frac{r_H - r_D}{2(t_e - t_a)}(x_{He} + x_{Ha})(t_e - t_a) \quad (5.10)$$

$$r_{obs} = r_H \frac{x_{He} + x_{Ha}}{2} + r_D \left(1 - \frac{x_{He} + x_{Ha}}{2} \right) \quad (5.11)$$

$$r_D = \frac{r_{obs} - r_H \frac{x_{He} + x_{Ha}}{2}}{1 - \frac{x_{He} + x_{Ha}}{2}} \quad (5.12)$$

Equation 5.12 allows for an easy correction of the observed initial rate in an experiment to determine the initial rate with isotopically labelled starting material in order to determine a KIE when there is also a high degree of H-D exchange going on during the reaction at a similar or even slightly higher rate.

5. Data Evaluation and Mathematical Derivations

KIE of benzylic C–H From the data points at hand the KIE value of the benzylic C–H bond using K_2CO_3 with an adsorbed water content of about 15% was determined to be 4.3 ± 0.6 indicating a significantly slower reaction using the corresponding deuterated compound. Correcting this KIE for the H–D exchange during the reaction assuming full deuteration before the start of the reaction a value of 4.9 ± 0.8 is obtained. Using K_2CO_3 with an adsorbed water content of only about 2% the KIE was 4.7 ± 0.6 , so basically the same showing that the KIE of the benzylic C–H bond is independent of the adsorbed water content of K_2CO_3 . The corrected KIE would be 5.2 ± 0.8 , so even more alike.

KIE of N–H Since the H-content of **1** was determined by IR analysis from the corresponding N–H and N–D stretching vibration bands the value could show a deviation due to a different H-content in the product of the reaction because the corresponding bands overlap. However, since in these experiments only about 5% of products were formed, the expected deviations in the H-content of **1** in a worst case scenario assuming only N–H being present in the product is only slightly outside the error margin (difference of 1.6 times the standard deviation to the determined value). In addition, the H-content in the product formed is expected to be similar to the H-content of the remaining starting material making this error effectively negligible.

5.2.1.2. Imine Intermediate Kinetics

In order to determine whether the reaction mechanism proceeds over the corresponding imine or not it was necessary to distinguish between the three general scenarios which are outlined in Figure 3.9. For the following mathematical derivation several variables are used.

- a ... Relative concentration of A (starting material)
- i ... Relative concentration of I (intermediate)
- p ... Relative concentration of P (product)
- t ... Time
- k_1 ... First-order rate constant for the reaction of A to I
- k_2 ... First-order rate constant for the forward reaction of I to P
- k_{-2} ... First-order rate constant for the backward reaction of P to I

It should be noted that all the rate constants are positive and for all the other variables values are bigger than or equal to 0, in general. Based on these mechanistic scenarios a method was developed to distinguish between them from kinetic data. First the following simplified kinetic model is assumed.



5. Data Evaluation and Mathematical Derivations

Based on this simplified kinetic model the following system of differential equations can be formulated.

$$\frac{da}{dt} = -k_1a \quad (5.14)$$

$$\frac{di}{dt} = k_1a + k_{-2}p - k_2i \quad (5.15)$$

$$\frac{dp}{dt} = -k_{-2}p + k_2i \quad (5.16)$$

In addition, it is assumed that the sum of the concentrations of A, I and P equals 1.

$$a + i + p = 1 \quad (5.17)$$

The solution of this system of differential equations is straightforward and will not be discussed in detail. The initial conditions were that at time 0 the relative concentration of A is 1 and those of I and P are 0, respectively.

$$a(0) = 1 \quad (5.18)$$

$$i(0) = 0 \quad (5.19)$$

$$p(0) = 0 \quad (5.20)$$

The following solutions for the time-dependent relative concentrations of A, I and P are obtained in case that k_1 does not equal the sum of k_{-2} and k_2 .

$$a(t) = e^{-k_1t} \quad (5.21)$$

$$i(t) = \frac{k_{-2}}{k_{-2} + k_2} (1 - e^{-(k_{-2}+k_2)t}) + \frac{k_1 - k_{-2}}{k_{-2} + k_2 - k_1} (e^{-k_1t} - e^{-(k_{-2}+k_2)t}) \quad (5.22)$$

$$p(t) = 1 - e^{-k_1t} - \frac{k_{-2}}{k_{-2} + k_2} (1 - e^{-(k_{-2}+k_2)t}) - \frac{k_1 - k_{-2}}{k_{-2} + k_2 - k_1} (e^{-k_1t} - e^{-(k_{-2}+k_2)t}) \quad (5.23)$$

As the difference of the sum of k_{-2} and k_2 and k_1 appears in the denominator in the functions for the relative concentrations of I and P this term is assumed to be unequal to 0 (which of course has to be assumed already during the derivation). In the case this equals 0 different solutions for the time course of the relative concentrations of I and P are obtained.

$$i(t) = \frac{k_{-2}}{k_{-2} + k_2} (1 - e^{-(k_{-2}+k_2)t}) + (k_1 - k_{-2})te^{-(k_{-2}+k_2)t} \quad (5.24)$$

$$p(t) = 1 - e^{-k_1t} - \frac{k_{-2}}{k_{-2} + k_2} (1 - e^{-(k_{-2}+k_2)t}) - (k_1 - k_{-2})te^{-(k_{-2}+k_2)t} \quad (5.25)$$

To have a first idea of how these functions look like two plots were created. The values assigned to the rate constants to obtain the corresponding plots are also given (cf. Figure 5.1).

5. Data Evaluation and Mathematical Derivations

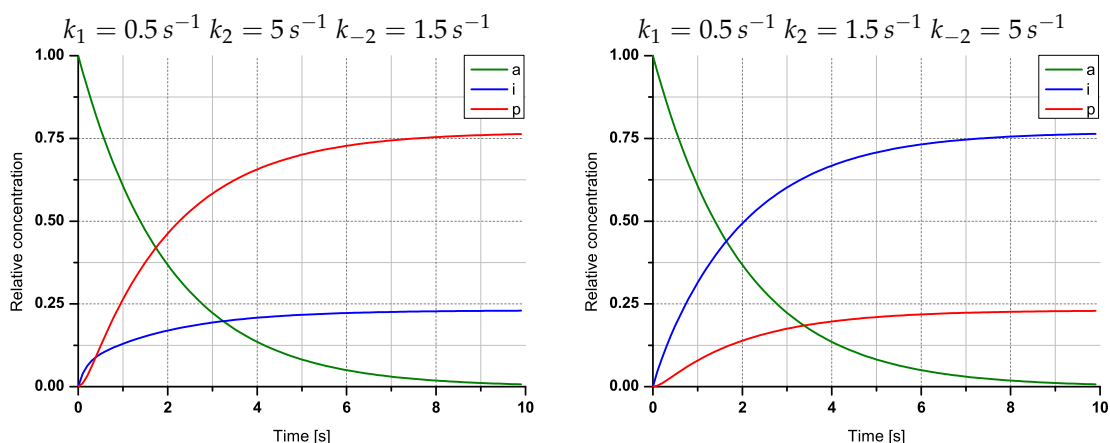


Figure 5.1.: Diagrams showing the time profiles of A, I and P in the simplified kinetic model with two distinct sets of rate constants. In the left diagram P is the major product, in the right diagram I is the major product.

It can be seen that, depending on the values of k_2 and k_{-2} , either I or P is the major product in this model. The method to distinguish between the three mechanistic scenarios is now based on the following feature. In an initial reaction period the intermediate I appears before the final product P does. This itself may already help to distinguish between the possible scenarios. However, in order to have a more general and reliable method instead of looking at the time profiles of I and P themselves the ratio of those should be calculated and plotted. This is done for the example plots (cf. Figure 5.2).

It can clearly be seen that the general trend of those two function is the same in both cases. Trying several values for the rate constants did not result in a change to the general trend. The function representing the ratio of I to P seems to be strictly decreasing for positive time and the function representing the inverse therefore is strictly increasing. The mathematical proof for the monotonicity of these functions is outlined below. The monotonicity only needs to be proven for one of the two since the monotonicity of its inverse directly follows from the initial function. In order to simplify these functions slightly for the following calculations a derived parameter is defined as follows.

$$k'_2 = k_{-2} + k_2 \quad (5.26)$$

The functions for the relative concentrations of I and P change slightly to the following.

$$i(t) = \frac{k_{-2}}{k'_2} (1 - e^{-k'_2 t}) + \frac{k_1 - k_{-2}}{k'_2 - k_1} (e^{-k_1 t} - e^{-k'_2 t}) \quad (5.27)$$

5. Data Evaluation and Mathematical Derivations

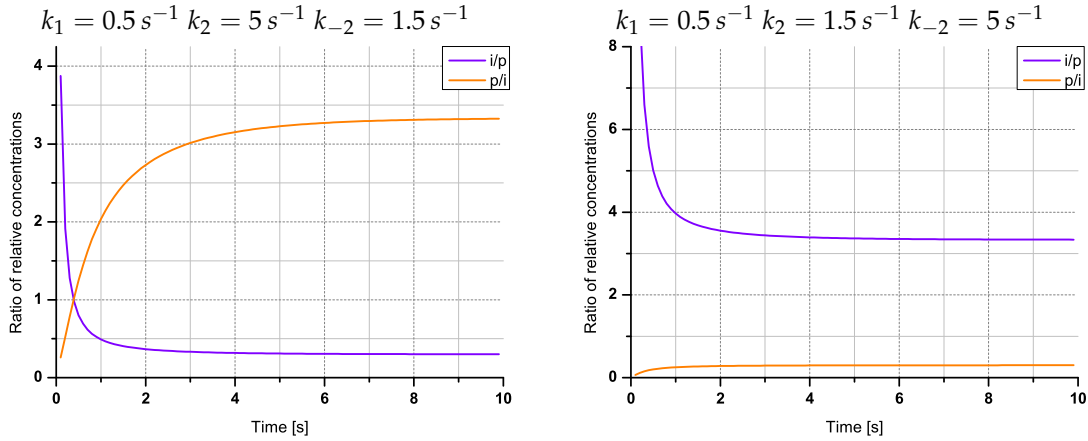


Figure 5.2.: Diagrams showing the time course of both the ratio of I to P and P to I for the two special cases with the specified values for the rate constants given above.

$$p(t) = 1 - e^{-k_1 t} - \frac{k_{-2}}{k'_2} (1 - e^{-k'_2 t}) - \frac{k_1 - k_{-2}}{k'_2 - k_1} (e^{-k_1 t} - e^{-k'_2 t}) \quad (5.28)$$

Now the function $r(t)$ is defined as the ratio of P to I.

$$r(t) = \frac{p(t)}{i(t)} = \frac{1 - e^{-k_1 t} - i(t)}{i(t)} \quad (5.29)$$

This function can now be slightly rearranged.

$$r(t) = \frac{1 - e^{-k_1 t} - i(t)}{i(t)} = \frac{1 - e^{-k_1 t}}{i(t)} - 1 \quad (5.30)$$

Keeping in mind that the numerator equals the sum of I and P this can be rearranged further.

$$r(t) = \frac{1 - e^{-k_1 t}}{i(t)} - 1 = \frac{i(t) + p(t)}{i(t)} - 1 \quad (5.31)$$

From this equation it can now clearly be seen that r will be strictly increasing if this fraction is strictly increasing. The numerator is strictly increasing which can directly be seen when its first derivative with respect to the time is determined. Now there are two possibilities. If $i(t)$ is decreasing it can trivially be seen that $r(t)$ is increasing. If $i(t)$ is increasing $r(t)$ is only increasing if the numerator is increasing to a higher degree than the denominator. This is the case if $p(t)$ is strictly increasing. Now $p(t)$ is strictly increasing if its first derivative is always positive. This needs to be shown. Therefore, the first derivative of $p(t)$ is determined.

$$p'(t) = k_1 e^{-k_1 t} - k_{-2} e^{-k'_2 t} - \frac{k_1 - k_{-2}}{k'_2 - k_1} (-k_1 e^{-k_1 t} + k'_2 e^{-k'_2 t}) \quad (5.32)$$

5. Data Evaluation and Mathematical Derivations

$$p'(t) = \frac{k_1 k'_2 - k_1^2}{k'_2 - k_1} e^{-k_1 t} - \frac{k_{-2} k'_2 - k_{-2} k_1}{k'_2 - k_1} e^{-k'_2 t} + \frac{k_1^2 - k_1 k_{-2}}{k'_2 - k_1} e^{-k_1 t} - \frac{k_1 k'_2 - k_{-2} k'_2}{k'_2 - k_1} e^{-k'_2 t} \quad (5.33)$$

$$p'(t) = \frac{k_1(k'_2 - k_{-2})}{k'_2 - k_1} (e^{-k_1 t} - e^{-k'_2 t}) \quad (5.34)$$

The numerator of this term is always positive. Therefore two possibilities remain. The denominator can be positive or negative.

$$k'_2 - k_1 > 0 \Leftrightarrow k'_2 > k_1 \Leftrightarrow -k'_2 t < -k_1 t \Leftrightarrow e^{-k'_2 t} < e^{-k_1 t} \Leftrightarrow e^{-k_1 t} - e^{-k'_2 t} > 0 \quad (5.35)$$

This clearly shows that if the denominator is positive the whole term is positive for positive time and $p(t)$ is strictly increasing. If the denominator is negative then also the difference of the two exponential functions is negative which can be seen by simply reversing all the inequations above and therefore $p(t)$ is also strictly increasing. Now there is only the case remaining that the denominator equals 0 where the other equation for $p(t)$ has to be taken (5.25). In this case the following is valid.

$$k_2 + k_{-2} = k_1 \quad (5.36)$$

The first derivative is calculated as follows starting with a simplification of the function $p(t)$ which results from combining equations 5.25 and 5.36.

$$p(t) = 1 - e^{-k_1 t} - \frac{k_{-2}}{k_1} (1 - e^{-k_1 t}) - (k_1 - k_{-2}) t e^{-k_1 t} \quad (5.37)$$

$$p'(t) = k_1 e^{-k_1 t} - k_{-2} e^{-k_1 t} - (k_1 - k_{-2}) e^{-k_1 t} + k_1 (k_1 - k_{-2}) t e^{-k_1 t} \quad (5.38)$$

$$p'(t) = k_1 (k_1 - k_{-2}) t e^{-k_1 t} \quad (5.39)$$

For positive time this term is always positive since k_1 is bigger than k_{-2} . Altogether it is shown that the function $r(t)$ representing the ratio of P to I is strictly increasing for positive time. Assuming that the function $r(t)$ does not vanish which is true for positive time it directly follows that the inverse function is strictly decreasing. Overall, this provides a method to distinguish between the first two mechanistic scenarios. It should be noted that so far the third mechanistic scenario where the first two pathways occur at a similar rate was not accounted for. This will be done mathematically considering an extended kinetic model. Therefore, one additional rate constant is needed and for convenience the variables are named differently.

- a ... Relative concentration of A (starting material)
- b ... Relative concentration of B (product 1)
- c ... Relative concentration of C (product 2)
- t ... Time
- k_1 ... First-order rate constant for the reaction of A to B
- k'_1 ... First-order rate constant for the reaction of A to C

5. Data Evaluation and Mathematical Derivations

k_2 ... First-order rate constant for the forward reaction of B to C

k_{-2} ... First-order rate constant for the backward reaction of C to B

Now the following extended kinetic model is considered.



Based on this kinetic model the following system of differential equations can be formulated.

$$\frac{da}{dt} = -(k_1 + k'_1)a \tag{5.41}$$

$$\frac{db}{dt} = k_1a + k_{-2}c - k_2b \tag{5.42}$$

$$\frac{dc}{dt} = -k_{-2}c + k_2b \tag{5.43}$$

In addition, it is also assumed that the sum of the concentrations of A, B and C equals 1.

$$a + b + c = 1 \tag{5.44}$$

The solution of this system of differential equations is straightforward as was the first one and will not be discussed in detail. The initial conditions were that at time 0 the relative concentration of A is 1 and those of B and C are 0.

$$a(0) = 1 \tag{5.45}$$

$$b(0) = 0 \tag{5.46}$$

$$c(0) = 0 \tag{5.47}$$

The following solutions for the time-dependent relative concentrations of A, B and C are obtained for the case that the sum of k_1 and k'_1 does not equal the sum of k_{-2} and k_2 .

$$a(t) = e^{-(k_1+k'_1)t} \tag{5.48}$$

$$b(t) = \frac{k_{-2}}{k_{-2} + k_2} + \frac{k_1 - k_{-2}}{k_{-2} + k_2 - k_1 - k'_1} e^{-(k_1+k'_1)t} + \left(\frac{k_{-2} - k_1}{k_{-2} + k_2 - k_1 - k'_1} - \frac{k_{-2}}{k_{-2} + k_2} \right) e^{-(k_{-2}+k_2)t}
 \tag{5.49}$$

$$c(t) = \frac{k_2}{k_{-2} + k_2} + \frac{k'_1 - k_2}{k_{-2} + k_2 - k_1 - k'_1} e^{-(k_1+k'_1)t} - \left(\frac{k_{-2} - k_1}{k_{-2} + k_2 - k_1 - k'_1} - \frac{k_{-2}}{k_{-2} + k_2} \right) e^{-(k_{-2}+k_2)t}
 \tag{5.50}$$

As the difference of the sum of k_{-2} and k_2 and the sum of k_1 and k'_1 appears in the denominator in the functions for the relative concentrations of B and C this term is assumed to be unequal to 0 (which of course has to be assumed during the

5. Data Evaluation and Mathematical Derivations

derivation). In the case this equals 0 different solutions for the time course of the relative concentrations of B and C are obtained.

$$b(t) = \frac{k_{-2}}{k_{-2} + k_2} (1 - e^{-(k_{-2} + k_2)t}) + (k_1 - k_{-2})te^{-(k_{-2} + k_2)t} \quad (5.51)$$

$$c(t) = \frac{k_2}{k_{-2} + k_2} (1 - e^{-(k_{-2} + k_2)t}) - (k_1 - k_{-2})te^{-(k_{-2} + k_2)t} \quad (5.52)$$

To have an idea of how these functions look like two plots were created. The values assigned to the rate constants in order to obtain the corresponding plots are also given. Since considering a mechanistic scenario like this makes only sense if both reactions occur at a similar rate, similar values for k_1 and k'_1 are taken in the examples (cf. Figure 5.3).

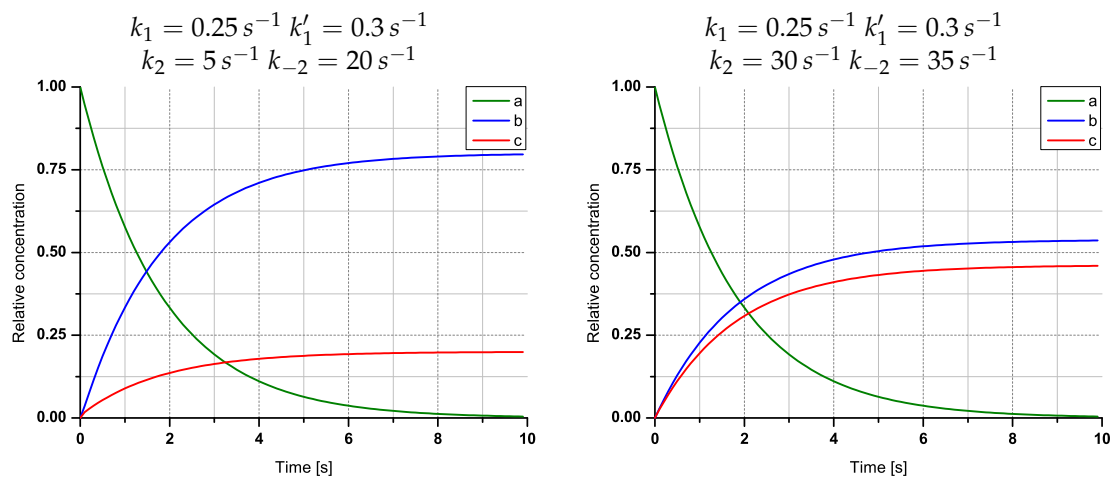


Figure 5.3.: Diagrams showing the time profiles of A, B and C in the extended kinetic model with two distinct sets of rate constants. In the left diagram there is one major product in the right diagram two products are formed in similar amounts.

It is again also looked at the ratios of B and C and the inverse (cf. Figure 5.4).

From these two examples it can already be seen that the general trend of the two ratios will be comparable to the general trend of the ratios I to P or P to I for the simplified kinetic model first discussed. A full curve discussion for the extended kinetic model will not be made but in general the ratios can show a very similar time course compared to the simplified kinetic model. The main differences are at the beginning. Assuming that both pathways occur the slopes of the concentration curves of products B and C are both finite at time 0 whereas the concentration curve of product P in the other kinetic model has a slope of 0. This has also a consequence to the ratio curves. For the extended kinetic model both curves have

5. Data Evaluation and Mathematical Derivations

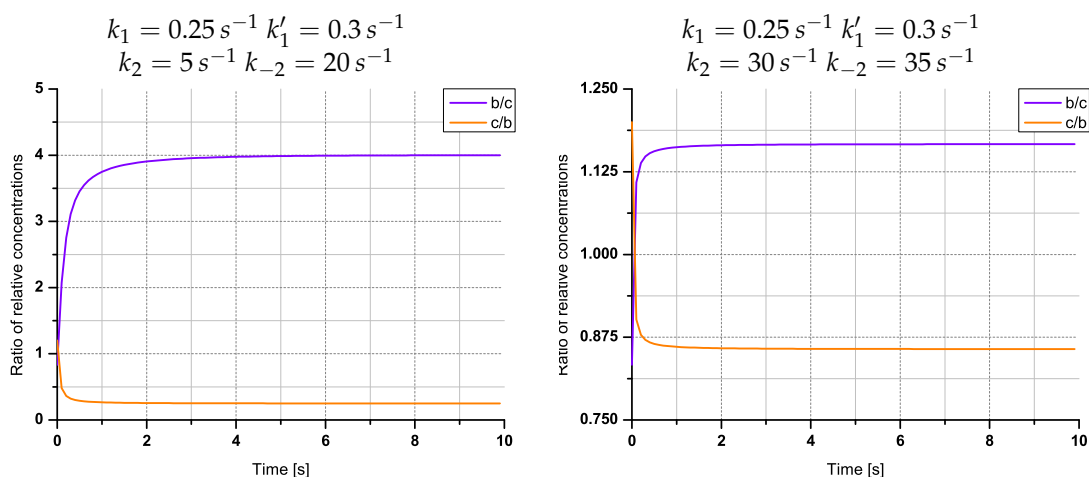


Figure 5.4.: Diagrams showing the time profiles of A, B and C in the extended kinetic model with two distinct sets of rate constants. In the left diagram there is one major product in the right diagram two products are formed in similar amounts.

a finite value at time 0 whereas in the kinetic model allowing only one pathway the ratio of intermediate to product is converging infinity when time converges 0 and the ratio of product to intermediate is converging 0 when time converges 0.

The problem with these differences in curve forms is that they are observed at time 0 which is experimentally not accessible. Even if it can be approximated to an infinitely small difference limits of detection and quantification of the corresponding products will limit the determination of their concentrations. Extrapolation from sufficiently near time points will not be reliable since the corresponding ratio curves have very high slopes in that time period. That are the reasons it is in principle impossible to distinguish those two mechanistic scenarios experimentally by this method.

This already shows the limits of the newly developed method. By looking at the time course of the product ratios it allows to easily distinguish between the first two mechanistic scenarios. However, an overlap of both mechanistic scenarios (i.e. mechanistic scenario 3) cannot be excluded by this method. Similar methods to investigate reaction mechanisms are readily employed in the determination of biochemical reaction mechanisms.⁵⁵

Now with the mathematical foundations of this method at hand this is the means to exclude one of the three mechanistic scenarios for the direct alkylation of **1** using alkenes (Figure 3.9) by looking at the time course of the ratio of the alkylated imine **11** to the main reaction product **2**. This was already previously shown for the kinetic profile using K_2CO_3 in stoichiometric amounts (cf. Figure 3.10). The corresponding diagrams determined from the kinetic profile using K_2CO_3 in catalytic amounts and

5. Data Evaluation and Mathematical Derivations

the experiments to investigate the temperature dependence of the initial reaction rate are given in Figures 5.5-5.10.

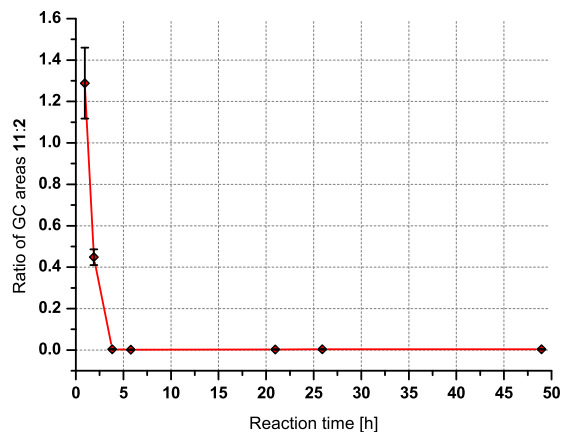


Figure 5.5.: Ratio of GC areas of **11** to **2** at 150 °C obtained from the kinetic time course using K_2CO_3 in catalytic amounts.

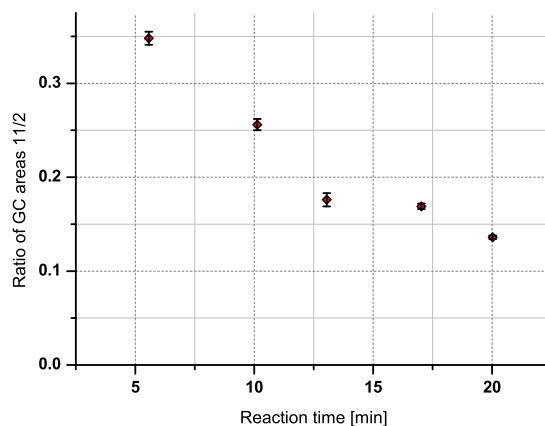


Figure 5.6.: Ratio of GC areas of **11** to **2** at 130 °C obtained from the temperature-dependence experiments.

In all diagrams the ratio of alkylated imine **11** to the main reaction product **2** is decreasing over time.

5. Data Evaluation and Mathematical Derivations

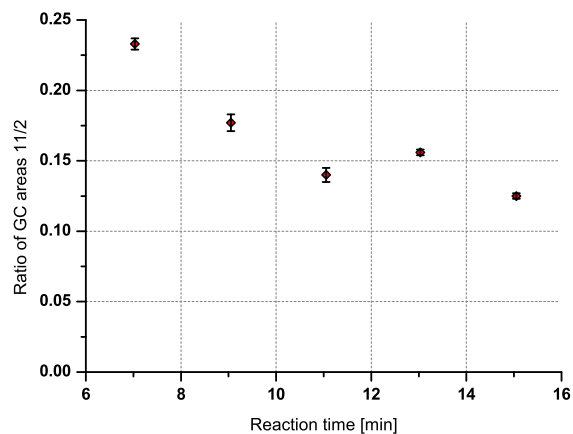


Figure 5.7.: Ratio of GC areas of **11** to **2** at 135 °C obtained from the temperature-dependence experiments.

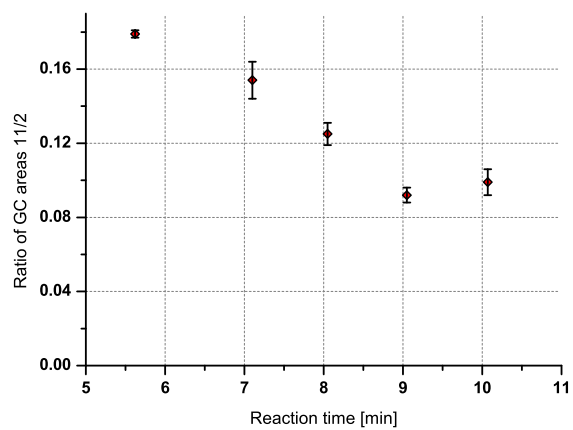


Figure 5.8.: Ratio of GC areas of **11** to **2** at 140 °C obtained from the temperature-dependence experiments.

5. Data Evaluation and Mathematical Derivations

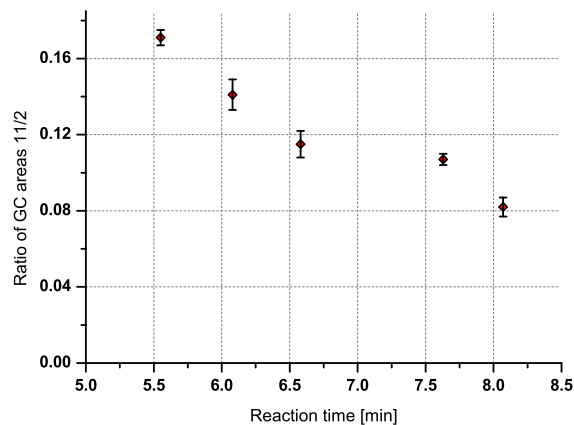


Figure 5.9.: Ratio of GC areas of **11** to **2** at 145 °C obtained from the temperature-dependence experiments.

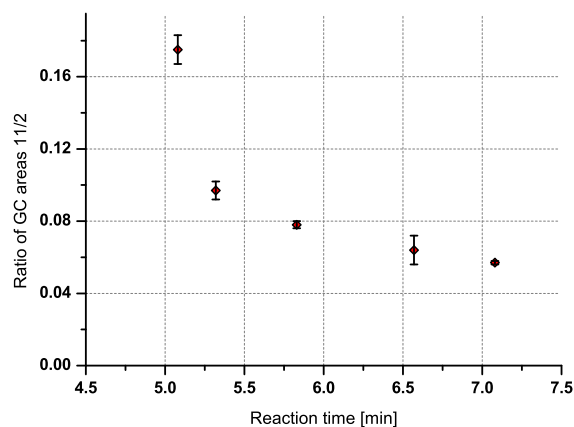


Figure 5.10.: Ratio of GC areas of **11** to **2** at 150 °C obtained from the temperature-dependence experiments.

5.2.2. Investigations into the Kinetic Modelling

5.2.2.1. Initial Rate Experiments

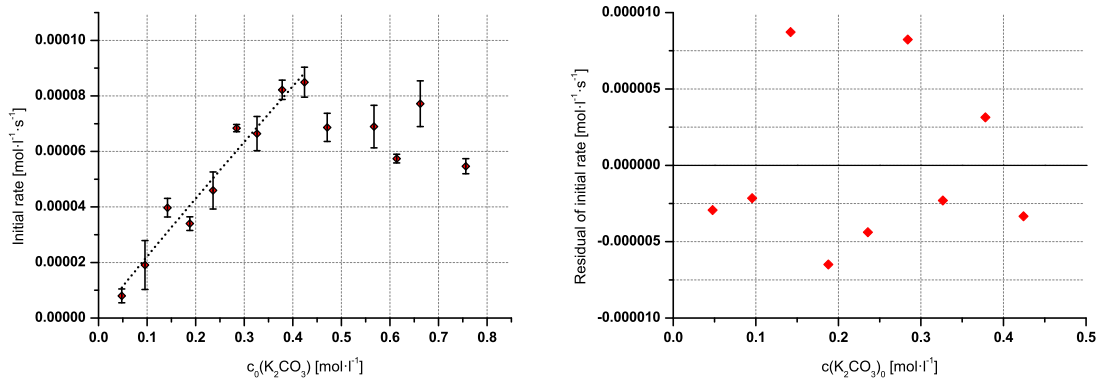
General Remarks First, the initial reaction period must be defined. Assuming the kinetic time profile for the formation of **2** would exactly follow the mathematical function determined by regression (vide infra), the relative error of the initial rate approximated by the method of initial rates at a product yield of 12% is only 10%, at a product yield of 18% the relative error is already 15% and at a product yield of 24% the relative error reaches a value of 20%. Therefore, in experiments using the method of initial rates the product yield should not reach values higher than 20% in order to keep the relative error in a reasonable range. So the method of initial rates is applied to a time period where the yield of the product is at least below 20%.

Initial rate dependence on K_2CO_3 The dependence of the initial rate on the K_2CO_3 concentration shows basically two regimes. From low concentrations until about 0.4 mol l^{-1} the initial rate shows more or less linear dependence on the concentration which is confirmed by a partial reaction order of 0.96 ± 0.10 obtained by a non-linear fit to a power function and also the good agreement to a linear regression (Figure 5.11). Further increasing the concentration does not result in higher initial rates. In fact the initial rate seems to slightly decrease. However, since the dependence in this region remains rather unclear no mathematical function was fitted to these data points. Qualitatively, it can be said that in the lower concentration region the reaction shows a partial reaction order of 1 with respect to K_2CO_3 . In the higher concentration region the partial reaction order actually seems to be even slightly negative but still close to 0. The somewhat negative partial reaction order could be explained by incipient off-cycle binding of carbonate to Rh forming a catalytically non-active species. However, this needs to be confirmed by additional experiments.

Initial rate dependence on **1** The dependence of the initial rate on the concentration of **1** shows over the whole investigated concentration range a linear course which is confirmed by a partial reaction order of 0.91 ± 0.07 obtained by a non-linear fit to a power function and also the good agreement to a linear regression (Figure 5.12). Qualitatively, it can be said that the reaction shows a partial reaction order of 1 with respect to **1** over the whole concentration region investigated.

Initial rate dependence on $[RhCl(cod)]_2$ The dependence of the initial rate on the concentration of $[RhCl(cod)]_2$ shows also two regimes. From low concentrations until about 0.006 mol l^{-1} the initial rate shows linear dependence on the concentration which is confirmed by a partial reaction order of 0.96 ± 0.07 obtained

5. Data Evaluation and Mathematical Derivations



$$y = ax^b$$

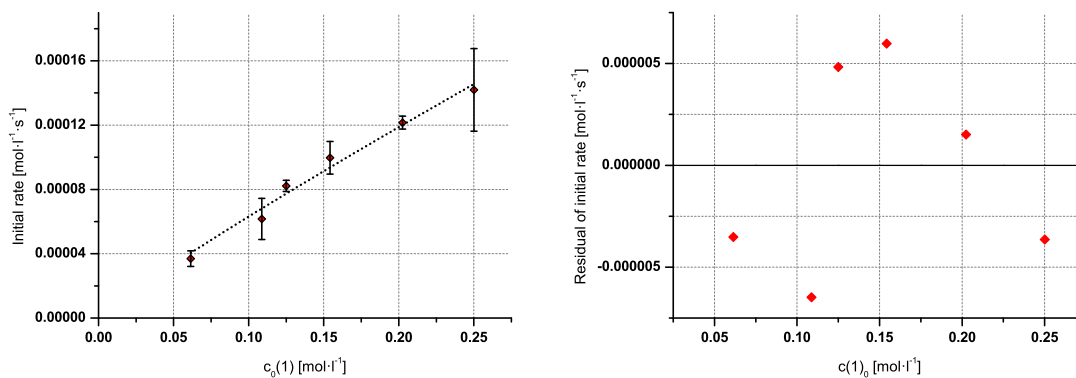
a		b		Statistics	
Value	Error	Value	Error	R ²	F
$2.0 \cdot 10^{-4}$	$0.3 \cdot 10^{-4}$	0.96	0.10	0.95894	401.52

$$y = ax$$

a		Statistics	
Value	Error	R ²	F
$2.11 \cdot 10^{-4}$	$0.07 \cdot 10^{-4}$	0.99114	894.48

Figure 5.11.: Dependence of the initial rate on the K₂CO₃ concentration (left) and residual plot of the power regression in the lower concentration range (right). The used regression equations and the regression results are shown in the lower section.

5. Data Evaluation and Mathematical Derivations



$$y = ax^b$$

Value	a		b		Statistics	
	Value	Error	Value	Error	R ²	F
5.15 · 10 ⁻⁴	0.63 · 10 ⁻⁴		0.91	0.07	0.98271	878.30

$$y = ax$$

Value	a		Statistics	
	Value	Error	R ²	F
5.97 · 10 ⁻⁴	0.15 · 10 ⁻⁴	0.99682	1569.09	

Figure 5.12.: Dependence of the initial rate on the concentration of **1** (left) and residual plot of the power regression in the lower concentration range (right). The used regression equations and the regression results are shown in the lower section.

5. Data Evaluation and Mathematical Derivations

by a non-linear fit to a power function and also the good agreement to a linear regression (Figure 5.13). Further increasing the concentration results in a region of more or less constant initial rate. This is confirmed by a partial reaction order of 0.03 ± 0.13 obtained by a non-linear fit to a power function. Qualitatively, it can be said that in the lower concentration region the reaction shows a partial reaction order of 1 with respect to $[\text{RhCl}(\text{cod})]_2$. In the higher concentration region the partial reaction order is 0.

Initial rate dependence on hex-1-ene Over the investigated concentration range the initial rate shows no dependence on the concentration of hex-1-ene which is confirmed by a partial reaction order of 0.02 ± 0.04 obtained by a non-linear fit to a power function (Figure 5.14). Qualitatively, it can be said that the reaction shows a partial reaction order of 0 with respect to hex-1-ene.

5.2.2.2. K_2CO_3 Studies

Figures 5.15-5.20 show the particle size distributions and the particle size distribution densities, respectively, for all the K_2CO_3 batches used (2 m% water, 15 m% water, dried from 2 m% water, hydrate original, hydrate comminuted). It should be noted that the K_2CO_3 batch with 15 m% adsorbed water was dried before it was subjected to the analysis.

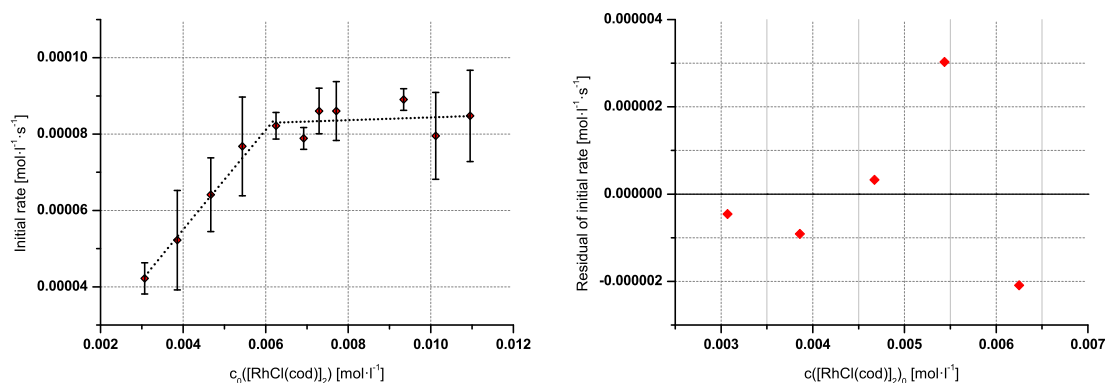
Table 5.1 gives the particle size modes, medians and means of all the K_2CO_3 batches as determined from the particle size distribution densities.

Table 5.1.: Particle size modes, medians and means for all the K_2CO_3 batches used.

Base batch	Mode [μm]	Median [μm]	Mean [μm]
2 m% H_2O	0.30	0.34	0.44
15 m% H_2O	0.78	0.95	1.14
Dried from 2 m% H_2O	0.30	0.33	0.43
Hydrate original	1.03	1.17	1.59
Hydrate comminuted	0.78	1.03	1.27

It should be noted that the K_2CO_3 batch with 2 m% adsorbed water and the one which was dried from the same batch show more or less the same particle size distributions and particle size distribution densities. This shows that under the chosen drying conditions the particle size does not change significantly. This is especially important for the particle size distribution determined for the batch with an adsorbed water content of 15 m% since this batch could not be subjected

5. Data Evaluation and Mathematical Derivations



Lower concentration region:

$$y = ax^b$$

a		b		Statistics	
Value	Error	Value	Error	R ²	F
0.0108	0.0040	0.96	0.07	0.96873	2172.05

$$y = ax$$

a		Statistics	
Value	Error	R ²	F
0.0136	0.0002	0.99916	3565.28

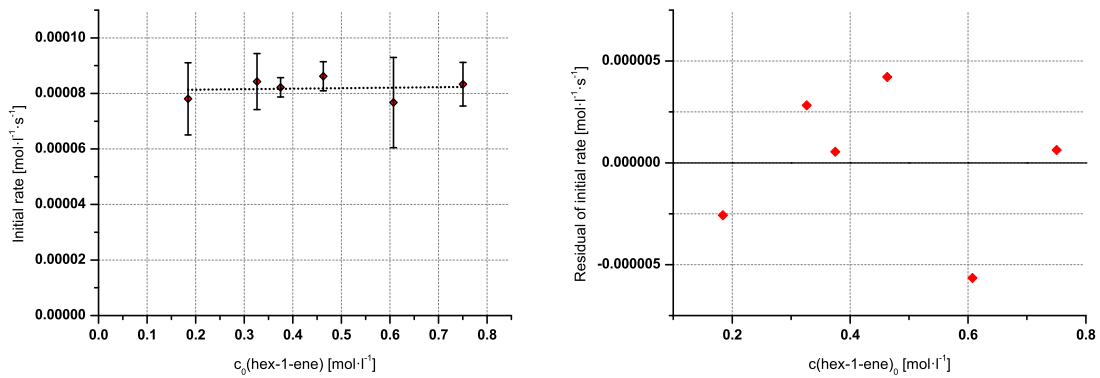
Higher concentration region:

$$y = ax^b$$

a		b		Statistics	
Value	Error	Value	Error	R ²	F
$9.6 \cdot 10^{-5}$	$5.8 \cdot 10^{-5}$	0.03	0.13	0.01292	1064.50

Figure 5.13.: Dependence of the initial rate on the [RhCl(cod)]₂ concentration (left) and residual plot of the power regression in the lower concentration range (right). The used regression equations and the regression results are shown in the lower section.

5. Data Evaluation and Mathematical Derivations



$$y = ax^b$$

	a		b		Statistics	
	Value	Error	Value	Error	R ²	F
	$8.3 \cdot 10^{-5}$	$0.4 \cdot 10^{-5}$	0.02	0.04	0.03985	1234.51

Figure 5.14.: Dependence of the initial rate on the hex-1-ene concentration (left) and residual plot of the power regression in the lower concentration range (right). The used regression equation and the regression results are shown in the lower section.

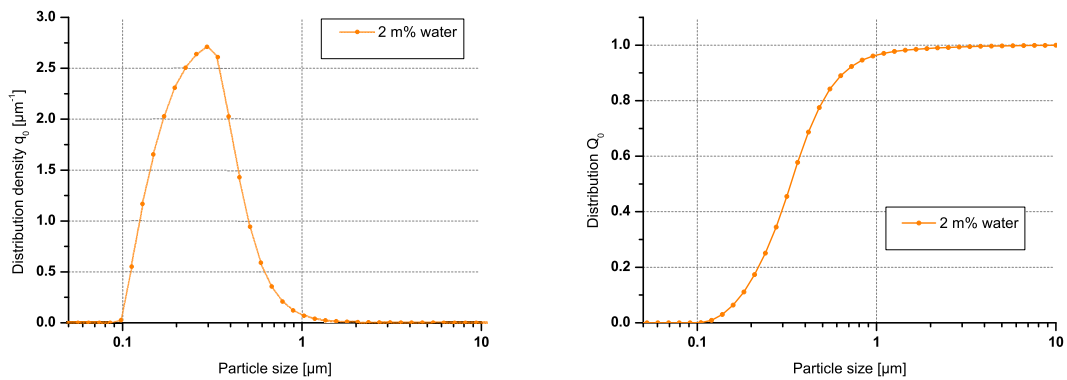


Figure 5.15.: Particle size distribution and particle size distribution density for the K₂CO₃ batch with 2 m% adsorbed water.

5. Data Evaluation and Mathematical Derivations

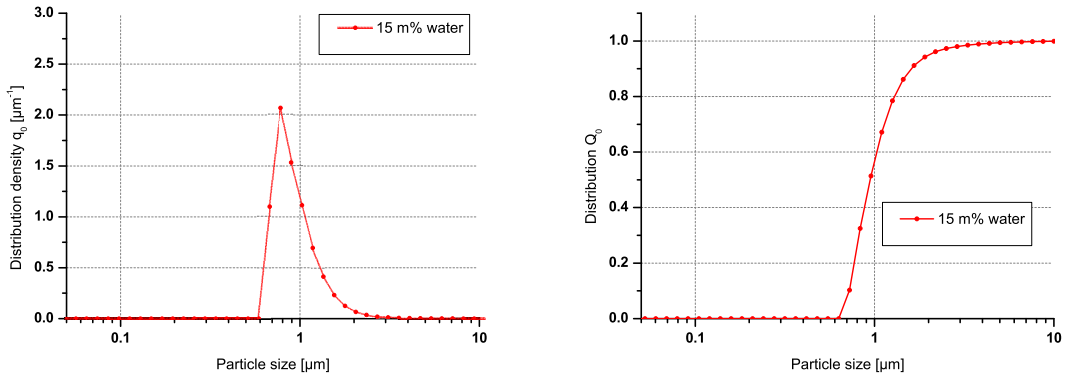


Figure 5.16.: Particle size distribution and particle size distribution density for the K_2CO_3 batch with 15 m% adsorbed water.

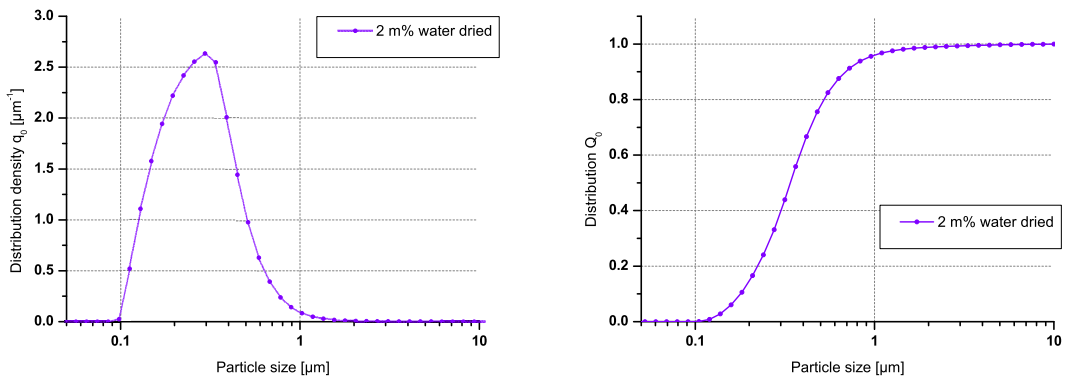


Figure 5.17.: Particle size distribution and particle size distribution density for the K_2CO_3 batch with 2 m% adsorbed water after drying.

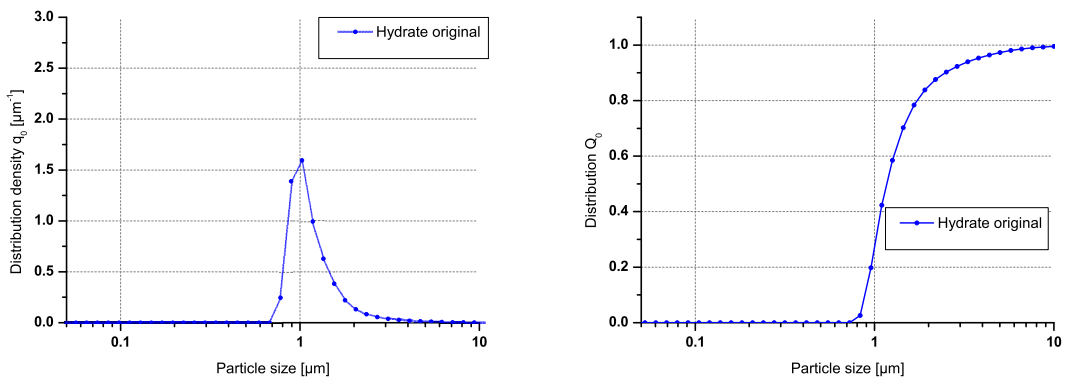


Figure 5.18.: Particle size distribution and particle size distribution density for the original $\text{K}_2\text{CO}_3 \cdot 1.5 \text{H}_2\text{O}$ batch.

5. Data Evaluation and Mathematical Derivations

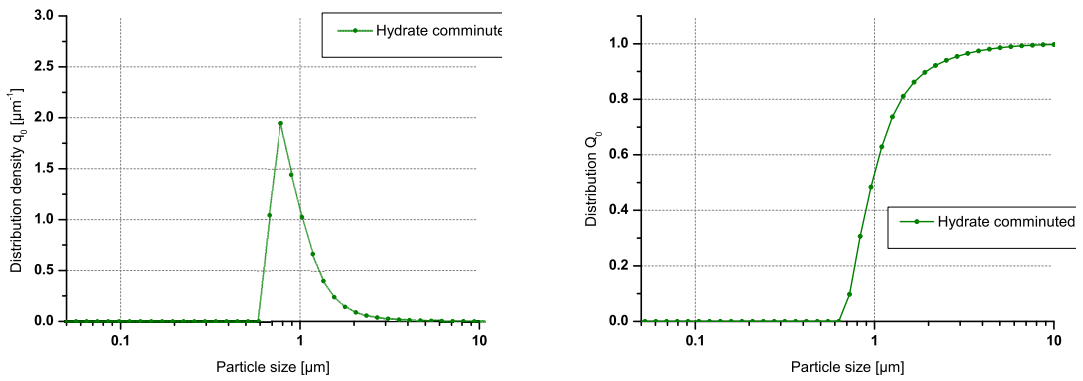


Figure 5.19.: Particle size distribution and particle size distribution density for the comminuted $\text{K}_2\text{CO}_3 \cdot 1.5 \text{H}_2\text{O}$ batch.

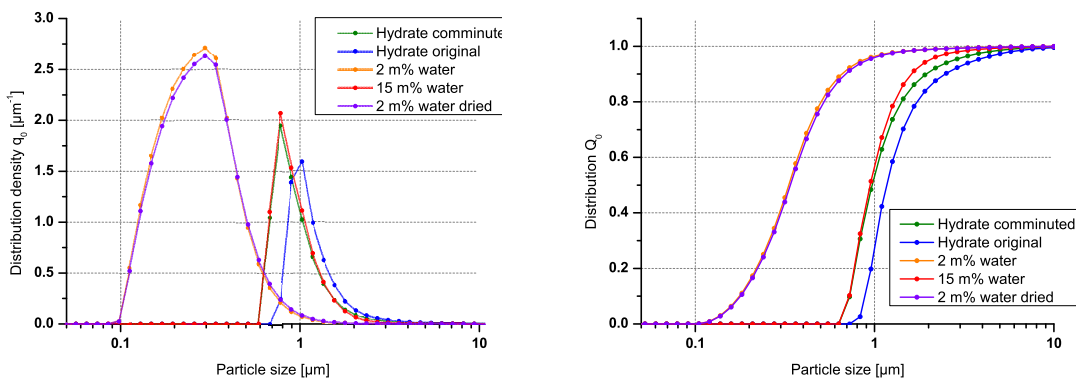


Figure 5.20.: Overlays of the particle size distributions and particle size distribution densities for all K_2CO_3 batches investigated.

5. Data Evaluation and Mathematical Derivations

directly to laser diffraction analysis and had to be dried prior to the measurements in order to ensure a uniform sample transport into the analyser.

Figures 5.21-5.25 show the nitrogen adsorption and desorption isotherms for all the K_2CO_3 batches together with the residual plots of the linear regressions performed in order to determine the BET surface area of the K_2CO_3 batches.

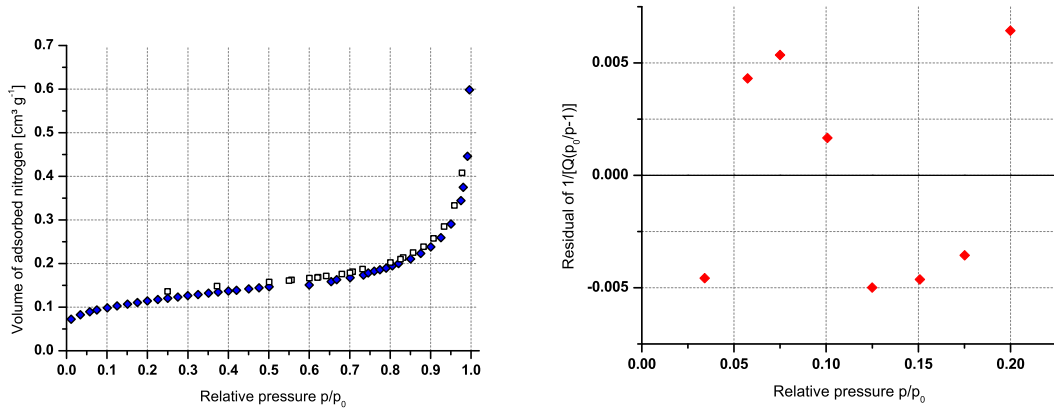


Figure 5.21.: Adsorption (blue) and desorption (white) isotherms (left) and residual plot of the linear regression to determine the BET surface area (right) for the K_2CO_3 batch with 2 m% adsorbed water.

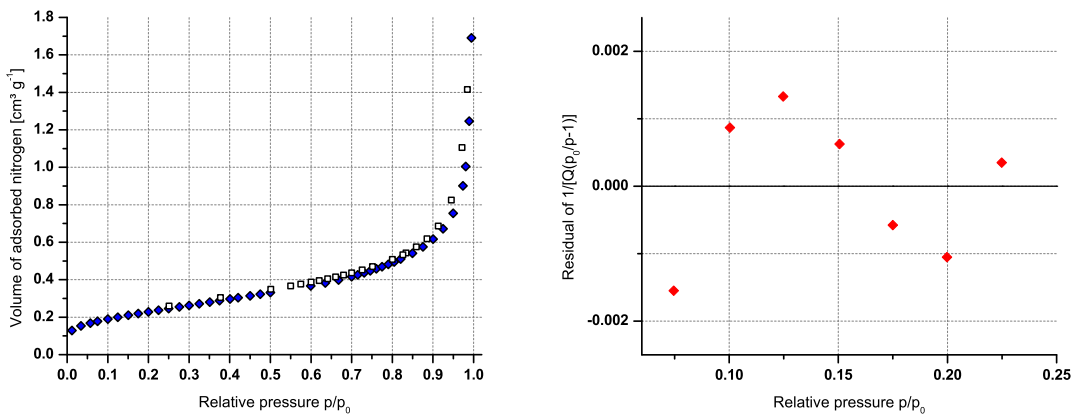


Figure 5.22.: Adsorption (blue) and desorption (white) isotherms (left) and residual plot of the linear regression to determine the BET surface area (right) for the K_2CO_3 batch with 15 m% adsorbed water.

Tables 5.2 and 5.3 summarises both the statistical parameters and the results of the BET surface area determinations.

5. Data Evaluation and Mathematical Derivations

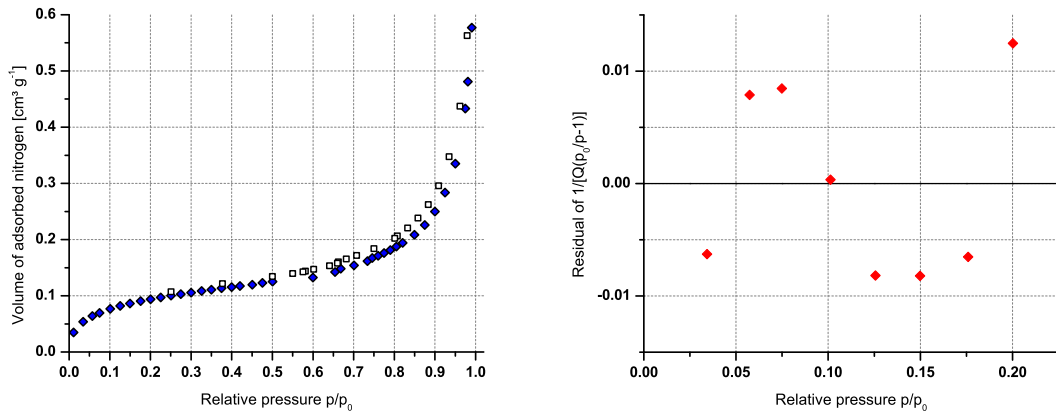


Figure 5.23.: Adsorption (blue) and desorption (white) isotherms (left) and residual plot of the linear regression to determine the BET surface area (right) for the K_2CO_3 batch with 2 m% adsorbed water after drying.

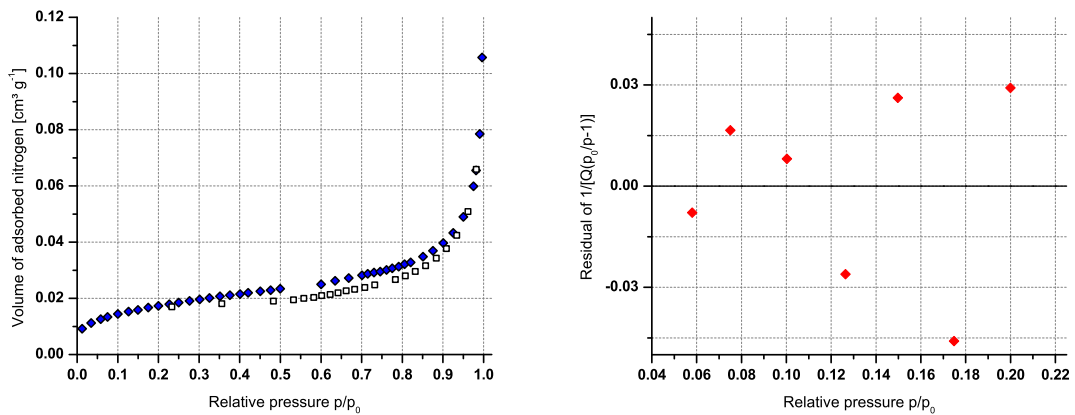


Figure 5.24.: Adsorption (blue) and desorption (white) isotherms (left) and residual plot of the linear regression to determine the BET surface area (right) for the original $K_2CO_3 \cdot 1.5 H_2O$ batch.

5. Data Evaluation and Mathematical Derivations

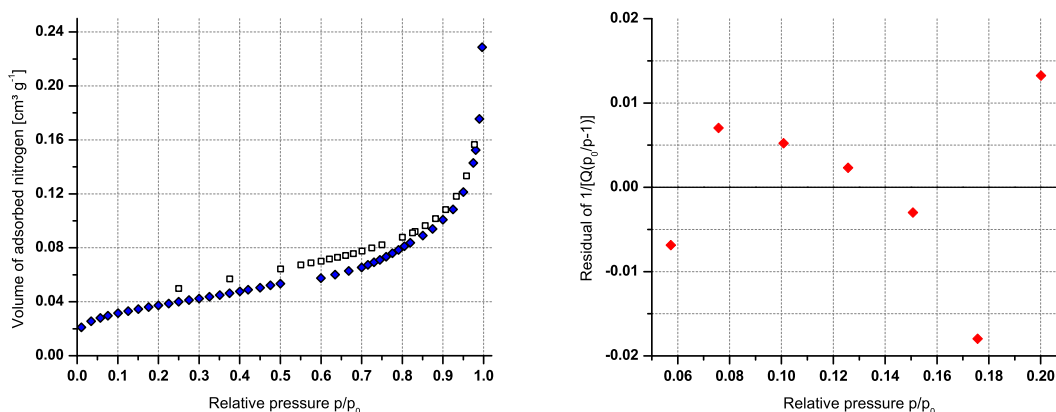


Figure 5.25.: Adsorption (blue) and desorption (white) isotherms (left) and residual plot of the linear regression to determine the BET surface area (right) for the comminuted $\text{K}_2\text{CO}_3 \cdot 1.5 \text{H}_2\text{O}$ batch.

Table 5.2.: Statistical parameters and results of the BET surface area determinations of all K_2CO_3 batches investigated.

Base batch	Slope k [g cm^{-3}]	Intercept d [g cm^{-3}]	Points	R^2	F
2 m% H_2O	10.60 ± 0.03	0.071 ± 0.004	8	0.99994	93356
15 m% H_2O	5.102 ± 0.009	0.075 ± 0.001	7	0.99998	331001
Dried from 2 m% H_2O	11.99 ± 0.06	0.257 ± 0.008	8	0.9999	40760
Hydrate original	67.1 ± 0.2	1.00 ± 0.03	7	0.99994	77634
Hydrate comminuted	31.62 ± 0.09	0.37 ± 0.01	7	0.99996	129104

Table 5.3.: Specific surface areas and BET constants of all K_2CO_3 batches investigated. Specific surface areas are reported with a relative uncertainty of 10 %.

Base batch	Specific surface area [$\text{m}^2 \text{g}^{-1}$]	BET constant C
2 m% H_2O	0.41 ± 0.04	149 ± 9
15 m% H_2O	0.84 ± 0.08	69 ± 1
Dried from 2 m% H_2O	0.36 ± 0.04	48 ± 1
Hydrate original	0.064 ± 0.006	68 ± 2
Hydrate comminuted	0.14 ± 0.01	87 ± 3

5. Data Evaluation and Mathematical Derivations

The specific surface area data points reveal that the K_2CO_3 batch with the highest adsorbed water content also has the highest specific surface area. It should be noted that this batch had to be dried in order to analyse it using nitrogen adsorption in order to ensure a proper degassing process. However, drying did not show a significant influence on the specific surface area of the K_2CO_3 batch with an adsorbed water content of 2 m%. The specific surface area results explain the significant difference between the initial rates of the comminuted $K_2CO_3 \cdot 1.5 H_2O$ batch and the K_2CO_3 batch with an adsorbed water content of 15 m%. The latter batch even has a higher specific surface area than the K_2CO_3 batch with an adsorbed water content of 2 m%, which had a significantly lower particle size.

5.2.2.3. Kinetic Profile with K_2CO_3 in Stoichiometric Amounts

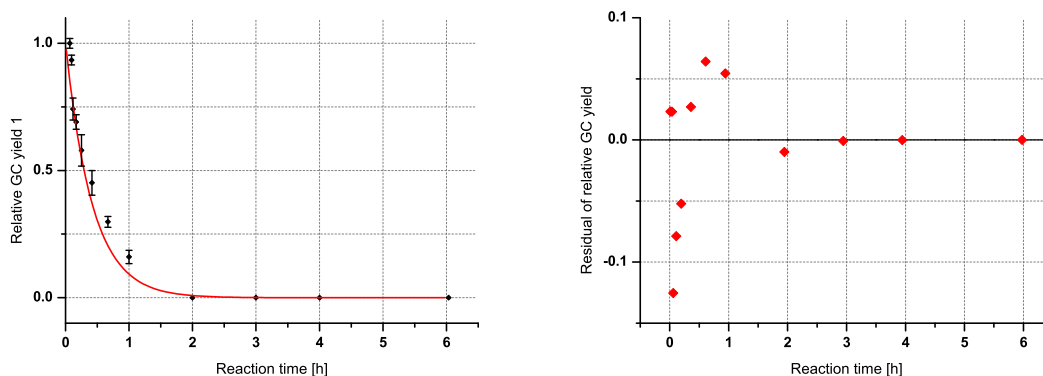
Since complete kinetic profiles were obtained for **1** and the products **2**, **3** and **4** mathematical functions were fitted to the data points. The function forms used for the regressions were derived from the exact solutions of simple kinetic models which are also shortly outlined below. Regression parameters were determined by non-linear regression. In order to get more reliable regression parameters the time values were corrected for the time needed for the reaction mixture to reach a constant temperature which is given at the end of this section. This is necessary since kinetic profiles show the biggest changes in the beginning and without the correction the obtained regression parameters are significantly different.

The kinetic profile for the consumption of **1** was fitted to a simple exponential decomposition which is valid for unimolecular irreversible decomposition (cf. Figure 5.26). The residual plot shows bigger residuals at the beginning and very small residuals at later reaction times. However, this is the case because the concentration of **1** approaches and also reaches 0. At the constant value of 0 the error naturally cannot be high. The graph showing the data points together with the fitted function shows that the used mathematical function is only able to describe the kinetic profile of **1** roughly and not very accurately. However, a better plausible mathematical function with a reasonable number of parameters could not be found. It was decided to make a reasonable compromise between number of parameters and accuracy of the resulting fit.

The kinetic profile for the formation of **2** was fitted to an equation which is valid for the formation of the product in an unimolecular reversible reaction (Figure 5.27). The residual plot reveals that the residuals are basically homoscedastic. Hence, the chosen mathematical function describes the kinetic behaviour of **2** in this reaction under these conditions quite accurately.

The kinetic profile for the formation of **3** was fitted to the same equation as used for the formation of **2** (Figure 5.28). The residual plot reveals that the used function may not be suitable to describe the kinetic behaviour at the beginning. However, the deviation is not too big. The deviation comes from the presence of a short

5. Data Evaluation and Mathematical Derivations



$$y = e^{-ax}$$

a		Statistics	
Value	Error	R ²	F
2.38	0.2	0.97883	1151.4

Figure 5.26.: Regression result (left) and residual plot (right) for the consumption of **1**. The used regression equation and the regression result are shown in the lower section.

induction period for the formation of **3** since it is formed in a consecutive reaction from the initial product **2**.

The kinetic profile for the formation of **4** was tried to be fitted to an equation which describes the formation of C in the following kinetic scheme (cf. Figure 5.29).



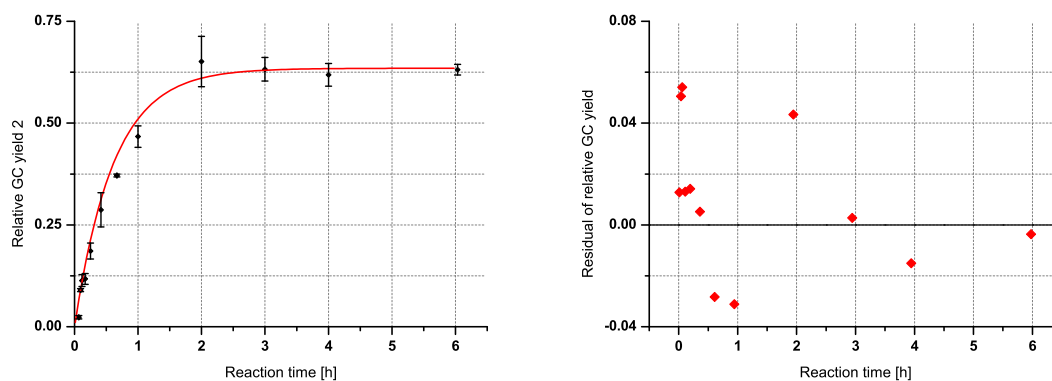
The corresponding mathematical function has the following form.^a

$$y = 1 - e^{-ax} - \frac{c}{b}[1 - e^{-bx}] - \frac{a-c}{b-c}[e^{-ax} - e^{-bx}] \quad (5.54)$$

However, since the resulting parameters yielded an insignificant result the mathematical form was slightly changed. The problem was that the resulting values for a, b and c were very similar, resulting in a difference very similar to zero with a significantly higher standard error. However, omitting the last term was sufficient to yield significantly better values. The residual plot shows slightly bigger residuals at later reaction times but the differences are not significant and the standard deviations of those data points are also bigger.

^aThe parameters a, b and c are derived from the rate constants in the above kinetic model.

5. Data Evaluation and Mathematical Derivations

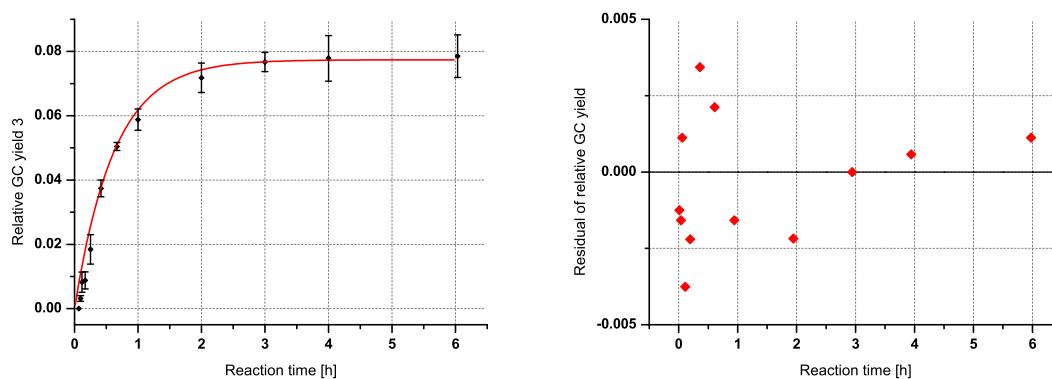


$$y = \frac{a}{a+b} [1 - e^{-(a+b)x}]$$

a		b		Statistics	
Value	Error	Value	Error	R ²	F
1.03	0.08	0.60	0.07	0.98472	1057.03

Figure 5.27.: Regression result (left) and residual plot (right) for the formation of **2**. The used regression equation and the regression result are shown in the lower section.

5. Data Evaluation and Mathematical Derivations

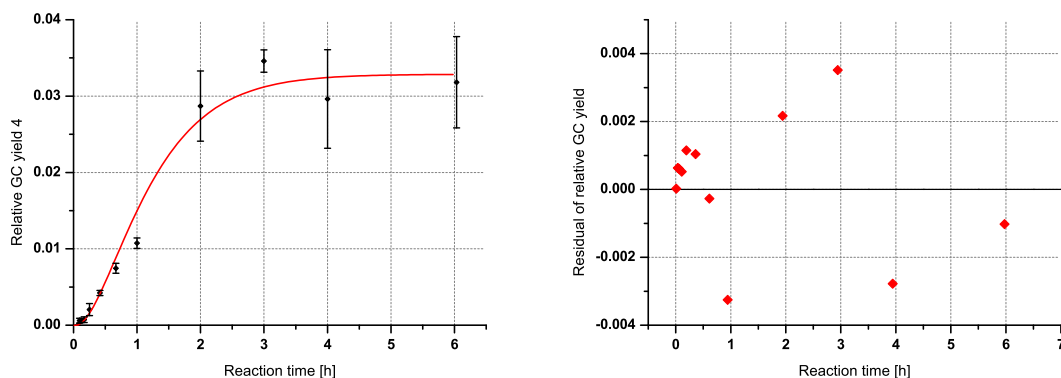


$$y = \frac{a}{a+b} [1 - e^{-(a+b)x}]$$

a		b		Statistics	
Value	Error	Value	Error	R ²	F
0.12	0.01	1.48	0.08	0.99556	3146.41

Figure 5.28.: Regression result (left) and residual plot (right) for the formation of **3**. The used regression equation and the regression result are shown in the lower section.

5. Data Evaluation and Mathematical Derivations



$$y = 1 - e^{-ax} - c[1 - e^{-bx}]$$

a		b		c		Statistics	
Value	Error	Value	Error	Value	Error	R ²	F
1.6	0.3	1.6	0.3	0.967	0.001	0.98184	305.01

Figure 5.29.: Regression result (left) and residual plot (right) for the formation of **4**. The used regression equation and the regression result are shown in the lower section.

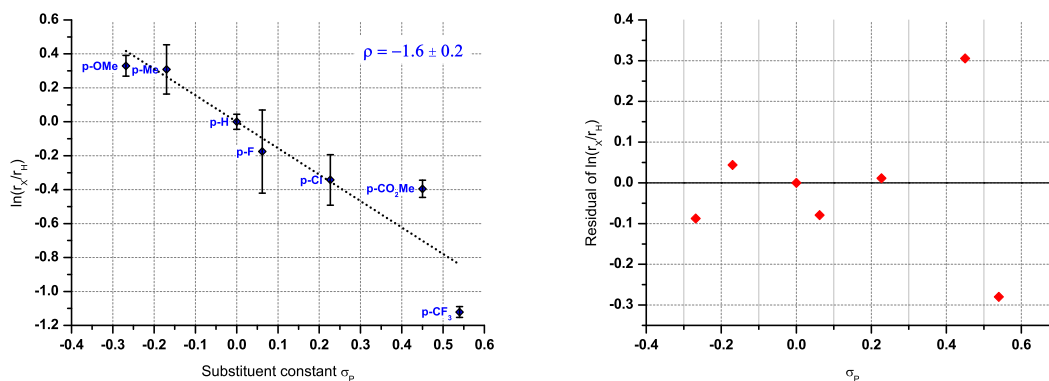
From the kinetic profile of the alkene reaction it was also needed to extrapolate the data to determine the point at which the reaction starts formally. Therefore, it was assumed, that under these conditions the formation of product is a linear function of time in the initial reaction period (This assumption is reasonable since based on the data of the kinetic profiles and especially the experiments to determine the temperature dependence of the reaction rate no considerable induction period was observed). The reason this needs to be done is because the reaction mixture needs some time to reach a constant temperature. Experiments were conducted to determine how long it takes the reaction mixture to reach a constant temperature, and for reactions at 150 °C (i.e. the temperature of the aluminium block) after 4 min the temperature remains more or less constant. However, even after 3 min the reaction temperature does not change significantly thereafter. Therefore, it is reasonable that a line through the two data points at 4 min and at 5.75 min would result in a good estimate of the formal reaction starting point since between those data points the assumption of a linear increase in the product concentration is satisfied best. It should be noted that this in fact only influences the absolute initial rate values obtained and therefore rate constants derived from initial rate experiments. However, partial reaction orders and other relative magnitudes are not affected at all. The effective reaction start in initial rate experiments was determined to be 3.4 min. This value is used as the second data point for all initial rate experiments

5. Data Evaluation and Mathematical Derivations

having product amounts of 0% in order to determine initial rates.

5.2.2.4. Electronic Influence on Benzylic Amines

The reaction constant ρ was determined from the experimental results by linear regression. First, the intercept was not assumed to be 0 but since the regression result showed a value for the intercept near zero with a standard error significantly higher than the value itself a linear regression with the intercept assumed to be 0 was performed. The results are depicted in Figure 5.30.



$$y = ax$$

a		Statistics	
Value	Error	R ²	F
-1.6	0.2	0.89358	50.38

Figure 5.30.: Hammett plot from the electronic influence of substituents on benzylic amines (left) and residual plot of the linear regression (right). The used regression equation and the regression results are shown in the lower section.

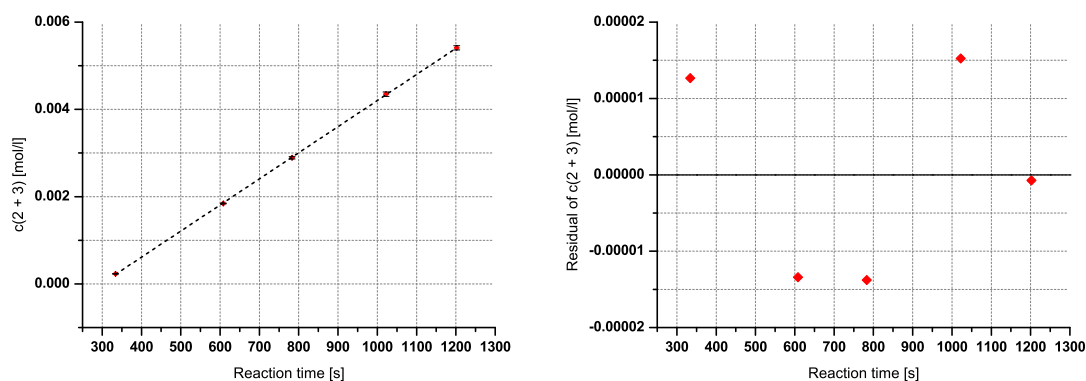
The correlation is not very high but still reasonable with an F value of just above 50. The residual plot shows slightly higher residuals for the electron-withdrawing groups but the number of data points is too low in order to be able to say the residuals are not homoscedastic.

5.2.2.5. Temperature Dependence of the Initial Rate

In order to determine the temperature dependence of the reaction rate and obtain the activation parameters of the reaction an Eyring plot⁷⁷ was constructed by determining the initial reaction rates at 5 different temperatures. In order to accurately determine the initial reaction rates 5 data points at different reaction times at

5. Data Evaluation and Mathematical Derivations

a certain temperature were determined. The initial rates at each temperature were determined by linear regression from the 5 data points determined. The slope of the linear regression is the initial reaction rate. Figures 5.31-5.35 show the regression results at all 5 temperatures.



$$y = ax + b$$

a		b		Statistics	
Value	Error	Value	Error	R ²	F
$5.98 \cdot 10^{-6}$	$0.02 \cdot 10^{-6}$	-0.00178	0.00002	0.99995	65333.38

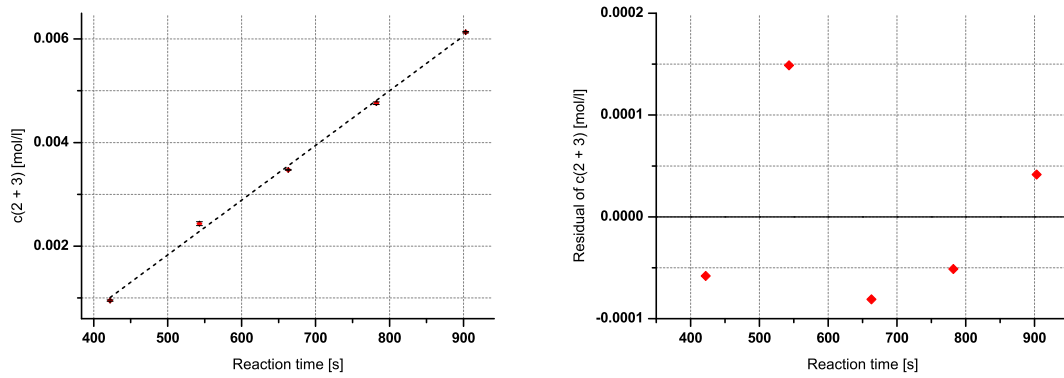
Figure 5.31.: Determination of the initial rate at 130 °C (left) and residual plot of the linear regression (right). The used regression equation and the regression results are shown in the lower section.

Basically, a high degree of linearity is observed at all 5 temperatures. The F values are in all 5 cases good to excellent being at least higher than 1000 and the residual plots show no significant outlier and are in general homoscedastic. The regression results for all 5 temperatures are summarised in Table 5.4. This Table contains together with the determined initial rates also the derived rate constants assuming a second order rate law (k_2) as determined from the previous experiments. So in order to determine k_2 the initial reaction rates were divided by the concentrations of **1** and $[\text{RhCl}(\text{cod})]_2$ at the beginning.

From these data points the activation parameters were determined based on the Eyring equation.⁷⁷ They were determined both using non-linear regression and linear regression with transformed coordinates (i.e. after linearisation). The corresponding regression results are given in Figures 5.36 and 5.37.

The regression parameters of the non-linear regression are the values for the activation parameters. For the linear regression the activation parameters need to be derived from the slope and the intercept, respectively. Table 5.5 gives the activation parameters from both methods. The differences are not big, but evident, especially

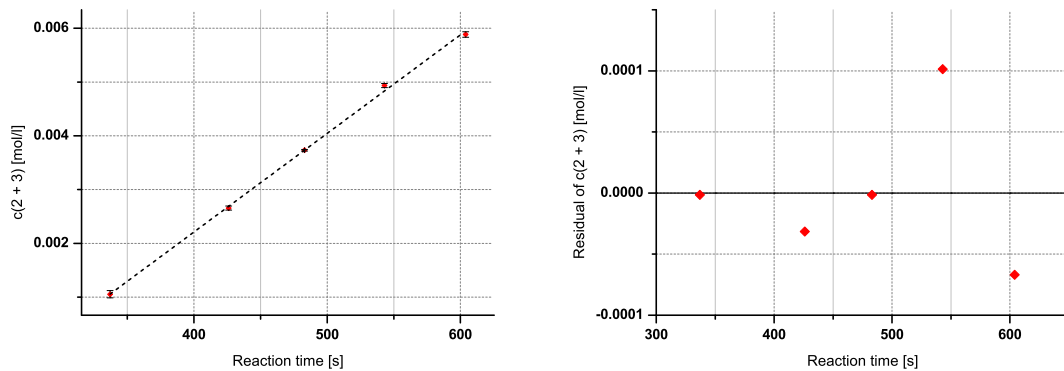
5. Data Evaluation and Mathematical Derivations



$$y = ax + b$$

a		b		Statistics	
Value	Error	Value	Error	R ²	F
$1.06 \cdot 10^{-5}$	$0.03 \cdot 10^{-5}$	-0.0035	0.0002	0.99775	1328.03

Figure 5.32.: Determination of the initial rate at 135 °C (left) and residual plot of the linear regression (right). The used regression equation and the regression results are shown in the lower section.

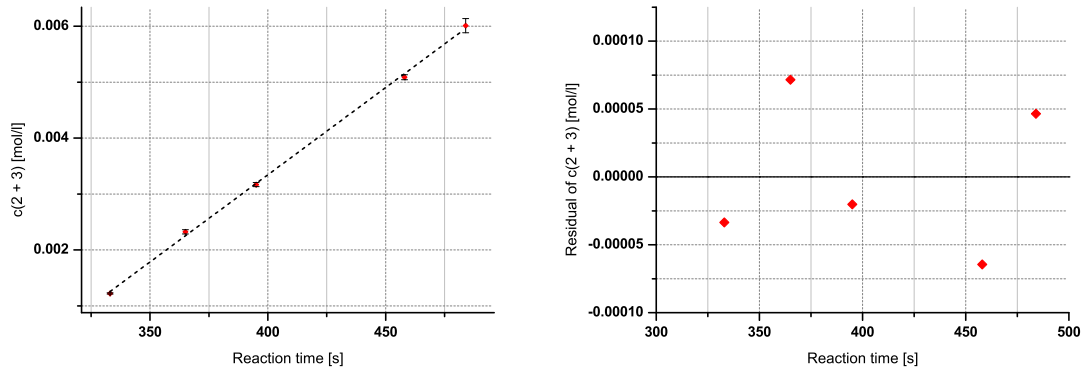


$$y = ax + b$$

a		b		Statistics	
Value	Error	Value	Error	R ²	F
$1.83 \cdot 10^{-5}$	$0.04 \cdot 10^{-5}$	-0.0051	0.0002	0.99890	2735.56

Figure 5.33.: Determination of the initial rate at 140 °C (left) and residual plot of the linear regression (right). The used regression equation and the regression results are shown in the lower section.

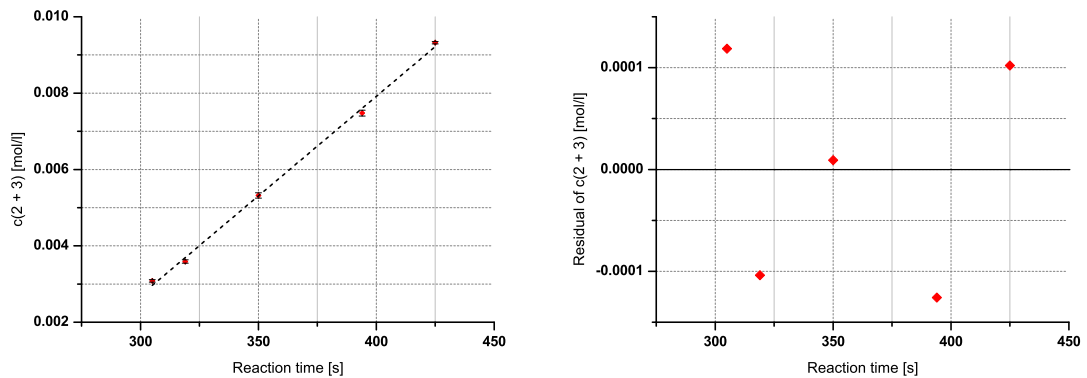
5. Data Evaluation and Mathematical Derivations



$$y = ax + b$$

a		b		Statistics	
Value	Error	Value	Error	R ²	F
$3.12 \cdot 10^{-5}$	$0.05 \cdot 10^{-5}$	-0.0091	0.0002	0.99916	3575.91

Figure 5.34.: Determination of the initial rate at 145 °C (left) and residual plot of the linear regression (right). The used regression equation and the regression results are shown in the lower section.



$$y = ax + b$$

a		b		Statistics	
Value	Error	Value	Error	R ²	F
$5.21 \cdot 10^{-5}$	$0.13 \cdot 10^{-5}$	-0.0129	0.0005	0.99815	1619.93

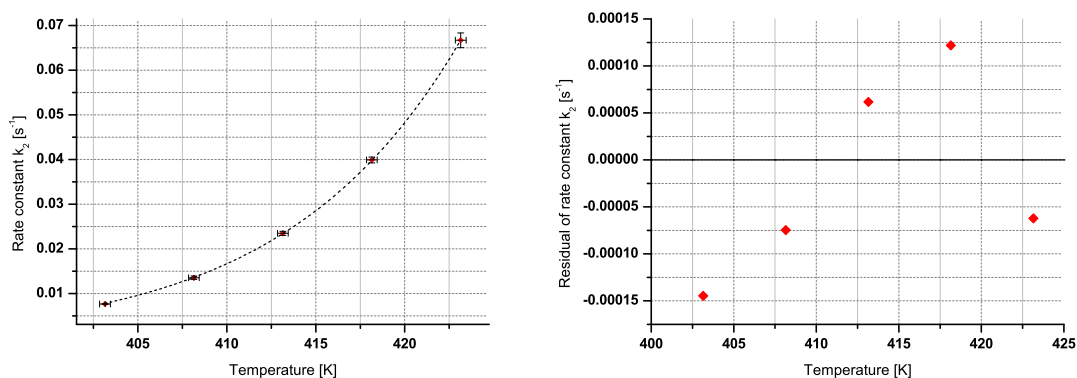
Figure 5.35.: Determination of the initial rate at 150 °C (left) and residual plot of the linear regression (right). The used regression equation and the regression results are shown in the lower section.

5. Data Evaluation and Mathematical Derivations

Table 5.4.: Rate constants at different temperatures determined by linear regression over the corresponding data points.

T [K]	Error of T ^a	k ₂ [10 ⁻² s ⁻¹]	Error of k ₂ [10 ⁻² s ⁻¹]
403.15	0.3	0.765	0.003
408.15	0.3	1.35	0.04
413.15	0.3	2.35	0.04
418.15	0.3	3.99	0.07
423.15	0.3	6.7	0.2

^aEstimated as worst case scenario.

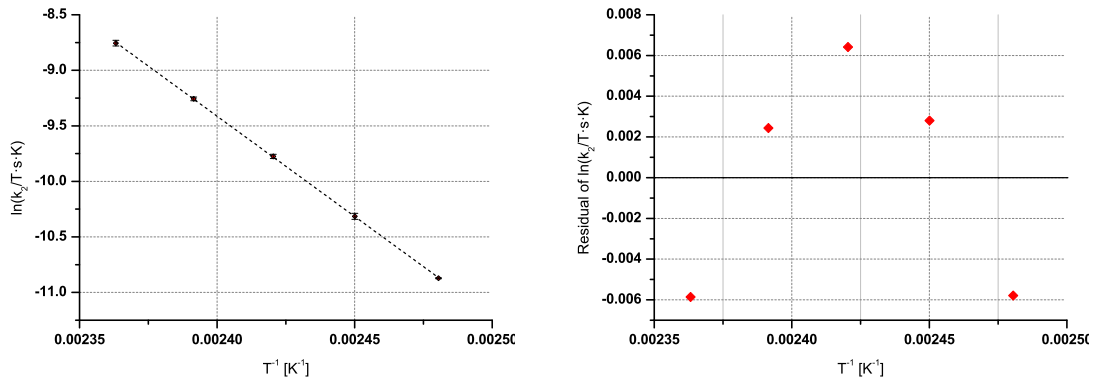


$$y = \frac{k_B T}{h} e^{\frac{\Delta S^\ddagger}{R}} e^{\frac{\Delta H^\ddagger}{R_x}}$$

ΔS^\ddagger		ΔH^\ddagger		Statistics	
Value	Error	Value	Error	R ²	F
81	1	148.8 · 10 ³	0.7 · 10 ³	0.99997	208961.57

Figure 5.36.: Determination of the activation parameters using non-linear regression (left) and the corresponding residual plot (right). The used regression equation and the regression results are shown in the lower section.

5. Data Evaluation and Mathematical Derivations



$$y = ax + b$$

Value	a		b		Statistics	
	Value	Error	Value	Error	R ²	F
$1.805 \cdot 10^4$	$0.007 \cdot 10^4$		33.9	0.2	0.99996	68366.55

Figure 5.37.: Determination of the activation parameters using linear regression of transformed coordinates (left) and the corresponding residual plot (right). In the logarithmic term of the ordinate the number is formally multiplied by the inverse of its unit. The used regression equation and the regression results are shown in the lower section.

5. Data Evaluation and Mathematical Derivations

for the entropy of activation. In general, the results from the non-linear regression are more significant since the data points are weighed equally and errors in the data points are accounted for correctly. However, since the linear regression of the transformed coordinates is still commonly used in literature^{82–86} to determine the activation parameters from the temperature-dependence of the rate constants, the respective values should be taken for comparison to other values, which were determined by the same method.

Table 5.5.: Activation parameters obtained from both non-linear regression and linear regression of transformed coordinates assuming a first order rate law.

Regression	ΔH^\ddagger [kJ mol ⁻¹]	ΔS^\ddagger [J mol ⁻¹ K ⁻¹]	ΔH^\ddagger [kcal mol ⁻¹]	ΔS^\ddagger [eu]
Non-linear	148.8 ± 0.7	81.4 ± 1.4	35.6 ± 0.2	19.5 ± 0.3
Linear	150.1 ± 0.6	84.4 ± 1.4	35.9 ± 0.1	20.2 ± 0.3

In addition, the Arrhenius parameters have also been determined from the same data and are given in Table 5.6.

Table 5.6.: Arrhenius parameters obtained from both non-linear and linear regression of transformed coordinates assuming a second order rate law (pre-exponential factor A_2).

Regression	E_a [kJ mol ⁻¹]	A_2 [10 ¹⁷ l mol ⁻¹ s ⁻¹]
Non-linear	152.3 ± 0.7	4.2 ± 0.7
Linear	153.5 ± 0.6	6 ± 1

Both the non-linear regression and the linear regression using transformed coordinates show a very high F value and therefore give very good results with respect to the fitness of the chosen regression functions. However, the quite small errors for both the enthalpy and the entropy of activation should be viewed with caution since errors associated with the rate constants for each temperature are higher than the corresponding residuals of the regression.

The enthalpy of activation shows a quite high value explaining the big temperature dependence of the reaction rate and the entropy of activation shows a significant positive value showing that a significant degree of disorder is generated prior to or in the turnover-limiting step.

Comparing the initial rate at 150 °C obtained from this experiment series [(5.2 ± 0.1) · 10⁻⁵ mol l⁻¹ s⁻¹] and the initial rate obtained from the initial rate

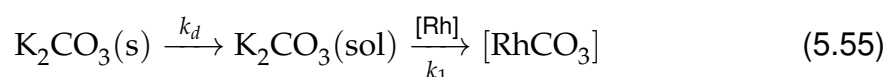
5. Data Evaluation and Mathematical Derivations

experiments $[(8.2 \pm 0.3) \cdot 10^{-5} \text{ mol l}^{-1} \text{ s}^{-1}]$ the two values show a significant difference. This discrepancy comes most probably from the fact that the experiments in order to determine the temperature dependence were conducted both in a different experimental setting (heating in oil bath, significantly different stirring rate) and the initial rate was determined differently (linear regression over 5 data points as compared to assumed start time and only one data point at a fixed time which was determined in triplicate). However, this discrepancy cannot be interpreted quantitatively by now and should be investigated further.

5.2.2.6. Kinetic Modelling

In the following section all aspects of the proposed kinetic model for the direct alkylation using alkenes (cf. Figure 3.20) are derived and investigated from a mathematical point of view. There are two parts of this kinetic model, the reaction of K_2CO_3 and a Rh-species in solution, denoted as [Rh], to form the catalytically active species, denoted formally as $[\text{RhCO}_3]$, and the catalytic cycle for the direct alkylation of **1** using hex-1-ene to form the corresponding alkylated product **2**.

First the reaction of K_2CO_3 and [Rh] to form the catalytically active species $[\text{RhCO}_3]$ will be discussed (cf. Equation 5.55).



K_2CO_3 is almost insoluble in the reaction mixture but a very small portion of it is still able to be dissolved. This very small portion of dissolved K_2CO_3 reacts with [Rh], a Rh-species which is derived from the $[\text{RhCl}(\text{cod})_2]$ complex used as catalyst precursor in this reaction. Mathematically, the dissolution of a big crystal of a solid having a planar surface in a solvent which is vigorously stirred can be described by the following Equation (cf. Equation 5.56).⁷⁵

$$\frac{dc}{dt} = \frac{D A}{V \delta} (c_s - c) \quad (5.56)$$

c ... Concentration of the solid in solution $[\text{mol l}^{-1}]$

t ... Time [s]

D ... Diffusion coefficient of the solid dissolved in the solvent $[\text{m}^2 \text{ s}^{-1}]$

A ... Surface of the solid $[\text{m}^2]$

V ... Volume of the solution $[\text{m}^3]$

δ ... Thin static solvent layer (Solvent adheres tightly to the surface) [m]

c_s ... Saturation concentration of the solid in solution $[\text{mol l}^{-1}]$

Equation 5.56 can be slightly rearranged by using the specific surface S of the solid, the molar mass M of the solid and the amount n of the solid (cf. Equations 5.57 and 5.58).

5. Data Evaluation and Mathematical Derivations

$$A = n M S \quad (5.57)$$

n ... Amount of the solid [mol]

M ... Molar mass of the solid [g mol^{-1}]

S ... Specific surface of the solid [$\text{m}^2 \text{g}^{-1}$]

$$\frac{dc}{dt} = \frac{D M S n}{V \delta} (c_s - c) \quad (5.58)$$

This is now simplified further by defining the fraction $\frac{n}{V}$ as the molar loading of undissolved solid $c[(s)]$. It is not termed a concentration because it is not dissolved. This yields the following.

$$\frac{dc}{dt} = \frac{D M S c[(s)]}{\delta} (c_s - c) \quad (5.59)$$

This description of the dissolution of a solid is applied in the proposed kinetic model for the dissolution of $\text{K}_2\text{CO}_3(s)$. Therefore, the following differential equation for the concentration of $\text{K}_2\text{CO}_3(\text{sol})$, denoted simply as c in the following discussion, can be formulated.

$$\frac{dc}{dt} = \frac{D M S c[\text{K}_2\text{CO}_3(s)]}{\delta} (c_s - c) - k_1 c([\text{Rh}]) c \quad (5.60)$$

Now it is assumed that the dissolved amount of K_2CO_3 is significantly lower compared to the remaining undissolved solid. Therefore, it can be assumed that the specific surface S does not change significantly in the dissolution process. In addition, on the basis of this assumption $c[\text{K}_2\text{CO}_3(s)]$ can also be assumed constant and equal to the initial molar loading $c_0(\text{K}_2\text{CO}_3)$. It should be noted here that this assumption is only valid when K_2CO_3 is used in excess in the reaction. If K_2CO_3 is used in catalytic amounts the analytic expressions for the concentration profiles of all the species involved in the induction period will be different. In order to simplify the mathematical derivations further k_d is introduced (cf. Equations 5.61 and 5.62).

$$k_d = \frac{D M S}{\delta} \quad (5.61)$$

$$\frac{dc}{dt} = k_d c_0(\text{K}_2\text{CO}_3) (c_s - c) - k_1 c([\text{Rh}]) c \quad (5.62)$$

The differential equation for the consumption of $[\text{Rh}]$ to form $[\text{RhCO}_3]$ is formulated as follows.

$$\frac{dc([\text{Rh}])}{dt} = -k_1 c([\text{Rh}]) c \quad (5.63)$$

As mentioned before, the solubility of K_2CO_3 in toluene is very low. Therefore, the concentration of K_2CO_3 in solution, i.e. c , is always very low and the steady state approximation can be applied (cf. Equation 5.64).

5. Data Evaluation and Mathematical Derivations

$$\frac{dc}{dt} = k_d c_0(K_2CO_3) (c_s - c) - k_1 c([Rh]) c = 0 \quad (5.64)$$

Rearranging equation 5.64 for c then yields equation 5.65.

$$c = \frac{k_d c_0(K_2CO_3) c_s}{k_d c_0(K_2CO_3) + k_1 c([Rh])} \quad (5.65)$$

Equation 5.65 is now substituted in equation 5.63.

$$\frac{dc([Rh])}{dt} = -k_1 c([Rh]) \frac{k_d c_0(K_2CO_3) c_s}{k_d c_0(K_2CO_3) + k_1 c([Rh])} \quad (5.66)$$

Now, this differential equation is solved by separating the variables and integration (cf. Equations 5.67-5.70).

$$-dt = \frac{dc([Rh])}{k_1 c_s c([Rh])} + \frac{dc([Rh])}{k_d c_s c_0(K_2CO_3)} \quad (5.67)$$

$$-\int_0^t dt = \int_{c_0([Rh])}^{c([Rh])} \frac{dc([Rh])}{k_1 c_s c([Rh])} + \int_{c_0([Rh])}^{c([Rh])} \frac{dc([Rh])}{k_d c_s c_0(K_2CO_3)} \quad (5.68)$$

$$-t = \frac{1}{k_1 c_s} \ln \frac{c([Rh])}{c_0([Rh])} + \frac{1}{k_d c_s c_0(K_2CO_3)} (c([Rh]) - c_0([Rh])) \quad (5.69)$$

$$t = \frac{1}{k_1 c_s} \ln \frac{c_0([Rh])}{c([Rh])} + \frac{1}{k_d c_s c_0(K_2CO_3)} (c_0([Rh]) - c([Rh])) \quad (5.70)$$

This equation now needs to be investigated. In the initial rate experiments a first order dependence on the initial molar loading of K_2CO_3 is observed. This dependence can only be explained on the basis of equation 5.70 if the first term can be neglected compared to the second because the first term does not show any dependence on the initial molar loading of K_2CO_3 . The first term can be neglected only if the rate constant k_1 is big and therefore only, if the reaction of $[Rh]$ with dissolved K_2CO_3 to form $[RhCO_3]$ is very fast compared to the rate of the dissolution of K_2CO_3 . This is not unreasonable since ligand substitution reaction are known to be potentially very fast.³⁷ Therefore, equation 5.70 is simplified to yield equation 5.71.

$$t = \frac{1}{k_d c_s c_0(K_2CO_3)} (c_0([Rh]) - c([Rh])) \quad (5.71)$$

Rearranging equation 5.71 for $c([Rh])$ yields equation 5.72.

$$c([Rh])(t) = c_0([Rh]) - k_d c_s c_0(K_2CO_3) t \quad (5.72)$$

5. Data Evaluation and Mathematical Derivations

Since $[RhCO_3]$ is formed from the reaction of $[Rh]$ with dissolved K_2CO_3 the concentration of $[RhCO_3]$ as a function of time can be determined according to equation 5.73.

$$c([RhCO_3])(t) = k_d c_s c_0(K_2CO_3) t \quad (5.73)$$

This equation means that as long as $[Rh]$ is present in solution, i.e. during the induction period, it will react with dissolved K_2CO_3 and there will be a linear increase of the concentration of $[RhCO_3]$. For the purpose of discussions equation 5.61 is resubstituted into equation 5.73 for k_d to yield equation 5.74.

$$c([RhCO_3])(t) = \frac{DMS}{\delta} c_s c_0(K_2CO_3) t \quad (5.74)$$

Before this result is discussed the kinetic model for the catalytic cycle of the direct alkylation of **1** using hex-1-ene to form the corresponding alkylated product **2** is derived. On the basis of the experimental results presented previously it is proposed that $[RhCO_3]$ is the predominant form of Rh in solution under the reaction conditions and therefore is also the resting state of the reaction. In addition, for the formation of both intermediates $[Rh \cdot \mathbf{1} \cdot CO_3]$ and $[Rh - \mathbf{1} \cdot CO_3]$ the equilibrium approximation is assumed. Therefore, the following equations can be derived (cf. Equations 5.75-5.78).

$$K_3 = \frac{c([Rh - \mathbf{1} \cdot CO_3])}{c([Rh \cdot \mathbf{1} \cdot CO_3])} \quad (5.75)$$

$$c([Rh - \mathbf{1} \cdot CO_3]) = K_3 c([Rh \cdot \mathbf{1} \cdot CO_3]) \quad (5.76)$$

$$K_2 = \frac{c([Rh \cdot \mathbf{1} \cdot CO_3])}{c([RhCO_3]) c_0(\mathbf{1})} \quad (5.77)$$

$$c([Rh \cdot \mathbf{1} \cdot CO_3]) = K_2 c([RhCO_3]) c_0(\mathbf{1}) \quad (5.78)$$

Substituting equation 5.78 into equation 5.76 yields the following expression for the concentration of $[Rh - \mathbf{1} \cdot CO_3]$.

$$c([Rh - \mathbf{1} \cdot CO_3]) = K_3 K_2 c([RhCO_3]) c_0(\mathbf{1}) \quad (5.79)$$

Now, the mass balance of Rh must be taken into account (cf. Equation 5.80). It should be noted that in the proposed kinetic model all Rh-species are assumed to be monomeric. However, on the basis of the experimental results at hand this cannot be determined and the catalytic cycle may as well proceed over dimeric Rh-species as is the catalyst precursor $[RhCl(cod)]_2$. This does not change the significance of the proposed kinetic model since most of the explanations and observations do not rely on whether the catalytically active Rh-species are monomeric, dimeric or oligomeric in general.

5. Data Evaluation and Mathematical Derivations

$$2 c_0([RhCl(cod)]_2) = c([RhCO_3]) + c([Rh \cdot \mathbf{1} \cdot CO_3]) + c([Rh - \mathbf{1} \cdot CO_3]) \quad (5.80)$$

Substituting the equations for the concentrations of $[Rh \cdot \mathbf{1} \cdot CO_3]$ and $[Rh - \mathbf{1} \cdot CO_3]$ into equation 5.80 results in the following.

$$2 c_0([RhCl(cod)]_2) = c([RhCO_3]) [1 + K_2 c_0(\mathbf{1}) + K_3 K_2 c_0(\mathbf{1})] \quad (5.81)$$

$$c([RhCO_3]) = \frac{2 c_0([RhCl(cod)]_2)}{1 + c_0(\mathbf{1}) K_2 (1 + K_3)} \quad (5.82)$$

The overall rate is determined by the rate of the turnover-limiting step (cf. Equation 5.83).

$$r = k_4 c([Rh - \mathbf{1} \cdot CO_3]) = k_4 K_3 K_2 c([RhCO_3]) c_0(\mathbf{1}) \quad (5.83)$$

Substituting equation 5.82 into equation 5.83 gives the rate law of the reaction.

$$r = \frac{2 k_4 K_3 K_2 c_0([RhCl(cod)]_2) c_0(\mathbf{1})}{1 + c_0(\mathbf{1}) K_2 (1 + K_3)} \quad (5.84)$$

Since in the initial rate experiments a first order dependence on the concentration of $\mathbf{1}$ was observed over a wide concentration region this rate law can be further simplified. Obviously, the second term in the denominator of equation 5.84 is negligible compared to the first. From a chemical point of view this means that almost all of the Rh is present in the form of $[RhCO_3]$ which seems reasonable since it is also proposed to be the resting state. The derived rate law is given in equation 5.85.

$$r = 2 k_4 K_3 K_2 c_0([RhCl(cod)]_2) c_0(\mathbf{1}) = k_{obs} c_0([RhCl(cod)]_2) c_0(\mathbf{1}) \quad (5.85)$$

Now the result from the kinetic modelling of the induction period (i.e. Equations 5.73 and 5.74) is discussed. On the basis of the proposed kinetic model the reaction rate does not possess first order dependence (in a kinetic sense) on the initial molar loading of K_2CO_3 . In order to explain this the results from both parts of the kinetic model need to be combined. Under the optimised reaction conditions no significant induction period is observed in the kinetic profile and at higher molar loadings of K_2CO_3 no increase is observed which is in accordance to the proposed kinetic model. However, when the loading of K_2CO_3 is reduced, the extent of the induction period increases. The time course of the final reaction product during the induction period can be mathematically described as follows introducing p as the concentration of the reaction product and introducing a and b to simplify the constant factors in the equations, respectively.

5. Data Evaluation and Mathematical Derivations

$$r = \frac{dp}{dt} = k_4 K_3 K_2 c([\text{RhCO}_3]) c_0(\mathbf{1}) = a c([\text{RhCO}_3]) c_0(\mathbf{1}) \quad (5.86)$$

$$c([\text{RhCO}_3])(t) = \frac{DMS}{\delta} c_s c_0(\text{K}_2\text{CO}_3) t = b c_0(\text{K}_2\text{CO}_3) t \quad (5.87)$$

$$\frac{dp}{dt} = a b c_0(\text{K}_2\text{CO}_3) c_0(\mathbf{1}) t \quad (5.88)$$

$$\int_0^p dp = \int_0^t a b c_0(\text{K}_2\text{CO}_3) c_0(\mathbf{1}) t dt \quad (5.89)$$

$$p(t) = \frac{a b}{2} c_0(\text{K}_2\text{CO}_3) c_0(\mathbf{1}) t^2 \quad (5.90)$$

In the experiments the initial rate is determined as the slope of a line between the start point (i.e. formally the point $t = 0$, $p = 0$) of the reaction and the product amount after a certain time which was the same in all experiments, which is denoted as t_i in the following equations. The initial rate r is therefore approximated by the following expression denoted r_i which actually is determined in the initial rate experiments, not the true initial rate r .

$$r \approx r_i = \frac{p(t_i) - p(0)}{t_i - 0} = \frac{a b}{2} c_0(\text{K}_2\text{CO}_3) c_0(\mathbf{1}) \frac{t_i^2}{t_i} = \frac{a b}{2} c_0(\text{K}_2\text{CO}_3) c_0(\mathbf{1}) t_i \quad (5.91)$$

From equation 5.91 it can now be seen that if t_i is held constant over all the experiments, as was the case in the initial rate experiments performed, the apparent initial rate r_i , which is determined in these experiments, shows a linear dependence on the initial molar K_2CO_3 loading. This explains why a first order dependence on the initial molar K_2CO_3 loading is observed, even though kinetically there is no first order dependence. It is a result of both the intrinsic kinetic behaviour of the system during the induction period and the experimental methods that were used to deduce the kinetic dependence. Technically, in the experiments with the lower K_2CO_3 loading the initial rates would have needed to be determined after the induction period which should then show no first order dependence on the basis of the proposed kinetic model.

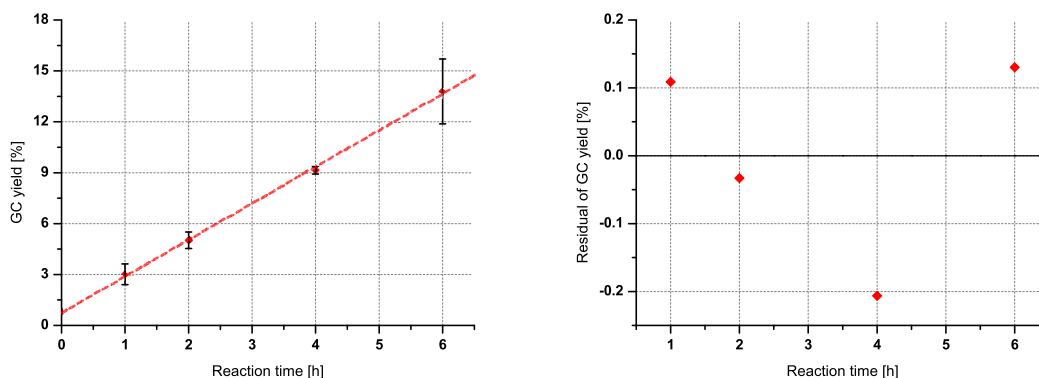
5.3. Direct Alkylations using Alkylbromides

5.3.1. Kinetic Profile Comparison

Since the reaction using 1-bromohexane was still in the initial reaction period it was not tried to fit mathematical functions to the data points of 1-bromohexane and **1**.

5. Data Evaluation and Mathematical Derivations

However, the increase of product amount showed a linear time profile and the initial rate of the formation of **2** was determined by linear regression through all the data points (cf. Figure 5.38). From the slope of the resulting line the initial rate was determined.



$$y = ax + b$$

a		b		Statistics	
Value	Error	Value	Error	R ²	F
2.15	0.05	0.8	0.2	0.99841	1884.95

Figure 5.38.: Regression result (left) and residual plot (right) for the formation of **2**. The used regression equation and the regression result are shown in the lower section.

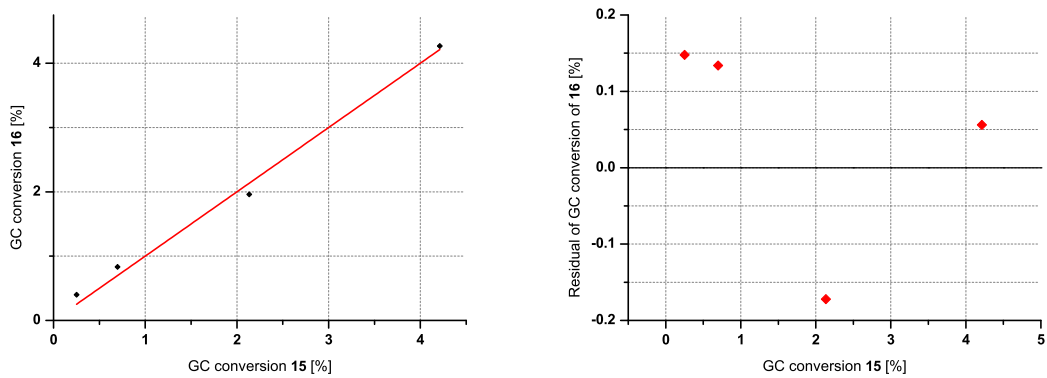
The initial rate of formation of **2** was determined to be $(7.5 \pm 0.2) 10^{-7} \text{ mol l}^{-1} \text{ s}^{-1}$ which is about 2 orders of magnitude slower compared to the initial rate observed for the formation of **2** in the direct alkylation of **1** using hex-1-ene.

5.3.2. Investigations into all Major Sideproducts

In order to investigate whether the formation of sideproducts **15** and **16** is potentially correlated their corresponding GC conversion data points were plotted against each other and the corresponding linear regression was determined. The results are given in Figure 5.39. The corresponding data points are found in the Appendix.

The conversions of the two sideproducts show basically the same kinetic profile which is confirmed by the high correlation between the corresponding data points. This indicates that the formation of both **15** and **16** could also be chemically correlated.

5. Data Evaluation and Mathematical Derivations



$$y = ax$$

a		Statistics	
Value	Error	R ²	F
1.00	0.03	0.99683	944.53

Figure 5.39.: Regression result (left) and residual plot (right) for the correlation of the GC conversions of **15** and **16**. The used regression equation and the regression result are shown in the lower section.

Bibliography

- [1] Mousseau, J. J.; Charette, A. B. *Acc. Chem. Res.* **2012**, *46*, 412–424.
- [2] Colby, D. A.; Tsai, A. S.; Bergman, R. G.; Ellman, J. A. *Acc. Chem. Res.* **2011**, *45*, 814–825.
- [3] Shi, G.; Zhang, Y. *Adv. Synth. Catal.* **2014**, *356*, 1419–1442.
- [4] Thirunavukkarasu, V. S.; Kozhushkov, S. I.; Ackermann, L. *Chem. Commun.* **2014**, *50*, 29–39.
- [5] Xie, J.; Jin, H.; Xu, P.; Zhu, C. *Tetrahedron Lett.* **2014**, *55*, 36–48.
- [6] Webb, J. R.; Burgess, S. A.; Cundari, T. R.; Gunnoe, T. B. *Dalton Trans.* **2013**, *42*, 16646–16665.
- [7] Yan, G.; Wu, X.; Yang, M. *Org. Biomol. Chem.* **2013**, *11*, 5558–5578.
- [8] Li, B.-J.; Shi, Z.-J. *Chem. Soc. Rev.* **2012**, *41*, 5588–5598.
- [9] Rouquet, G.; Chatani, N. *Angew. Chem. Int. Ed.* **2013**, *52*, 11726–11743.
- [10] Tsurugi, H.; Yamamoto, K.; Nagae, H.; Kaneko, H.; Mashima, K. *Dalton Trans.* **2014**, *43*, 2331–2343.
- [11] Gao, K.; Yoshikai, N. *Acc. Chem. Res.* **2014**, *47*, 1208–1219.
- [12] Shul'pin, G. B. *Dalton Trans.* **2013**, *42*, 12794–12818.
- [13] Sun, X.; Li, J.; Huang, X.; Sun, C. *Curr. Inorg. Chem.* **2012**, *2*, 64–85.
- [14] Okamoto, K.; Zhang, J.; Housekeeper, J. B.; Marder, S. R.; Luscombe, C. K. *Macromolecules* **2013**, *46*, 8059–8078.
- [15] Zhou, L.; Lu, W. *Chemistry-A European Journal* **2014**, *20*, 634–642.
- [16] Kapdi, A. R. *Dalton Trans.* **2014**, *43*, 3021–3034.
- [17] Wencel-Delord, J.; Colobert, F. *Chem.-Eur. J.* **2013**, *19*, 14010–14017.
- [18] Rossi, R.; Bellina, F.; Lessi, M.; Manzini, C. *Adv. Synth. Catal.* **2014**, *356*, 17–117.

Bibliography

- [19] Shang, X.; Liu, Z.-Q. *Chem. Soc. Rev.* **2013**, *42*, 3253–3260.
- [20] Li, B.; Dixneuf, P. H. *Chem. Soc. Rev.* **2013**, *42*, 5744–5767.
- [21] Girard, S. A.; Knauber, T.; Li, C.-J. *Angew. Chem. Int. Ed.* **2014**, *53*, 74–100.
- [22] Ramirez, T. A.; Zhao, B.; Shi, Y. *Chem. Soc. Rev.* **2012**, *41*, 931–942.
- [23] Dastbaravardeh, N.; Christakakou, M.; Haider, M.; Schnürch, M. *Synthesis* **2014**, *46*, 1421–1439.
- [24] Cavaliere, V. N.; Mindiola, D. J. *Chem. Sci.* **2012**, *3*, 3356–3365.
- [25] Qin, Y.; Lv, J.; Luo, S. *Tetrahedron Lett.* **2014**, *55*, 551–558.
- [26] Albrecht, M. *Chem. Rev.* **2009**, *110*, 576–623.
- [27] Granell, J.; Martínez, M. *Dalton Trans.* **2012**, *41*, 11243–11258.
- [28] Van der Boom, M. E.; Milstein, D. *Chem. Rev.* **2003**, *103*, 1759–1792.
- [29] Omae, I. *J. Organomet. Chem.* **2011**, *696*, 1128–1145.
- [30] Engle, K. M.; Mei, T.-S.; Wasa, M.; Yu, J.-Q. *Acc. Chem. Res.* **2011**, *45*, 788–802.
- [31] Han, Y.-F.; Jin, G.-X. *Chem. Soc. Rev.* **2014**, *43*, 2799–2823.
- [32] Johnson, K. R.; Hayes, P. G. *Chem. Soc. Rev.* **2013**, *42*, 1947–1960.
- [33] Dastbaravardeh, N.; Kirchner, K.; Schnürch, M.; Mihovilovic, M. D. *J. Org. Chem.* **2013**, *78*, 658–672.
- [34] Dastbaravardeh, N.; Schnürch, M.; Mihovilovic, M. D. *Eur. J. Org. Chem.* **2013**, *14*, 2878–2890.
- [35] Pollice, R. Mechanistic & substrate scope investigation of direct alkylation reactions by C-H activation. B.Sc. Thesis, Vienna University of Technology, 2013.
- [36] Crabtree, R. H. *Dalton Trans.* **2001**, 2437–2450.
- [37] Hartwig, J. *Organotransition Metal Chemistry: From Bonding to Catalysis*, 1st ed.; University Science Books: Sausalito, California, 2010.
- [38] He, T.; Li, H.; Li, P.; Wang, L. *Chem. Commun.* **2011**, *47*, 8946–8948.
- [39] Xia, J.-B.; Zhu, C.; Chen, C. *J. Am. Chem. Soc.* **2013**, *135*, 17494–17500.
- [40] Balcells, D.; Clot, E.; Eisenstein, O. *Chem. Rev.* **2010**, *110*, 749–823.

Bibliography

- [41] Song, G.; Wang, F.; Li, X. *Chem. Soc. Rev.* **2012**, *41*, 3651–3678.
- [42] Liu, Q.; Jackstell, R.; Beller, M. *Angew. Chem. Int. Ed.* **2013**, *52*, 13871–13873.
- [43] Bugaut, X.; Glorius, F. *Angew. Chem. Int. Ed.* **2011**, *50*, 7479–7481.
- [44] Zhang, S.-Y.; He, G.; Nack, W. A.; Zhao, Y.; Li, Q.; Chen, G. *J. Am. Chem. Soc.* **2013**, *135*, 2124–2127.
- [45] Jun, C.-H.; Hwang, D.-C.; Na, S.-J. *Chem. Commun.* **1998**, 1405–1406.
- [46] Zhang, Q.; Yu, H.-Z.; Li, Y.-T.; Liu, L.; Huang, Y.; Fu, Y. *Dalton Trans.* **2013**, *42*, 4175–4184.
- [47] Luo, X.; Tang, D.; Li, M. *J. Mol. Struct.* **2005**, *731*, 139–147.
- [48] Finger, M.; Reek, J. N.; de Bruin, B. *Organometallics* **2011**, *30*, 1094–1101.
- [49] Xu, R.; Bittner, M.; Klatt, G.; Köppel, H. *J. Phys. Chem. A* **2008**, *112*, 13139–13148.
- [50] Cramer, N.; Seiser, T. *Synlett* **2011**, *4*, 449–460.
- [51] Siegbahn, P. E.; Blomberg, M. R. *J. Am. Chem. Soc.* **1992**, *114*, 10548–10556.
- [52] Rytchinski, B.; Milstein, D. *Angew. Chem. Int. Ed.* **1999**, *38*, 870–883.
- [53] Jun, C.-H.; Moon, C. W.; Lee, D.-Y. *Chem. Eur. J.* **2002**, *8*, 2422–2428.
- [54] Jo, E.-A.; Lee, J.-H.; Jun, C.-H. *Chem. Commun.* **2008**, *44*, 5779–5781.
- [55] Crampin, E.; Schnell, S.; McSharry, P. *Progress in biophysics and molecular biology* **2004**, *86*, 77–112.
- [56] Nagashima, H.; Tatebe, K.; Ishibashi, T.; Nakaoka, A.; Sakakibara, J.; Itoh, K. *Organometallics* **1995**, *14*, 2868–2879.
- [57] Sunada, Y.; Fujimura, Y.; Nagashima, H. *Organometallics* **2008**, *27*, 3502–3513.
- [58] McBee, J. L.; Escalada, J.; Tilley, T. D. *J. Am. Chem. Soc.* **2009**, *131*, 12703–12713.
- [59] Gangopadhyay, S.; Basak, P.; Drew, M.; Gangopadhyay, P. K. *Chem. Commun.* **2010**, *46*, 7436–7438.
- [60] Ampt, K. A.; Duckett, S. B.; Perutz, R. N. *Dalton Trans.* **2004**, 3331–3337.

Bibliography

- [61] Xu, L.; Zhu, Q.; Huang, G.; Cheng, B.; Xia, Y. *J. Org. Chem.* **2012**, *77*, 3017–3024.
- [62] Karshtedt, D.; Bell, A. T.; Tilley, T. D. *Organometallics* **2006**, *25*, 4471–4482.
- [63] Esqueda, A. C.; Conejero, S.; Maya, C.; Carmona, E. *Organometallics* **2010**, *29*, 5481–5489.
- [64] Douglas, T. M.; Weller, A. S. *New J. Chem.* **2008**, *32*, 966–969.
- [65] Yadav, M.; Singh, A. K.; Pandey, D. S. *Organometallics* **2009**, *28*, 4713–4723.
- [66] Cross, W. B.; Daly, C. G.; Boutadla, Y.; Singh, K. *Dalton Trans.* **2011**, *40*, 9722–9730.
- [67] Gierz, V.; Urbanaite, A.; Seyboldt, A.; Kunz, D. *Organometallics* **2012**, *31*, 7532–7538.
- [68] Shende, V. S.; Shingote, S. K.; Deshpande, S. H.; Kuriakose, N.; Vanka, K.; Kelkar, A. A. *RSC Adv.* **2014**, *4*, 46351–46356.
- [69] Marche, C.; Ferronato, C.; De Hemptinne, J.-C.; Jose, J. *J. Chem. Eng. Data* **2006**, *51*, 355–359.
- [70] Zheng, Y.; Xiong, T.; Lv, Y.; Zhang, J.; Zhang, Q. *Org. Biomol. Chem.* **2013**, *11*, 7923–7930.
- [71] Gu, Z.-S.; Chen, W.-X.; Shao, L.-X. *J. Org. Chem.* **2014**, *79*, 5806–5811.
- [72] Zhao, Y.-B.; Mariampillai, B.; Candito, D. A.; Laleu, B.; Li, M.; Lautens, M. *Angew. Chem. Int. Ed.* **2009**, *121*, 1881–1884.
- [73] Jiao, L.; Bach, T. *J. Am. Chem. Soc.* **2011**, *133*, 12990–12993.
- [74] Freeman, D. L.; Doll, J. *J. Chem. Phys.* **1983**, *78*, 6002–6009.
- [75] Wedler, G. *Lehrbuch der Physikalischen Chemie*, 5th ed.; WILEY-VCH: Weinheim, Germany, 2004.
- [76] Hammett, L. P. *J. Am. Chem. Soc.* **1937**, *59*, 96–103.
- [77] Eyring, H. *J. Chem. Phys.* **1935**, *3*, 107–115.
- [78] Yang, H.-M.; Wu, P.-I. *Appl. Catal. A* **2001**, *209*, 17–26.
- [79] Aihara, Y.; Tobisu, M.; Fukumoto, Y.; Chatani, N. *J. Am. Chem. Soc.* **2014**, *136*, 15509–15518.

Bibliography

- [80] Marcé, P.; Godard, C.; Feliz, M.; Yáñez, X.; Bo, C.; Castellón, S. *Organometallics* **2009**, *28*, 2976–2985.
- [81] Jun, C.-H.; Lee, D.-Y.; Lee, H.; Hong, J.-B. *Angew. Chem. Int. Ed.* **2000**, *39*, 3070–3072.
- [82] Racowski, J. M.; Dick, A. R.; Sanford, M. S. *J. Am. Chem. Soc.* **2009**, *131*, 10974–10983.
- [83] Sevov, C. S.; Hartwig, J. F. *J. Am. Chem. Soc.* **2014**, *136*, 10625–10631.
- [84] Salzinger, S.; Soller, B. S.; Plikhta, A.; Seemann, U. B.; Herdtweck, E.; Rieger, B. *J. Am. Chem. Soc.* **2013**, *135*, 13030–13040.
- [85] Lutz, J. P.; Rathbun, C. M.; Stevenson, S. M.; Powell, B. M.; Boman, T. S.; Baxter, C. E.; Zona, J. M.; Johnson, J. B. *J. Am. Chem. Soc.* **2011**, *134*, 715–722.
- [86] Ball, N. D.; Gary, J. B.; Ye, Y.; Sanford, M. S. *J. Am. Chem. Soc.* **2011**, *133*, 7577–7584.

A. Appendices

A.1. Direct Alkylations using Alkenes

A.1.1. Investigations into the Mechanistic Outline

A.1.1.1. KIE Studies

The data points for the KIE studies are given in Tables A.1-A.2.

Table A.1.: Data points for the determination of the KIE of the benzylic C–H bond.

		1/1a	Hex-1-ene	[RhCl(cod)] ₂		
		0.125 mol l ⁻¹	0.375 mol l ⁻¹	0.006 25 mol l ⁻¹		
1/1a	H ₂ O ^a [m/m %]	c ₀ (K ₂ CO ₃) [mol l ⁻¹]	Rate [10 ⁻⁵ mol l ⁻¹ s ⁻¹]	Exchange ^b	2 + 3^c	
1	0.152	0.378	8.2 ± 0.3	-	9.5 %	
1a	0.152	0.378	1.9 ± 0.2	7 %	1.9 %	
1	0.018	0.378	7.0 ± 0.4	-	8.2 %	
1a	0.018	0.379	1.5 ± 0.2	5 %	1.5 %	

^aAdsorbed H₂O on K₂CO₃.

^bH–D exchange was determined by ¹H-NMR analysis of the crude reaction mixture after filtration and removal of the solvent under reduced pressure.

^cGC-yield.

A.1.1.2. Imine Intermediate Kinetics

The data points for the investigation of the imine intermediate kinetics are given in Tables A.3-A.9.

A.1.2. Investigations into the Kinetic Modelling

A.1.2.1. Initial Rate Experiments

The data points for the initial rate experiments are given in Tables A.10-A.14.

A. Appendices

Table A.2.: Data points for the determination of the KIE of the N–H bond.

1/1b	Hex-1-ene	[RhCl(cod)] ₂		
0.125 mol l ⁻¹	0.375 mol l ⁻¹	0.006 25 mol l ⁻¹		

1/1b	H ₂ O ^a [m/m %]	c ₀ (K ₂ CO ₃) [mol l ⁻¹]	Rate [10 ⁻⁵ mol l ⁻¹ s ⁻¹]	Exchange ^b
1	0.018	0.378	7.0 ± 0.4	-
1b	0.018	0.378	6.3 ± 0.8	(56 ± 1) %

^aAdsorbed H₂O on K₂CO₃.

^bH–D exchange was determined by transmission IR analysis of the reaction mixture after filtration.

Table A.3.: Data points for the GC area ratios of alkylated imine **11** and amine **2** at 150 °C obtained from the experiment series to determine the kinetic time course of the reaction with stoichiometric amounts of K₂CO₃.

Time [min]	GC Area Ratio $\frac{11}{2}$
4	0.043 ± 0.004
7	0.016 ± 0.004
10	0.013 ± 0.004
15	0.009 ± 0.002
25	0.005 ± 0.002
40	0.0047 ± 0.0009
60	0.0054 ± 0.0006
120	0.006 ± 0.001
180	0.0052 ± 0.0009
240	0.0063 ± 0.0008
362	0.0056 ± 0.0008

A. Appendices

Table A.4.: Data points for the GC area ratios of alkylated imine **11** and amine **2** at 150 °C obtained from the experiment series to determine the kinetic time course of the reaction with catalytic amounts of K₂CO₃.

Time [h]	GC Area Ratio $\frac{11}{2}$
0.943	1.29 ± 0.17
1.887	0.45 ± 0.04
3.830	0.0037 ± 0.0004
5.774	0.0016 ± 0.0002
20.967	0.00283 ± 0.00014
25.911	0.0032 ± 0.0002
48.938	0.0033 ± 0.0002

Table A.5.: Data points for the GC area ratios of alkylated imine **11** and amine **2** at 130 °C obtained from the temperature-dependence experiments.

Time [min]	GC Area Ratio $\frac{11}{2}$
5.57	0.348 ± 0.007
10.13	0.256 ± 0.006
13.05	0.176 ± 0.007
17.03	0.169 ± 0.003
20.03	0.136 ± 0.002

Table A.6.: Data points for the GC area ratios of alkylated imine **11** and amine **2** at 135 °C obtained from the temperature-dependence experiments.

Time [min]	GC Area Ratio $\frac{11}{2}$
7.03	0.233 ± 0.004
9.05	0.177 ± 0.006
11.05	0.140 ± 0.005
13.03	0.156 ± 0.002
15.05	0.125 ± 0.002

A. Appendices

Table A.7.: Data points for the GC area ratios of alkylated imine **11** and amine **2** at 140 °C obtained from the temperature-dependence experiments.

Time [min]	GC Area Ratio $\frac{11}{2}$
5.62	0.179 ± 0.002
7.1	0.154 ± 0.010
8.05	0.125 ± 0.006
9.05	0.092 ± 0.004
10.07	0.099 ± 0.007

Table A.8.: Data points for the GC area ratios of alkylated imine **11** and amine **2** at 145 °C obtained from the temperature-dependence experiments.

Time [min]	GC Area Ratio $\frac{11}{2}$
5.55	0.171 ± 0.004
6.08	0.141 ± 0.008
6.58	0.115 ± 0.007
7.63	0.107 ± 0.003
8.07	0.082 ± 0.005

Table A.9.: Data points for the GC area ratios of alkylated imine **11** and amine **2** at 150 °C obtained from the temperature-dependence experiments.

Time [min]	GC Area Ratio $\frac{11}{2}$
5.08	0.175 ± 0.008
5.32	0.097 ± 0.005
5.83	0.078 ± 0.002
6.57	0.064 ± 0.008
7.08	0.057 ± 0.001

A. Appendices

Table A.10.: Data points for the dependence of the initial rate on the K_2CO_3 concentration.

1	Hex-1-ene	$[\text{RhCl}(\text{cod})]_2$
0.125 mol l^{-1}	0.375 mol l^{-1}	$0.00625 \text{ mol l}^{-1}$

$c_0(\text{K}_2\text{CO}_3) [\text{mol l}^{-1}]$	Rate [$10^{-5} \text{ mol l}^{-1} \text{ s}^{-1}$]	Error [$10^{-5} \text{ mol l}^{-1} \text{ s}^{-1}$]
0.048	0.8	0.2
0.096	1.9	0.9
0.142	4.0	0.3
0.188	3.4	0.2
0.236	4.6	0.7
0.284	6.8	0.1
0.326	6.6	0.6
0.378	8.2	0.3
0.424	8.5	0.5
0.471	6.9	0.5
0.567	6.9	0.8
0.614	5.7	0.2
0.662	7.7	0.8
0.756	5.5	0.3

Table A.11.: Data points for the dependence of the initial rate on the concentration of **1**.

Hex-1-ene	$[\text{RhCl}(\text{cod})]_2$
0.375 mol l^{-1}	$0.00625 \text{ mol l}^{-1}$

$c_0(\mathbf{1}) [\text{mol l}^{-1}]$	$c_0(\text{K}_2\text{CO}_3) [\text{mol l}^{-1}]$	Rate [$10^{-5} \text{ mol l}^{-1} \text{ s}^{-1}$]	Error [$10^{-5} \text{ mol l}^{-1} \text{ s}^{-1}$]
0.061	0.379	3.7	0.5
0.109	0.377	6.2	1.3
0.125	0.378	8.2	0.3
0.154	0.377	10	1
0.202	0.377	12.2	0.4
0.250	0.379	14.2	2.6

A. Appendices

Table A.12.: Data points for the dependence of the initial rate on the concentration of $[\text{RhCl}(\text{cod})]_2$.

	1	Hex-1-ene		
	0.125 mol l^{-1}	0.375 mol l^{-1}		

$c_0([\text{RhCl}(\text{cod})]_2) [\text{mol l}^{-1}]$	$c_0(\text{K}_2\text{CO}_3) [\text{mol l}^{-1}]$	Rate [$10^{-5} \text{ mol l}^{-1} \text{ s}^{-1}$]	Error [$10^{-5} \text{ mol l}^{-1} \text{ s}^{-1}$]
0.0031	0.38	4.2	0.4
0.0039	0.378	5.2	1.3
0.0047	0.379	6.4	1.0
0.0054	0.377	7.7	1.3
0.0063	0.378	8.2	0.3
0.0069	0.378	7.9	0.3
0.0073	0.378	8.6	0.6
0.0077	0.374	8.6	0.8
0.0093	0.378	8.9	0.3
0.0101	0.378	8.0	1.1
0.0110	0.378	8.5	1.2

Table A.13.: Data points for the dependence of the initial rate on the concentration of hex-1-ene.

	1	$[\text{RhCl}(\text{cod})]_2$		
	0.125 mol l^{-1}	$0.00625 \text{ mol l}^{-1}$		

$c_0(\text{hex-1-ene}) [\text{mol l}^{-1}]$	$c_0(\text{K}_2\text{CO}_3) [\text{mol l}^{-1}]$	Rate [10 ⁻⁵ mol l ⁻¹ s ⁻¹]	Error [10 ⁻⁵ mol l ⁻¹ s ⁻¹]
0.184	0.378	7.8	1.3
0.326	0.375	8.4	1.0
0.375	0.378	8.2	0.3
0.463	0.377	8.6	0.5
0.607	0.375	7.7	1.6
0.750	0.378	8.3	0.8

A. Appendices

Table A.14.: Initial rate with increased concentrations of both K_2CO_3 and $[RhCl(cod)]_2$ and initial rate with increased concentration of $[RhCl(cod)]_2$ and decreased concentration of K_2CO_3 . These data points were determined only from single experiments. The error is the error over three GC measurements, respectively.

		1	Hex-1-ene		
		0.125 mol l ⁻¹	0.375 mol l ⁻¹		
$c_0(K_2CO_3)$ [mol l ⁻¹]	$c_0([RhCl(cod)]_2)$ [mol l ⁻¹]	Rate [10 ⁻⁵ mol l ⁻¹ s ⁻¹]		Error [10 ⁻⁵ mol l ⁻¹ s ⁻¹]	
0.568	0.0094	8.7		0.1	
0.234	0.0094	4.8		0.1	

A.1.2.2. K_2CO_3 Studies

The data points for the K_2CO_3 studies are given in Tables A.15-A.17.

Table A.15.: Data points for the dependence of the initial rate on the adsorbed water content in K_2CO_3 .

		1	Hex-1-ene	$[RhCl(cod)]_2$
		0.125 mol l ⁻¹	0.375 mol l ⁻¹	0.006 25 mol l ⁻¹
Net $c_0(K_2CO_3)$ [mol l ⁻¹]	H_2O^a [m/m %]	Rate [10 ⁻⁵ mol l ⁻¹ s ⁻¹]		
0.371	0.000	0.77 ± 0.06		
0.371	0.018	7.0 ± 0.4		
0.360	0.152	8.5 ± 0.5		

^aAdsorbed H_2O on K_2CO_3 .

A.1.2.3. Kinetic Profiles

The data points for the kinetic profiles are given in Tables A.18-A.19.

A.1.2.4. Electronic Influence on Benzylic Amines

The data points for the determination of the electronic influence of benzylic amines on the initial reaction rate are given in Table A.20.

A. Appendices

Table A.16.: Data points for the influence of the specific surface area of $\text{K}_2\text{CO}_3 \cdot 1.5\text{H}_2\text{O}$ on the initial reaction rate.

1	Hex-1-ene	[RhCl(cod)] ₂
0.125 mol l ⁻¹	0.375 mol l ⁻¹	0.006 25 mol l ⁻¹

c ₀ (K ₂ CO ₃) [mol l ⁻¹]	Specific surface area [m ² g ⁻¹]	Rate [10 ⁻⁵ mol l ⁻¹ s ⁻¹]
0.377	0.064 ± 0.006	2.34 ± 0.08
0.378	0.14 ± 0.01	5.1 ± 0.8

Table A.17.: Initial reaction rate without stirring and dependence of the influence of agitation on the content of adsorbed water in K_2CO_3 .

	Hex-1-ene	[RhCl(cod)] ₂
	0.375 mol l ⁻¹	0.006 25 mol l ⁻¹

c ₀ (K ₂ CO ₃) [mol l ⁻¹]	c ₀ (1) [mol l ⁻¹]	H ₂ O ^a [m/m %]	Rate [10 ⁻⁵ mol l ⁻¹ s ⁻¹]
0.378	0.125	0.018	1.2 ± 0.5
0.379	0.125	0.152	4.9 ± 0.5
0.377	0.250	0.152	10 ± 1

^aAdsorbed H₂O on K₂CO₃.

A. Appendices

Table A.18.: Data points for the kinetic time course of direct C–H alkylation of **1** using hex-1-ene and stoichiometric amounts of K_2CO_3 . Percentages are calibrated GC-yields.

	1	Hex-1-ene	K_2CO_3	$[RhCl(cod)]_2$				
	0.125 mol l ⁻¹	0.375 mol l ⁻¹	0.377 mol l ⁻¹	0.006 25 mol l ⁻¹				
Time [h]	1	Error 1	3	Error 3	2	Error 2	4	Error 4
0.067	100 %	2 %	0.00 %	0.00 %	2.3 %	0.4 %	0.00 %	0.00 %
0.096	93 %	2 %	0.32 %	0.09 %	9.0 %	0.4 %	0.06 %	0.03 %
0.117	74 %	4 %	0.8 %	0.3 %	11.0 %	1.0 %	0.06 %	0.02 %
0.167	69 %	3 %	0.9 %	0.3 %	12.0 %	1.0 %	0.07 %	0.04 %
0.250	58 %	6 %	1.8 %	0.5 %	19 %	2 %	0.20 %	0.08 %
0.417	45 %	5 %	3.7 %	0.3 %	29 %	4 %	0.42 %	0.03 %
0.667	30 %	2 %	5.0 %	0.1 %	37.1 %	0.4 %	0.74 %	0.07 %
1.00	16 %	3 %	5.9 %	0.3 %	47 %	3 %	1.10 %	0.10 %
2.00	0.00 %	0.00 %	7.2 %	0.5 %	65 %	6 %	2.9 %	0.5 %
3.00	0.00 %	0.00 %	7.7 %	0.3 %	63 %	3 %	3.5 %	0.1 %
4.00	0.00 %	0.00 %	7.8 %	0.7 %	62 %	3 %	3.0 %	0.6 %
6.03	0.00 %	0.00 %	7.9 %	0.7 %	63 %	1 %	3.2 %	0.6 %

Table A.19.: Data points for the kinetic time course of direct C–H alkylation of **1** using hex-1-ene and catalytic amounts of K_2CO_3 . Percentages are calibrated GC-yields except for **11**. For **11** percentages are conversions determined with respect to dodecane as internal standard assuming a conversion factor of 1.

	1	Hex-1-ene	K_2CO_3	$[RhCl(cod)]_2$		
	0.125 mol l ⁻¹	0.375 mol l ⁻¹	0.012 mol l ⁻¹	0.006 25 mol l ⁻¹		
Time [h]	1 [%]	3 [%]	2 [%]	11 [%]	4 [%]	Balance
0.000	99 ± 3	0.00 ± 0.00	0.00 ± 0.00	0.000 ± 0.000	0.00 ± 0.00	99 ± 4 %
0.943	92 ± 2	0.03 ± 0.02	0.18 ± 0.01	0.33 ± 0.04	0.00 ± 0.00	93 ± 2 %
1.887	88 ± 2	0.04 ± 0.02	1.19 ± 0.05	0.75 ± 0.05	0.00 ± 0.00	90 ± 2 %
3.830	64.5 ± 0.3	0.85 ± 0.05	21.2 ± 0.2	0.111 ± 0.010	0.212 ± 0.006	87 ± 1 %
5.774	49.2 ± 1.0	1.13 ± 0.12	41.9 ± 0.8	0.093 ± 0.009	0.48 ± 0.03	93 ± 2 %
20.97	19.5 ± 0.9	1.88 ± 0.11	69.7 ± 1.0	0.276 ± 0.017	1.22 ± 0.07	93 ± 2 %
25.91	18.4 ± 1.1	1.98 ± 0.02	71.3 ± 1.7	0.319 ± 0.014	1.31 ± 0.10	93 ± 3 %
48.94	17.3 ± 0.8	2.05 ± 0.10	73.1 ± 0.2	0.33 ± 0.02	1.324 ± 0.013	94 ± 1 %

A. Appendices

Table A.20.: Data points for the determination of the electronic influence of benzylic amines on the reaction rate.

1/1c-h	Hex-1-ene	K_2CO_3	$[RhCl(cod)]_2$
0.125 mol l ⁻¹	0.375 mol l ⁻¹	0.377 mol l ⁻¹	0.006 25 mol l ⁻¹

Compound	Y ^a	σ_p^{76}	Rate [10 ⁻⁵ mol l ⁻¹ s ⁻¹]	$\ln \frac{r_X}{r_H}$
1	H	0.000	7.9 ± 0.2	0.00 ± 0.04
1h	CF ₃	0.54	2.59 ± 0.01	-1.12 ± 0.03
1f	Cl	0.227	5.6 ± 0.8	-0.3 ± 0.1
1e	F	0.062	6.7 ± 1.6	-0.2 ± 0.2
1c	OMe	-0.268	11.0 ± 0.6	0.33 ± 0.06
1d	Me	-0.17	10.8 ± 1.5	0.3 ± 0.1
1g	CO ₂ Me	0.45	5.4 ± 0.2	-0.40 ± 0.05

^aSubstituent on the para position on the benzylic amine.

A.1.2.5. Temperature Dependence of the Initial Rate

The data points for the determination of the temperature dependence of the initial rates are given in Tables A.21-A.26.

Table A.21.: Concentrations of all the starting materials used in the experiments to investigate the temperature dependence of the initial rate.

1	Hex-1-ene	K_2CO_3	$[RhCl(cod)]_2$
0.125 mol l ⁻¹	0.375 mol l ⁻¹	0.377 mol l ⁻¹	0.006 25 mol l ⁻¹

Table A.22.: Data points for the determination of the temperature dependence of the reaction rate at 130 °C.

Time [s]	c(2 + 3) [10 ⁻³ mol l ⁻¹]	Error of c [10 ⁻³ mol l ⁻¹]
334	0.231	0.003
608	1.84	0.01
783	2.89	0.03
1022	4.35	0.05
1202	5.41	0.05

A. Appendices

Table A.23.: Data points for the determination of the temperature dependence of the reaction rate at 135 °C.

Time [s]	$c(\mathbf{2} + \mathbf{3}) [10^{-3} \text{ mol l}^{-1}]$	Error of c [$10^{-3} \text{ mol l}^{-1}$]
422	0.95	0.01
543	2.43	0.04
663	3.47	0.01
782	4.76	0.03
903	6.13	0.01

Table A.24.: Data points for the determination of the temperature dependence of the reaction rate at 140 °C.

Time [s]	$c(\mathbf{2} + \mathbf{3}) [10^{-3} \text{ mol l}^{-1}]$	Error of c [$10^{-3} \text{ mol l}^{-1}$]
337	1.05	0.07
426	2.66	0.04
483	3.73	0.02
543	4.94	0.04
604	5.89	0.05

Table A.25.: Data points for the determination of the temperature dependence of the reaction rate at 145 °C.

Time [s]	$c(\mathbf{2} + \mathbf{3}) [10^{-3} \text{ mol l}^{-1}]$	Error of c [$10^{-3} \text{ mol l}^{-1}$]
333	1.22	0.01
365	2.32	0.04
395	3.17	0.04
458	5.09	0.05
484	6.01	0.13

Table A.26.: Data points for the determination of the temperature dependence of the reaction rate at 150 °C.

Time [s]	c(2 + 3) [10^{-3} mol l $^{-1}$]	Error of c [10^{-3} mol l $^{-1}$]
305	3.08	0.03
319	3.59	0.05
350	5.32	0.07
394	7.48	0.08
425	9.32	0.03

A.2. Direct Alkylations using Alkylbromides

A.2.1. Kinetic Profile Comparison

The data points for the kinetic profile of direct alkylation of **1** using 1-bromohexane are given in Table A.27.

Table A.27.: Data points for the kinetic time course of direct C–H alkylation of **1** using 1-bromohexane. Percentages are calibrated GC-yields.

	1	1-Bromohexane	K ₂ CO ₃	[RhCl(cod)] ₂		
	0.125 mol l $^{-1}$	0.375 mol l $^{-1}$	0.377 mol l $^{-1}$	0.006 25 mol l $^{-1}$		

Time [h]	1	Error 1	<i>n</i> -hex-Br	Error <i>n</i> -hex-Br	2	Error 2
1	102 %	3 %	97 %	2 %	3.0 %	0.6 %
2	91 %	3 %	91 %	1 %	5.0 %	0.5 %
4	78 %	6 %	83 %	1 %	9.2 %	0.2 %
6	68 %	6 %	76 %	3 %	14 %	2 %

A.2.2. Investigations into all Major Sideproducts

The data points for the kinetic profile of the sideproducts **14**, **15** and **16** in the direct alkylation of **1** using 1-bromohexane are given in Table A.28.

A.2.3. Optimisation of Reaction Conditions

The data points for the optimisation of reaction conditions of direct alkylation of **1** using 1-bromohexane (denoted as R-Br in the Tables) are given in Tables A.29-

A. Appendices

Table A.28.: Data points for the kinetic time course of the sideproducts in the direct C–H alkylation of **1** using 1-bromohexane. Percentages are GC-conversions relative to dodecane as internal standard assuming a conversion factor of 1.

Time [h]	14	Error 14	15	Error 15	16	Error 16	Sel.
1.00	0.38 %	0.13 %	0.25 %	0.10 %	0.40 %	0.15 %	4.1
2.00	0.50 %	0.11 %	0.70 %	0.14 %	0.8 %	0.3 %	3.6
4.00	0.83 %	0.11 %	2.1 %	0.3 %	2.0 %	0.3 %	2.7
6.00	1.35 %	0.08 %	4.2 %	1.6 %	4.3 %	1.5 %	2.0

A.31. In the data given the GC yields for sideproducts **3** and **4** are omitted since in almost all experiments amounts below 1 % of these compounds were formed and those sideproducts were therefore not the focus of the optimisation performed.

Table A.29.: Data points of the optimisation of conditions for direct alkylation of **1** using 1-bromohexane. Part 1

Entry	T [°C]	Solvent	Base	R-Br	Time	Additive(s)	R-Br	1	17	16	2	14	15	Sel. ^c	
1	160	toluene	K ₂ CO ₃ ^a	7.5 eq.	3.0 eq.	24 h	-	52.5 %	0.0 %	0.0 %	9.7 %	49.9 %	4.6 %	9.9 %	2.7
2	160	toluene	K ₂ CO ₃ ^a	4.0 eq.	3.0 eq.	24 h	-	67.1 %	0.0 %	0.0 %	12.3 %	51.8 %	3.8 %	12.8 %	2.4
3	160	toluene	K ₂ CO ₃ ^a	3.5 eq.	3.0 eq.	24 h	-	63.5 %	2.7 %	0.0 %	7.0 %	56.7 %	3.0 %	6.2 %	4.1
4	160	toluene	K ₂ CO ₃ ^a	3.5 eq.	3.0 eq.	20 h	-	100.5 %	5.0 %	0.0 %	14.3 %	45.2 %	3.3 %	15.6 %	1.7
5	160	toluene	K ₂ CO ₃ ^a	3.5 eq.	3.0 eq.	16 h	-	162.6 %	28.3 %	0.0 %	8.7 %	37.8 %	3.3 %	9.9 %	2.1
6	160	toluene	Ag ₂ CO ₃	3.5 eq.	3.0 eq.	24 h	-	197.2 %	50.9 %	0.0 %	0.2 %	0.4 %	0.2 %	0.0 %	1.5
7	160	toluene	Ag ₂ CO ₃	3.5 eq.	3.0 eq.	16 h	-	205.9 %	51.3 %	0.0 %	1.6 %	0.4 %	1.5 %	0.0 %	0.1
8	160	toluene	K ₂ CO ₃ ^a	3.5 eq.	3.0 eq.	24 h	Ag ₂ CO ₃ (0.2 eq.)	67.3 %	0.0 %	0.0 %	16.0 %	47.5 %	4.2 %	16.7 %	1.6
9	160	toluene	K ₂ CO ₃ ^a	3.5 eq.	3.0 eq.	24 h	AgNO ₃ (0.2 eq.)	177.4 %	44.9 %	0.0 %	5.9 %	16.3 %	1.9 %	4.1 %	1.8
10	160	toluene	K ₂ CO ₃ ^a	3.5 eq.	3.0 eq.	16 h	Ag ₂ CO ₃ (0.1 eq.)	156.1 %	12.9 %	0.0 %	9.0 %	52.4 %	2.8 %	9.6 %	2.7
11	160	toluene	K ₂ CO ₃ ^a	3.5 eq.	3.0 eq.	16 h	Ag ₂ CO ₃ (0.2 eq.)	159.1 %	26.5 %	0.0 %	8.2 %	29.6 %	3.2 %	8.5 %	1.8
12	160	toluene	K ₂ CO ₃ ^a	3.5 eq.	3.0 eq.	16 h	Ag ₂ CO ₃ (0.4 eq.)	148.2 %	32.9 %	0.0 %	9.3 %	19.9 %	4.3 %	10.6 %	1.0
13	160	toluene	K ₂ CO ₃ ^a	3.5 eq.	3.0 eq.	16 h	Ag ₂ CO ₃ (0.05 eq.)	77.7 %	0.0 %	0.0 %	11.4 %	60.8 %	2.4 %	11.5 %	2.6
14	150	toluene	K ₂ CO ₃ ^a	3.5 eq.	3.0 eq.	16 h	Ag ₂ CO ₃ (0.05 eq.)	158.0 %	15.8 %	0.0 %	13.4 %	42.8 %	2.7 %	15.3 %	1.8
15	150	toluene	K ₂ CO ₃ ^a	3.5 eq.	3.0 eq.	20 h	Ag ₂ CO ₃ (0.05 eq.)	111.1 %	6.0 %	0.0 %	16.9 %	46.6 %	3.0 %	18.7 %	1.6
16	150	toluene	K ₂ CO ₃ ^a	3.5 eq.	3.0 eq.	24 h	Ag ₂ CO ₃ (0.05 eq.)	67.8 %	2.8 %	0.0 %	17.8 %	49.5 %	2.9 %	20.0 %	1.5
17	160	toluene	K ₂ CO ₃ ^a	3.5 eq.	2.0 eq.	16 h	Ag ₂ CO ₃ (0.05 eq.)	47.1 %	12.4 %	0.0 %	13.6 %	58.8 %	3.4 %	13.0 %	2.4
18	160	toluene	K ₂ CO ₃ ^a	3.5 eq.	1.5 eq.	16 h	Ag ₂ CO ₃ (0.05 eq.)	25.7 %	15.4 %	0.0 %	7.9 %	39.2 %	2.9 %	7.1 %	2.5
19	160	toluene	K ₂ CO ₃ ^a	2.0 eq.	1.5 eq.	16 h	Ag ₂ CO ₃ (0.05 eq.)	19.0 %	21.2 %	0.0 %	10.1 %	36.3 %	2.9 %	9.4 %	2.0
20	160	toluene	K ₂ CO ₃ ^a	2.0 eq.	1.5 eq.	24 h	Ag ₂ CO ₃ (0.05 eq.)	36.0 %	16.2 %	0.0 %	6.8 %	38.7 %	2.6 %	6.7 %	2.9
21	160	toluene	K ₂ CO ₃ ^a	2.5 eq.	2.0 eq.	16 h	Ag ₂ CO ₃ (0.05 eq.)	56.7 %	4.0 %	0.0 %	8.4 %	51.8 %	2.1 %	7.9 %	3.3
22	160	toluene	K ₂ CO ₃ ^a	2.5 eq.	2.0 eq.	20 h	Ag ₂ CO ₃ (0.05 eq.)	43.7 %	7.1 %	0.0 %	10.8 %	44.9 %	2.6 %	10.0 %	2.3
23	150	toluene	K ₂ CO ₃ ^a	3.5 eq.	3.0 eq.	16 h	Ag ₂ CO ₃ (0.025 eq.)	157.7 %	15.0 %	0.0 %	13.5 %	35.7 %	2.6 %	14.5 %	1.6
24	150	toluene	K ₂ CO ₃ ^a	3.5 eq.	3.0 eq.	20 h	Ag ₂ CO ₃ (0.025 eq.)	102.8 %	7.7 %	0.0 %	18.8 %	39.4 %	3.8 %	21.2 %	1.2
25	150	toluene	K ₂ CO ₃ ^b	3.5 eq.	3.0 eq.	16 h	Ag ₂ CO ₃ (0.05 eq.)	156.2 %	9.7 %	0.0 %	10.3 %	49.1 %	2.0 %	11.5 %	2.6
26	150	toluene	K ₂ CO ₃ ^b	3.5 eq.	3.0 eq.	20 h	Ag ₂ CO ₃ (0.05 eq.)	145.0 %	6.5 %	0.0 %	10.6 %	50.1 %	2.0 %	11.5 %	2.6
27	150	toluene	K ₂ CO ₃ ^b	3.5 eq.	3.0 eq.	24 h	Ag ₂ CO ₃ (0.05 eq.)	95.5 %	0.0 %	0.0 %	12.5 %	54.6 %	2.1 %	13.8 %	2.2
28	160	toluene	K ₂ CO ₃ ^b	3.5 eq.	3.0 eq.	16 h	Ag ₂ CO ₃ (0.05 eq.)	153.7 %	5.0 %	0.0 %	6.8 %	58.1 %	1.5 %	6.2 %	4.3
29	150	toluene	K ₂ CO ₃ ^b	3.5 eq.	3.0 eq.	16 h	Ag ₂ CO ₃ (0.05 eq.), Et ₃ N (0.1 eq.)	93.9 %	0.0 %	1.1 %	7.8 %	57.2 %	1.2 %	8.1 %	3.1
30	140	toluene	K ₂ CO ₃ ^b	3.5 eq.	3.0 eq.	16 h	Ag ₂ CO ₃ (0.05 eq.), Et ₃ N (0.1 eq.)	139.2 %	15.5 %	1.5 %	8.8 %	44.8 %	1.4 %	10.0 %	2.4
31	140	toluene	K ₂ CO ₃ ^b	3.5 eq.	3.0 eq.	16 h	Ag ₂ CO ₃ (0.05 eq.), Et ₃ N (0.05 eq.)	197.0 %	26.0 %	0.7 %	5.4 %	30.2 %	1.0 %	6.3 %	2.9
32	140	toluene	K ₂ CO ₃ ^b	3.5 eq.	3.0 eq.	16 h	Ag ₂ CO ₃ (0.05 eq.), Et ₃ N (0.15 eq.)	158.3 %	11.7 %	1.7 %	4.5 %	46.8 %	1.0 %	5.1 %	4.2
33	140	toluene	K ₂ CO ₃ ^b	3.5 eq.	3.0 eq.	16 h	Ag ₂ CO ₃ (0.05 eq.), DIPEA (0.1 eq.)	221.3 %	46.7 %	0.0 %	5.5 %	21.5 %	1.1 %	6.4 %	2.2
34	140	toluene	K ₂ CO ₃ ^b	3.5 eq.	3.0 eq.	16 h	Ag ₂ CO ₃ (0.05 eq.), Et ₂ NH (0.1 eq.)	165.3 %	24.2 %	0.5 %	6.9 %	30.6 %	1.7 %	8.0 %	2.4
35	140	toluene	K ₂ CO ₃ ^b	3.5 eq.	3.0 eq.	16 h	Ag ₂ CO ₃ (0.05 eq.), TMEDA (0.05 eq.)	160.6 %	19.8 %	0.0 %	4.1 %	37.4 %	1.0 %	3.3 %	3.6
36	140	toluene	K ₂ CO ₃ ^b	3.5 eq.	3.0 eq.	16 h	Ag ₂ CO ₃ (0.05 eq.), TMEDA (0.1 eq.)	140.1 %	28.4 %	0.0 %	4.1 %	27.1 %	1.1 %	2.4 %	2.5
37	140	toluene	K ₂ CO ₃ ^b	3.5 eq.	3.0 eq.	16 h	Ag ₂ CO ₃ (0.05 eq.), Et ₃ N (0.2 eq.)	115.8 %	14.2 %	2.3 %	7.4 %	49.2 %	1.3 %	8.3 %	2.6

^aK₂CO₃ with an adsorbed water content of 2 m%, a particle size median of 0.3 μm and a specific BET Surface of 0.4 m² g⁻¹ was used.

^bK₂CO₃ with an adsorbed water content of 0 m%, a particle size median of 0.3 μm and a specific BET Surface of 0.4 m² g⁻¹ was used.

^cSelectivity is defined as ratio of **2** and all other sideproducts formed.

Table A.30.: Data points of the optimisation of conditions for direct alkylation of **1** using 1-bromohexane. Part 2

Entry	T [°C]	Solvent	Base	R-Br	Time	Additive(s)	R-Br	1	17	16	2	14	15	Sel. ^c	
38	140	toluene	K ₂ CO ₃ ^b	3.5 eq.	3.0 eq.	16 h	Ag ₂ CO ₃ (0.05 eq.), TBAB (0.1 eq.)	118.8 %	23.9 %	0.0 %	4.5 %	26.8 %	0.6 %	6.4 %	2.6
39	140	toluene	K ₂ CO ₃ ^b	3.5 eq.	3.0 eq.	16 h	Ag ₂ CO ₃ (0.05 eq.), TBAB (0.2 eq.)	152.5 %	43.0 %	0.0 %	1.9 %	14.6 %	0.3 %	1.3 %	3.8
40	140	toluene	K ₂ CO ₃ ^b	3.5 eq.	3.0 eq.	16 h	Ag ₂ CO ₃ (0.05 eq.), Et ₃ N (0.3 eq.)	133.4 %	11.7 %	1.8 %	4.6 %	44.2 %	0.7 %	4.4 %	3.3
41	140	toluene	K ₂ CO ₃ ^b	3.5 eq.	3.0 eq.	16 h	Ag ₂ CO ₃ (0.05 eq.), Et ₃ N (0.4 eq.)	87.8 %	8.1 %	2.4 %	5.3 %	39.0 %	0.9 %	5.8 %	2.6
42	140	toluene/octane (4:1)	K ₂ CO ₃ ^b	3.5 eq.	3.0 eq.	16 h	Ag ₂ CO ₃ (0.05 eq.), Et ₃ N (0.2 eq.)	96.9 %	5.3 %	1.7 %	14.5 %	46.1 %	2.1 %	18.1 %	1.6
43	140	toluene/DMSO (4:1)	K ₂ CO ₃ ^b	3.5 eq.	3.0 eq.	16 h	Ag ₂ CO ₃ (0.05 eq.), Et ₃ N (0.2 eq.)	7.4 %	74.8 %	0.0 %	3.4 %	0.0 %	0.0 %	0.0 %	0.0
44	140	toluene	K ₂ CO ₃ ^b	3.5 eq.	3.0 eq.	16 h	Ag ₂ CO ₃ (0.05 eq.), Et ₃ N (0.2 eq.), bipy (0.1 eq.)	217.6 %	81.0 %	0.0 %	0.0 %	1.3 %	0.4 %	0.0 %	1.6
45	140	toluene	K ₂ CO ₃ ^b	3.5 eq.	3.0 eq.	16 h	Ag ₂ CO ₃ (0.05 eq.), Et ₃ N (0.2 eq.), terpy (0.1 eq.)	265.9 %	92.7 %	0.0 %	0.0 %	0.0 %	0.0 %	0.0 %	-
46	140	toluene/dioxane (4:1)	K ₂ CO ₃ ^b	3.5 eq.	3.0 eq.	16 h	Ag ₂ CO ₃ (0.05 eq.), Et ₃ N (0.2 eq.)	78.3 %	4.0 %	1.8 %	7.3 %	53.5 %	0.8 %	8.6 %	2.7
47	140	toluene	K ₂ CO ₃ ^b	3.5 eq.	3.0 eq.	16 h	Ag ₂ CO ₃ (0.05 eq.), Et ₃ N (0.2 eq.), cod (0.1 eq.)	162.6 %	25.5 %	1.9 %	4.3 %	41.2 %	0.8 %	6.5 %	3.8
48	140	toluene	K ₂ CO ₃ ^b	3.5 eq.	3.0 eq.	16 h	Ag ₂ CO ₃ (0.05 eq.), Et ₃ N (0.2 eq.), 2,6-Lut (0.1 eq.)	133.7 %	16.2 %	2.0 %	6.2 %	43.1 %	1.5 %	7.0 %	2.5
49	140	toluene/dioxane (3:2)	K ₂ CO ₃ ^b	3.5 eq.	3.0 eq.	16 h	Ag ₂ CO ₃ (0.05 eq.), Et ₃ N (0.2 eq.)	52.8 %	2.2 %	1.9 %	9.4 %	48.3 %	0.7 %	11.2 %	2.6
50	140	toluene/glyme (4:1)	K ₂ CO ₃ ^b	3.5 eq.	3.0 eq.	16 h	Ag ₂ CO ₃ (0.05 eq.), Et ₃ N (0.2 eq.)	64.5 %	4.8 %	1.7 %	8.8 %	42.2 %	1.1 %	9.0 %	2.6
51	140	toluene	K ₂ CO ₃ ^b	3.5 eq.	3.0 eq.	16 h	Ag ₂ CO ₃ (0.05 eq.), Et ₃ N (0.2 eq.), coe (0.1 eq.)	142.7 %	13.8 %	2.1 %	5.8 %	46.9 %	1.0 %	6.2 %	4.1
52	140	dioxane	K ₂ CO ₃ ^b	3.5 eq.	3.0 eq.	16 h	Ag ₂ CO ₃ (0.05 eq.)	137.1 %	31.3 %	0.0 %	7.4 %	20.6 %	0.0 %	7.2 %	1.8
53	140	toluene	K ₂ CO ₃ ^b	3.5 eq.	3.0 eq.	16 h	AgBF ₄ , Et ₃ N (0.2 eq.)	173.1 %	22.2 %	2.2 %	4.2 %	34.0 %	1.6 %	4.3 %	3.6
54	140	toluene	K ₂ CO ₃ ^b	3.5 eq.	3.0 eq.	16 h	Ag ₂ CO ₃ (0.05 eq.), Bu ₃ N (0.2 eq.)	126.6 %	12.5 %	0.0 %	10.4 %	48.0 %	1.2 %	11.2 %	2.8
55	140	dioxane	K ₂ CO ₃ ^b	3.5 eq.	3.0 eq.	16 h	Ag ₂ CO ₃ (0.05 eq.), Et ₃ N (0.2 eq.)	56.5 %	8.8 %	0.7 %	15.4 %	34.5 %	0.0 %	18.7 %	1.3
56	140	toluene	K ₂ CO ₃ ^b	3.5 eq.	3.0 eq.	16 h	AgSbF ₆ , Et ₃ N (0.2 eq.)	119.8 %	12.5 %	2.0 %	8.3 %	49.6 %	1.1 %	8.8 %	3.2
57	140	toluene/dioxane (2:3)	K ₂ CO ₃ ^b	3.5 eq.	3.0 eq.	16 h	Ag ₂ CO ₃ (0.05 eq.), Et ₃ N (0.2 eq.)	116.6 %	16.1 %	0.7 %	11.0 %	33.6 %	1.0 %	12.6 %	1.7
58	140	toluene/dioxane (1:4)	K ₂ CO ₃ ^b	3.5 eq.	3.0 eq.	16 h	Ag ₂ CO ₃ (0.05 eq.), Et ₃ N (0.2 eq.)	21.9 %	4.0 %	1.8 %	13.1 %	45.4 %	0.8 %	16.3 %	1.8
59	140	toluene/dioxane (4:1)	K ₂ CO ₃ ^b	3.5 eq.	3.0 eq.	16 h	Ag ₂ CO ₃ (0.05 eq.), Et ₃ N (0.2 eq.), CyOH (0.5 eq.)	50.5 %	11.1 %	1.3 %	10.4 %	40.0 %	1.6 %	11.7 %	2.1
60	140	toluene/dioxane (4:1)	K ₂ CO ₃ ^b	3.5 eq.	3.0 eq.	16 h	Ag ₂ CO ₃ (0.05 eq.), Et ₃ N (0.2 eq.), CyOH (0.1 eq.)	61.5 %	4.5 %	1.8 %	11.7 %	46.3 %	1.2 %	12.8 %	2.2
61	140	toluene/dioxane (4:1)	K ₂ CO ₃ ^b	3.5 eq.	3.0 eq.	16 h	Ag ₂ CO ₃ (0.05 eq.), NH ₄ Cl (0.2 eq.)	186.9 %	31.8 %	0.0 %	8.9 %	20.4 %	3.1 %	6.7 %	1.5
62	140	toluene/dioxane (4:1)	K ₂ CO ₃ ^b	3.5 eq.	3.0 eq.	16 h	Ag ₂ CO ₃ (0.05 eq.), DABCO (0.2 eq.)	62.6 %	13.2 %	3.9 %	8.5 %	34.5 %	0.5 %	7.4 %	2.2
63	140	toluene/dioxane (4:1)	K ₂ CO ₃ ^b	3.5 eq.	3.0 eq.	16 h	Ag ₂ CO ₃ (0.05 eq.), Et ₃ N (0.2 eq.), CyOH (1 eq.)	42.7 %	15.4 %	1.5 %	8.9 %	42.3 %	2.0 %	10.0 %	2.4
64	140	toluene/dioxane (4:1)	K ₂ CO ₃ ^b	3.5 eq.	3.0 eq.	16 h	Ag ₂ CO ₃ (0.05 eq.), Et ₃ N (0.2 eq.), CyOH (2 eq.)	21.9 %	30.3 %	1.8 %	5.0 %	36.8 %	2.4 %	7.8 %	2.8
65	140	toluene/dioxane (4:1)	K ₂ CO ₃ ^b	3.5 eq.	3.0 eq.	16 h	Ag ₂ CO ₃ (0.05 eq.), chinuclidine(0.2 eq.)	42.1 %	35.8 %	0.0 %	5.5 %	22.8 %	0.9 %	2.6 %	2.6
66	140	toluene/dioxane (4:1)	K ₂ CO ₃ ^b	3.5 eq.	3.0 eq.	16 h	Ag ₂ CO ₃ (0.05 eq.), Et ₃ N (0.2 eq.), CyOH (3 eq.)	36.3 %	34.2 %	1.4 %	2.5 %	31.9 %	2.2 %	4.1 %	4.1
67	140	toluene/dioxane (4:1)	K ₂ CO ₃ ^b	3.5 eq.	3.0 eq.	16 h	Ag ₂ CO ₃ (0.05 eq.), Et ₃ N (0.2 eq.), CyOH (4 eq.)	105.0 %	44.3 %	0.9 %	0.7 %	22.3 %	2.4 %	0.8 %	6.2
68	140	toluene	K ₂ CO ₃ ^b	3.5 eq.	3.0 eq.	16 h	Ag ₂ CO ₃ (0.05 eq.), Et ₃ N (0.2 eq.), cod (0.05 eq.)	148.3 %	9.9 %	1.8 %	5.2 %	50.9 %	0.8 %	5.1 %	5.0
69	140	toluene	K ₂ CO ₃ ^b	3.5 eq.	3.0 eq.	16 h	Ag ₂ CO ₃ (0.05 eq.), Et ₃ N (0.2 eq.), cod (0.2 eq.)	139.3 %	7.1 %	1.5 %	6.5 %	55.9 %	0.5 %	5.8 %	5.0
70	140	toluene/dioxane (4:1)	K ₂ CO ₃ ^b	3.5 eq.	3.0 eq.	16 h	Ag ₂ CO ₃ (0.05 eq.), Et ₃ N (0.2 eq.), CyOH (3.5 eq.)	78.0 %	38.1 %	1.0 %	1.1 %	30.5 %	1.8 %	1.1 %	8.0
71	140	toluene/dioxane (4:1)	K ₂ CO ₃ ^b	3.5 eq.	3.0 eq.	16 h	Ag ₂ CO ₃ (0.05 eq.), Et ₃ N (0.2 eq.), CyOH (4.5 eq.)	115.1 %	46.3 %	1.2 %	0.6 %	23.0 %	1.6 %	0.4 %	8.3
72	140	toluene	K ₂ CO ₃ ^b	3.5 eq.	3.0 eq.	16 h	Ag ₂ CO ₃ (0.05 eq.), Et ₃ N (0.2 eq.), cod (0.3 eq.)	94.7 %	6.5 %	1.3 %	8.9 %	49.0 %	0.7 %	8.1 %	3.3
73	140	toluene	K ₂ CO ₃ ^b	3.5 eq.	3.0 eq.	16 h	Ag ₂ CO ₃ (0.05 eq.), Et ₃ N (0.2 eq.), cod (0.4 eq.)	107.1 %	5.9 %	1.3 %	9.0 %	52.9 %	0.5 %	9.0 %	3.5
74	140	toluene/dioxane (4:1)	K ₂ CO ₃ ^b	3.5 eq.	3.0 eq.	16 h	Ag ₂ CO ₃ (0.05 eq.), Et ₃ N (0.2 eq.), CyOH (6.5 eq.)	64.0 %	44.4 %	1.2 %	1.0 %	29.0 %	2.2 %	1.4 %	6.4
75	140	toluene/dioxane (4:1)	K ₂ CO ₃ ^b	3.5 eq.	3.0 eq.	16 h	Ag ₂ CO ₃ (0.05 eq.), Et ₃ N (0.2 eq.), CyOH (4.5 eq.)	32.0 %	38.9 %	1.5 %	1.8 %	31.0 %	2.3 %	3.3 %	4.5
76	140	toluene/dioxane (4:1)	K ₂ CO ₃ ^b	3.5 eq.	3.0 eq.	16 h	Ag ₂ CO ₃ (0.05 eq.), Et ₃ N (0.2 eq.), CyOH (6 eq.)	90.1 %	47.6 %	1.1 %	0.7 %	25.0 %	2.0 %	0.7 %	7.1
77	140	toluene/dioxane (4:1)	K ₂ CO ₃ ^b	3.5 eq.	3.0 eq.	16 h	Ag ₂ CO ₃ (0.05 eq.), Et ₃ N (0.2 eq.), Cyclopentanol (6 eq.)	86.3 %	57.1 %	3.1 %	0.0 %	19.3 %	2.3 %	0.0 %	5.0
78	140	toluene/dioxane (4:1)	K ₂ CO ₃ ^b	3.5 eq.	3.0 eq.	16 h	Ag ₂ CO ₃ (0.05 eq.), Et ₃ N (0.2 eq.), <i>i</i> PrOH (6 eq.)	134.2 %	61.9 %	1.7 %	0.0 %	13.9 %	2.5 %	0.0 %	4.7

^aK₂CO₃ with an adsorbed water content of 2 m%, a particle size median of 0.3 μm and a specific BET Surface of 0.4 m² g⁻¹ was used.

^bK₂CO₃ with an adsorbed water content of 0 m%, a particle size median of 0.3 μm and a specific BET Surface of 0.4 m² g⁻¹ was used.

^cSelectivity is defined as ratio of **2** and all other sideproducts formed.

Table A.31.: Data points of the optimisation of reaction for direct alkylation of **1** using 1-bromohexane. Part 3

Entry	T [°C]	Solvent	Base	R-Br	Time	Additive(s)	R-Br	1	17	16	2	14	15	Sel. ^c	
79	140	toluene/dioxane (4:1)	K ₂ CO ₃ ^b	3.5 eq.	3.0 eq.	16 h	Ag ₂ CO ₃ (0.05 eq.), Et ₃ N (0.2 eq.), <i>i</i> PrOH (5 eq.)	130.0 %	53.0 %	1.7 %	0.3 %	16.3 %	2.9 %	0.0 %	4.7
80	140	toluene/dioxane (4:1)	K ₂ CO ₃ ^b	3.5 eq.	3.0 eq.	16 h	Ag ₂ CO ₃ (0.05 eq.), Et ₃ N (0.2 eq.), <i>i</i> PrOH (4 eq.)	124.1 %	45.5 %	1.2 %	0.5 %	21.8 %	2.2 %	0.0 %	7.5
81	140	toluene/dioxane (4:1)	K ₂ CO ₃ ^b	3.5 eq.	3.0 eq.	16 h	Ag ₂ CO ₃ (0.05 eq.), Et ₃ N (0.2 eq.), <i>i</i> PrOH (3 eq.)	146.1 %	52.7 %	1.7 %	0.5 %	16.3 %	1.9 %	0.0 %	5.2
82	140	toluene/dioxane (4:1)	K ₂ CO ₃ ^b	3.5 eq.	3.0 eq.	16 h	Ag ₂ CO ₃ (0.05 eq.), N-Methylpyrrolidine (0.2 eq.)	44.1 %	31.2 %	0.0 %	7.2 %	26.9 %	0.9 %	3.0 %	2.7
83	140	toluene/dioxane (4:1)	K ₂ CO ₃ ^b	3.5 eq.	3.0 eq.	16 h	Ag ₂ CO ₃ (0.05 eq.), Me ₃ N · HCl (0.2 eq.)	78.0 %	16.6 %	0.8 %	6.0 %	38.2 %	0.8 %	6.4 %	3.4
84	140	toluene/dioxane (4:1)	K ₂ CO ₃ ^b	3.5 eq.	3.0 eq.	16 h	Ag ₂ CO ₃ (0.05 eq.), Et ₃ N (0.2 eq.), <i>i</i> PrOH (2 eq.)	144.7 %	45.6 %	1.6 %	0.6 %	20.8 %	1.8 %	0.0 %	6.9
85	140	toluene/dioxane (4:1)	K ₂ CO ₃ ^b	3.5 eq.	3.0 eq.	16 h	Ag ₂ CO ₃ (0.05 eq.), Et ₃ N (0.2 eq.), <i>i</i> PrOH (1 eq.)	149.0 %	43.7 %	0.7 %	0.7 %	24.5 %	1.2 %	0.3 %	11.1
86	140	toluene/dioxane (4:1)	K ₂ CO ₃ ^b	3.5 eq.	3.0 eq.	16 h	Ag ₂ CO ₃ (0.05 eq.), Et ₃ N (0.2 eq.), <i>i</i> PrOH (0.5 eq.)	57.3 %	15.7 %	1.5 %	10.6 %	39.8 %	1.7 %	12.8 %	2.0
87	140	toluene/dioxane (4:1)	K ₂ CO ₃ ^b	3.5 eq.	3.0 eq.	16 h	Ag ₂ CO ₃ (0.05 eq.), Et ₃ N (0.2 eq.), EtOH (1 eq.)	212.1 %	62.1 %	0.0 %	0.0 %	3.4 %	0.4 %	1.7 %	2.3
88	140	toluene/dioxane (4:1)	K ₂ CO ₃ ^b	3.5 eq.	3.0 eq.	16 h	Ag ₂ CO ₃ (0.05 eq.), Et ₃ N (0.2 eq.), <i>t</i> BuOH (1 eq.)	76.9 %	2.1 %	2.0 %	9.0 %	55.9 %	0.9 %	10.9 %	3.0
89	140	toluene/dioxane (4:1)	K ₂ CO ₃ ^b	3.5 eq.	3.0 eq.	16 h	Ag ₂ CO ₃ (0.05 eq.), Et ₃ N (0.2 eq.), cod (0.2 eq.), <i>i</i> PrOH (1 eq.)	120.5 %	41.0 %	0.7 %	1.0 %	32.0 %	1.2 %	1.1 %	10.2
90	150	toluene	K ₂ CO ₃ ^b	3.5 eq.	3.0 eq.	24 h	Ag ₂ CO ₃ (0.05 eq.), TEMPO (0.1 eq.)	153.7 %	3.6 %	0.0 %	7.8 %	53.3 %	0.5 %	7.8 %	4.5
91	150	toluene/dioxane (4:1)	K ₂ CO ₃ ^b	3.5 eq.	3.0 eq.	16 h	Ag ₂ CO ₃ (0.05 eq.), Et ₃ N (0.2 eq.), cod (0.2 eq.), <i>i</i> PrOH (1 eq.)	132.9 %	37.5 %	0.7 %	0.9 %	28.7 %	1.2 %	0.5 %	11.2
92	160	toluene/dioxane (4:1)	K ₂ CO ₃ ^b	3.5 eq.	3.0 eq.	16 h	Ag ₂ CO ₃ (0.05 eq.), Et ₃ N (0.2 eq.), cod (0.2 eq.), <i>i</i> PrOH (1 eq.)	126.3 %	36.4 %	0.8 %	1.3 %	31.1 %	1.4 %	0.7 %	10.1
93	140	toluene/dioxane (4:1)	K ₂ CO ₃ ^b	3.5 eq.	3.0 eq.	24 h	Ag ₂ CO ₃ (0.05 eq.), Et ₃ N (0.2 eq.), cod (0.2 eq.), <i>i</i> PrOH (1 eq.)	79.3 %	26.4 %	0.8 %	2.8 %	38.9 %	1.5 %	3.6 %	5.9
94	130	toluene/dioxane (4:1)	K ₂ CO ₃ ^b	3.5 eq.	3.0 eq.	16 h	Ag ₂ CO ₃ (0.05 eq.), Et ₃ N (0.2 eq.), cod (0.2 eq.), <i>i</i> PrOH (1 eq.)	65.7 %	27.6 %	1.4 %	10.6 %	34.6 %	1.7 %	13.0 %	1.7
95	140	toluene/dioxane (4:1)	K ₂ CO ₃ ^b	3.5 eq.	3.0 eq.	72 h	Ag ₂ CO ₃ (0.05 eq.), Et ₃ N (0.2 eq.), cod (0.2 eq.), <i>i</i> PrOH (1 eq.)	23.9 %	13.2 %	1.3 %	6.0 %	45.4 %	2.5 %	7.2 %	3.6
96	140	toluene/dioxane (4:1)	K ₂ CO ₃ ^b	3.5 eq.	3.0 eq.	72 h	Ag ₂ CO ₃ (0.05 eq.), Et ₃ N (0.2 eq.), cod (0.2 eq.), <i>i</i> PrOH (1.5 eq.)	62.1 %	34.7 %	0.7 %	1.2 %	26.0 %	1.8 %	1.6 %	6.3

^aK₂CO₃ with an adsorbed water content of 2 m%, a particle size median of 0.3 μm and a specific BET Surface of 0.4 m² g⁻¹ was used.

^bK₂CO₃ with an adsorbed water content of 0 m%, a particle size median of 0.3 μm and a specific BET Surface of 0.4 m² g⁻¹ was used.

^cSelectivity is defined as ratio of **2** and all other sideproducts formed.